P-146
GRANT / AMES

IN-21534

APPLIED SUPERCONDUCTIVITY CENTER

UNIVERSITY OF WISCONSIN

1500 JOHNSON DRIVE

MADISON, WISCONSIN 53706

THERMAL AND ELECTRICAL CONTACT CONDUCTANCE STUDIES

Final Report, covering period June 1, 1983 - August 31, 1985

Grant Number: NAG2-242

Authors: M. Nilles
S. W. Van Sciver - Principal Investigator

THERMAL AND ELECTRICAL CONTACT RESISTANCE OF OFHC CU FROM 4K TO 290K

Michael John Nilles

under the supervision of Professor Steven W. Van Sciver

Prediction of electrical and thermal contact resistance for pressed, nominally flat contacts is complicated by the large number of variables which influence contact formation. This is reflected in experimental results as a wide variation in contact resistances, spanning up to six orders of magnitude. A series of experiments have been carried out to observe the effects of oxidation and surface roughness on contact resistance. Electrical contact resistance and thermal contact conductance from 4K to 290K on OFHC Cu contacts are reported. Electrical contact resistance is measured with a 4-wire DC technique. Thermal contact conductance is determined by steady-state longitudinal heat flow. Corrections for the bulk contribution to the overall measured resistance are made, with the remaining resistance due solely to the presence of the contact. Electrical contact resistance data differ markedly from the bulk behavior. The residual resistance ratio (RRR) of the contacts is always between 2 and 3, whereas the bulk RRR = 112. A contact assembled under an inert atmosphere

of dry nitrogen gas had a RRR = 11, indicating the dominant influence of the oxide present on the metal contact surface. Thermal contact conductance increased by a factor of 80 as the temperature increased from 4K to 290K. The low temperature variation of the thermal contact conductance followed a power law, with the temperature exponent ranging from 1.2 to 2. The increase in the exponent follows the increase in oxidation, again indicating the importance of the oxide layer on contact resistance. Lorenz numbers calculated from electrical and thermal contact resistance data are always greater than the Lorenz number for bulk Cu. The majority of the load bearing area of the contact must be electrically insulated, presumably by the oxide present. No systematic variation of contact resistance with respect to surface roughness was observed. The rms roughness ranged from 0.1um to 0.4um. In order to achieve larger thermal contact conductances, efforts must be directed to removing the oxide present on these types of contacts.

ACKNOWLEDGEMENTS

A number of people have contributed in various ways to this thesis and my development as a graduate student. First and foremost is my advisor, Prof. Steven W. Van Sciver. Under his guidance, I have had the freedom to work out details and develop the methods used in this study as I saw best. Of course, I can "see" better now, at the end of my graduate studies, than I did at the beginning. My improved "vision" has resulted from working through experimental aspects and recognizing when to attack a problem from a different perspective and when to abandon an idea altogether. The experience gained is invaluable and can only be learned through experience. Prof. Van Sciver has my sincere thanks.

The members of the cryogenics group have made my stay in graduate school enjoyable. They include: Susan Breon, Ed Canavan, Ben Helvensteijn, Scott Holmes, Ali Kashani, Jim Maddocks, Johm Pfotenhauer and John Weisend. Their discussions and helpful suggestions have been welcome.

Ed Drier and Oscar Petry always managed to deliver my liquid helium order, no matter how little notice I had given them. Their efforts to meet my experimental schedule are greatly appreciated.

Ray Thomas and Cary Pico aided my efforts on the Auger machine and Richard Knoll assisted with the scanning electron microscopy. The materials science program at the University of Wisconsin-Madison provided the facilities and funds.

Jim Babson printed the photos and machined the knife-edge clamps used in the experimental work.

Finally, my wife Anne and my children, Christine and Matthew, have put up with long nights and lonely weekends while this thesis was being written. Their love and support during this time was unwavering. I can only offer my love in return and to them, I dedicate this thesis.

TABLE OF CONTENTS page

TABLE OF CONTENTS page

TABLE OF CONTENTS page

Figure	List of Figures	page

Figure	List of Figures	page

Figure	List of Figures	page

Figure	List of Figures	page

List of Figures

List of Tables

List of Tables

CHAPTER 1 -- INTRODUCTION

Electrical and thermal contact resistance are important for a number of low temperature technologies. Low temperature refrigeration systems, space cryogenics and superconducting magnet technology are a few examples. The specific interest in contact resistance depends on the particular application. For example, applications in space cryogenics are concerned primarily with high thermal contact conductance joints, independent of the electrical contact resistance. Superconducting magnet applications require low electrical contact resitance joints, to minimize Ohmic losses during magnet energization and high thermal contact conductance to ensure adequate thermal stability of the joint.

Because of the varied and continuing interest in contact resistance, a number of investigations have been undertaken. The range of reported values spans several orders of magnitude. Also, the particular contact geometry, especially for electrical contact resistance, may not model conditions appropriate for technical applications.

The prediction of contact resistance is treated in a statistical manner, with the load bearing area determined by the distribution of peak heights and peak radii and by the applied load. It is usually possible to predict the

contact resistance within an order of magnitude at room temperature. Low temperature contact resistance has been estimated by extrapolation of the bulk behavior. If better accuracy is required, experimental measurements modeling the appropriate conditions are required.

There are some notable features of contact resistance apparant in the literature. The temperature range of interest for thermal contact conductance has generally been below 4K and near room temperature. Low temperature thermal contact conductance can be described with a power law dependence below 4K, although it is unclear how much higher in temperature this behavior exists. Separate results on electrical contact resistance and thermal contact conductance exist, but little information is available with regard to the relationship between the two when measured on the same contact. Some evidence indicates that most of the load supporting area of the contact is covered with an insulating film.

A series of experiments were undertaken to measure the electrical contact resistance and thermal contact conductance of OFHC Cu from 4K to 290K. Variables include the oxidation state of the contact surface and surface roughness. A unique aspect of these experiments is that both quantities are measured on the same contact. The load is a constant.

We explored three oxidation conditions. They are: 1) clean, a freshly prepared contact is assembled in air, attempting to minimize exposure time; 2) oxidation of 15min at 200C; 3) oxidation of 30min at 200C. The 200C oxidations are carried out in laboratory air. Three surface finishes were prepared for each oxidation state. The rms roughnesses are 0.4um, 0.2um and 0.1um. In addition, one sample was prepared under a N_2 atmosphere to prevent oxygen from reacting with the newly exposed metal contact surface. In order to observe the effect of soft metallic bonding agents on the overall contact conductance, a .003" In foil was inserted in between the contact faces of a 0.2um clean contact.

The remainder of this report is organized as follows. Chapter 2 contains the basic concepts of contact resistance and the data relavent to low temperature applications. In Chapter 3, we describe in detail the experimental techniques and procedures involved in the present study. Results and discussion are presented in Chapter 4. Chapter 5 contains our conclusions and suggestions for further work.

CHAPTER 2 -- ASPECTS OF CONTACT RESISTANCE

2.0 INTRODUCTION

A large number of interelated factors influence contact resistance. Roughness, mechanical behavior and surface contaminants affect contact resistance. For example, surface films can insulate load bearing areas which otherwise would be in metallic contact, rough surfaces may rupture oxide layers more easily than smooth surfaces, and some oxides are tough, existing on a soft substrate, e.g. Al_2O_3.

A large body of literature exists, dealing with many facets of contact resistance. An excellent starting point is R. Holm's Electric Contacts, 4th ed. While dealing with electrical contact resistance, many aspects are analogous with thermal contact resistance. This chapter contains a review of the basic concepts of contact resistance, as it pertains to rough, nominally flat contacts, and results applicable to low temperature environments.

2.1 FUNDAMENTALS

2.1.1 SINGLE, ISOLATED CONTACT

Consider a single circular contact, of radius a. Maxwell (1) solved

$$\nabla^2 V(\vec{r}) = 0 \qquad (2.1)$$

in oblate spherical coordinates. The solution is

$$V(\vec{r}) = \pm V_o \left[1 - \frac{2}{\pi} \tan^{-1} (1/\xi) \right] \qquad (2.2)$$

where $\pm$ refers to both sides of the contact and ξ is defined in terms of cylindrical polar coordinates r,z by

$$r^2 / a^2 = (1 + \xi)^2 (1 - z^2/\xi^2 a^2) \qquad (2.3)$$

where a is the radius of the constricting orifice. The resistance of the contact is found by dividing the voltage drop, $2V_o$, by the total current flow I, with

$$I = \int_0^{2\pi} d\varphi \int_0^{2\pi} r\, dr\, \sigma [\partial V/\partial z]_{z=0} \qquad (2.4)$$

where σ is the electrical conductivity. The resistance is then given by

$$R_c = \rho / 2a \qquad (2.5)$$

where $\rho = 1/\sigma$. This equation has been verified for a wide variety of practical contacts (2). Note that this is commonly referred to as the "constriction resistance". It arises from the constriction of current flowing through the contact region, essentially a boundary condition on the electrostatic potential, and not from any scattering mechanism operating in the contact region.

If the radius of the contact point is smaller than the scattering length of the electrons, l, the contact

resistance is determined only by the electron acceleration in the contact region. For large l/a, Sharvin (3) has estimated the contact resistance as

$$R_s = \rho l / 4a^2 \qquad (2.6)$$

Note that the contact resistance has an inverse quadratic dependence on the contact radius, as opposed to eqn. (2.5).

A formula interpolating between the two regimes was derived by Wexler (4). It is

$$R = \frac{\Gamma(l/a)}{2\sigma a} + \frac{4(l/a)}{3\pi\sigma a} \qquad (2.7)$$

where $\Gamma(l/a)$ is a slowly varying function of (l/a) with $\Gamma(0) = 1$ and $\Gamma(\infty) = 9\pi^2/128$.

2.1.2 THERMAL CONTACT RESISTANCE

In a manner analogous to electrical contact resistance, one solves

$$\nabla^2 T(\vec{r}) = 0 \qquad (2.8)$$

and calculates a thermal contact resistance W_c

$$W_c = 1/k2a \qquad (2.9)$$

where k is the bulk thermal conductivity and a is the contact spot radius.

2.1.3 GEOMETRICAL EFFECTS

The preceding formulas for contact resistance assume a circular contact spot. Depending on surface roughness, contact geometry and load, this assumption may not be valid. Therefore, Poisson's equation must be solved for various geometries. The results may be expressed as

$$R_c' = \psi R_c \qquad (2.10)$$

where ψ is a constriction factor with $0.5 \leq \psi \leq 2$ depending on geometry (5-8).

2.1.4 FILM COVERED CONTACTS

Surface films, including oxide or tarnish layers, are present on all metal surfaces that have been exposed to air. As the resistivities of these films are much greater than the metal substrate, the film resistance is determined by Ohm's law,

$$R_f = \rho_f d_f / \pi a^2 \qquad (2.11)$$

where the f subscript refers to the film, ρ and d are the film resistivity and thickness and a is the contact spot radius. However, ρ_f varies depending on the electron transport mechanism. These effects are discussed later while interpreting some experimental results. Also, electrical contact resistance is affected to a much

greater degree than is thermal contact conductance, owing to the substantial thermal conductivity of these films at room temperature.

2.1.5 MULTIPLE CONTACTS

The formulas presented above are for single, isolated contact areas. In a real system, contact occurs over a set of points determined by the load and surface roughness. If the points are "far" apart, the total resistance is determined by all the parallel paths. When the spacing is close enough, the current flow through one contact point will affect the current flow through the adjacent points. In a circular cluster of radius σ, that is uniformly covered with n contact points of mean radius a, the resistance of the cluster is (9,10)

$$R = \rho(1/2\sigma + 1/2na) \qquad (2.12)$$

where the first term is due to the self-interaction among closely spaced points and the last term is the resistance of n points all in parallel.

2.2 LOAD BEHAVIOR

Understanding of contact resistance between real surfaces is somewhat quantitative. A schematic of an ideal and a real contact region is shown in Fig. 2-1.

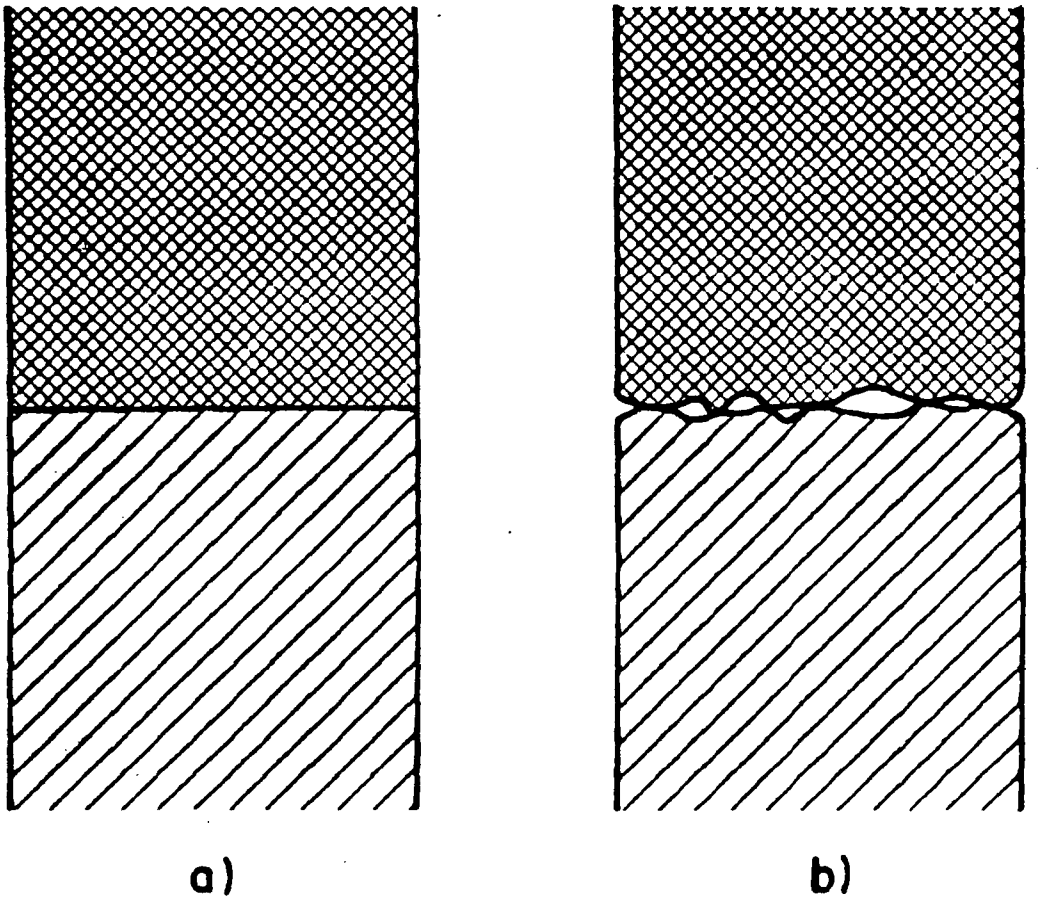

Fig. 2-1. Schematic of a) ideal contact and b) real contact between two solid bodies.

Actual contact over the apparent surface area of the contact occurs as a set of discrete points, due to the microscopic surface roughness of the contacting faces. Obviously, the pressure on these points is very high, initially at least, to yield the highest asperities. This allows more points to touch, lowering the pressure on the individual contact points. Eventually, equilibrium is reached, with the total load bearing area determined by;

1) microscopic hardness of the surface
2) plastic or elastic deformation of contacting asperities
3) total load applied to the contact

At equilibrium, some portion of the load must be supported elastically (11). Thus, mixed modes of deformation are present. The possibility of the roughness distribution changing during contact loading cannot be excluded either.

2.2.1 PREDICTION OF CONTACT RESISTANCE VS LOAD

A model of elastic contact has been proposed by Greenwood and Williamson (12). Assuming a gaussian height distribution and a constant surface slope distribution, a criteria differentiating between elastic and plastic deformation is derived. A "plasticity index", Ψ , is defined as,

$$\psi = (E'/H)\sqrt{s/b} \qquad (2.13)$$

where H is the microhardness, s is the standard deviation of the height distribution, b is the radius of all asperity summits and E'is

$$E' = E_1 E_2 / \left[E_2 (1-\nu_1)^2 + E_1 (1-\nu_2)^2 \right] \qquad (2.14)$$

where E is the modulus of elasticity and v is Poisson's ratio for the material. For $\psi > 1$, plastic deformation occurs for low load, while for $\psi < 0.6$, elastic deformation dominates unless a very large load is applied.

Figure 2-2 shows resistance vs load as calculated in their model. A power law dependence is found with

$$R_c = a L^{-0.94} \qquad (2.15)$$

Further, as seen in Fig. 2-3, the contact area depends only on load and not on the nominal pressure. For an apparent contact area differing by a factor of 10, there is essentially no difference in the contact resistance.

A similar model developed by Mikić (13) includes deformation of the underlying substrate. Again, contact conductance vs load follows eqn. (2.15). The variation with load for both plastic and elastic deformation is the same, although the total conductance is higher for the elastic mode, Fig. 2-4. In plastic deformation, surface

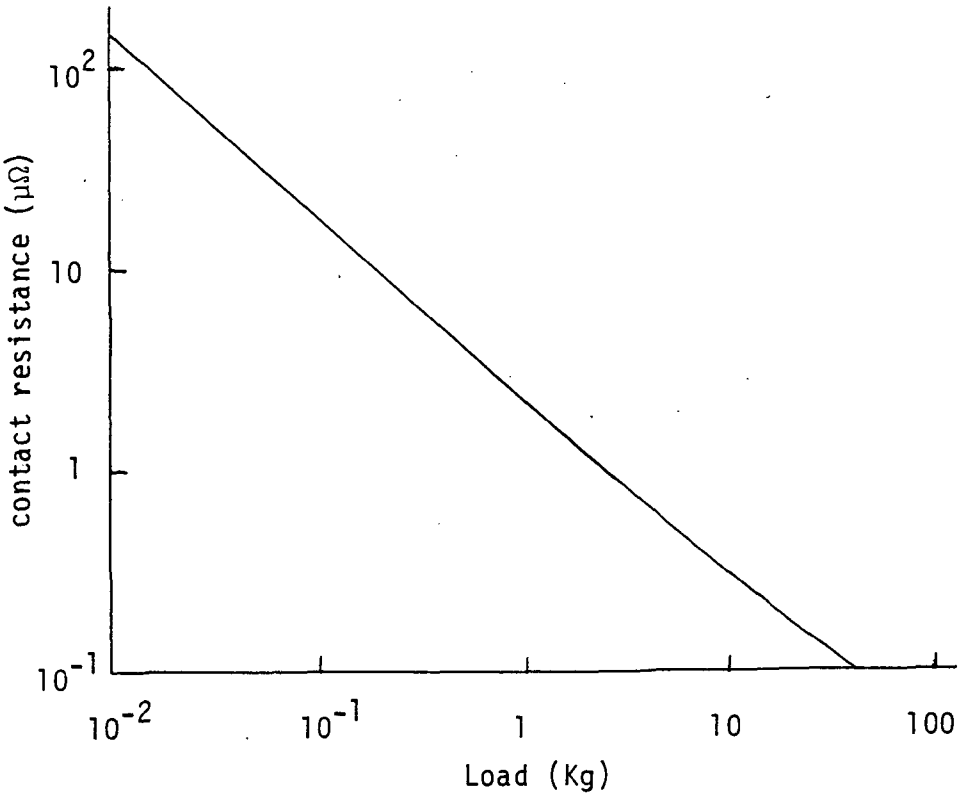

Fig. 2-2. Contact resistance vs load (ref. 12).

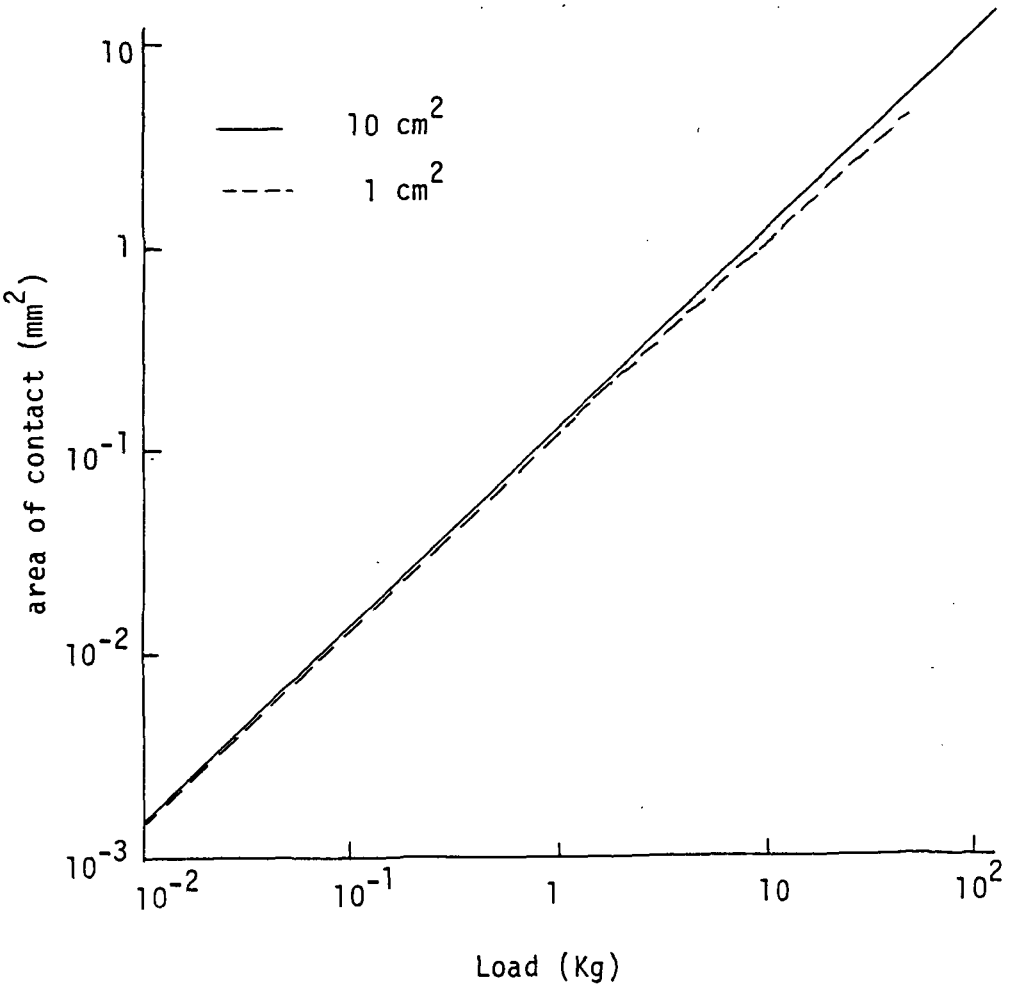

Fig. 2-3. Effect of nominal contact area on the load bearing contact area. —— $10cm^2$ — — — $1cm^2$ (ref. 12).

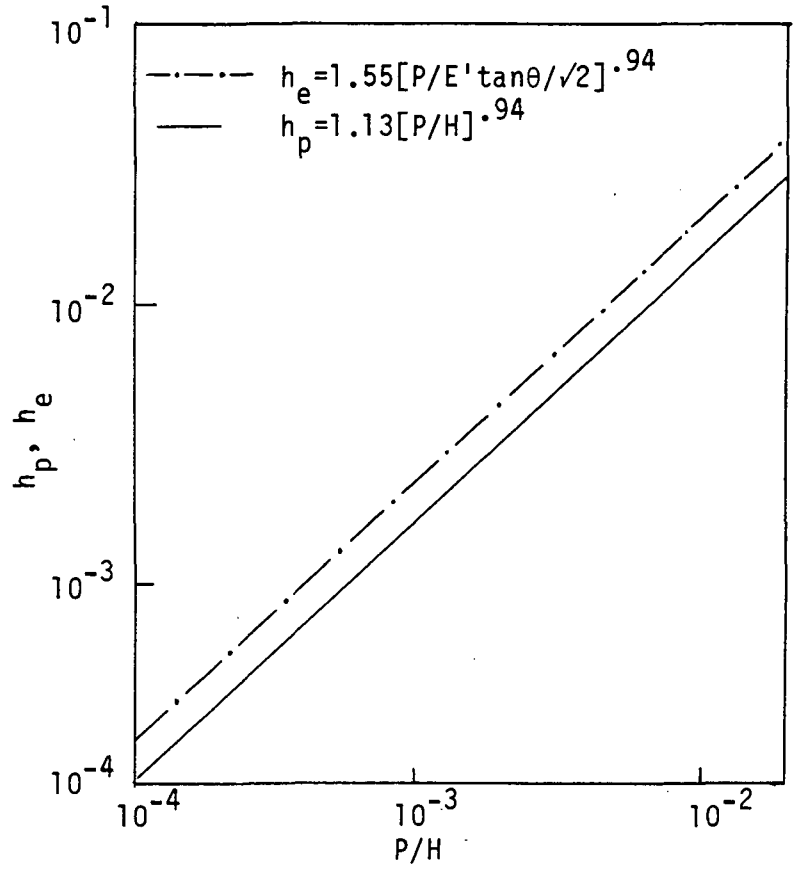

Fig. 2-4. Thermal contact conductance for elastic (he) and plastic (hp) deformation modes (ref. 13).

roughness and the slope of the asperities plays an important role, whereas in pure elastic deformation, only roughness is important. The deformation mode can be distinguished by γ, defined as

$$\gamma = H/(E' \tan\theta) \qquad (2.16)$$

with H and E' defined as before and tanθ is the mean of the absolute slope of the surface profile. Elastic deformation results when $\gamma > 3$ and plastic deformation dominates for $\gamma \leq 1/3$. Elastic deformation of the substrate increases the contact conductance. This effects is stronger at lower load and causes a change in the conductance vs load slope, lowering the slope at lower load.

Empirical correlations have been developed, attempting to predict contact conductance for a variety of circumstances (14-17). An example is shown in Fig. 2-5. The solid line is a function of the form

$$h = 1.45\, k\, (P_a / H)^{0.985} / (s \tan\theta) \qquad (2.17)$$

where h is the thermal contact conductance, k is the thermal conductivity, s is the rms roughness, tanθ is the average absolute asperity angle, P_a is the apparent contact pressure and H is the hardness. The agreement is

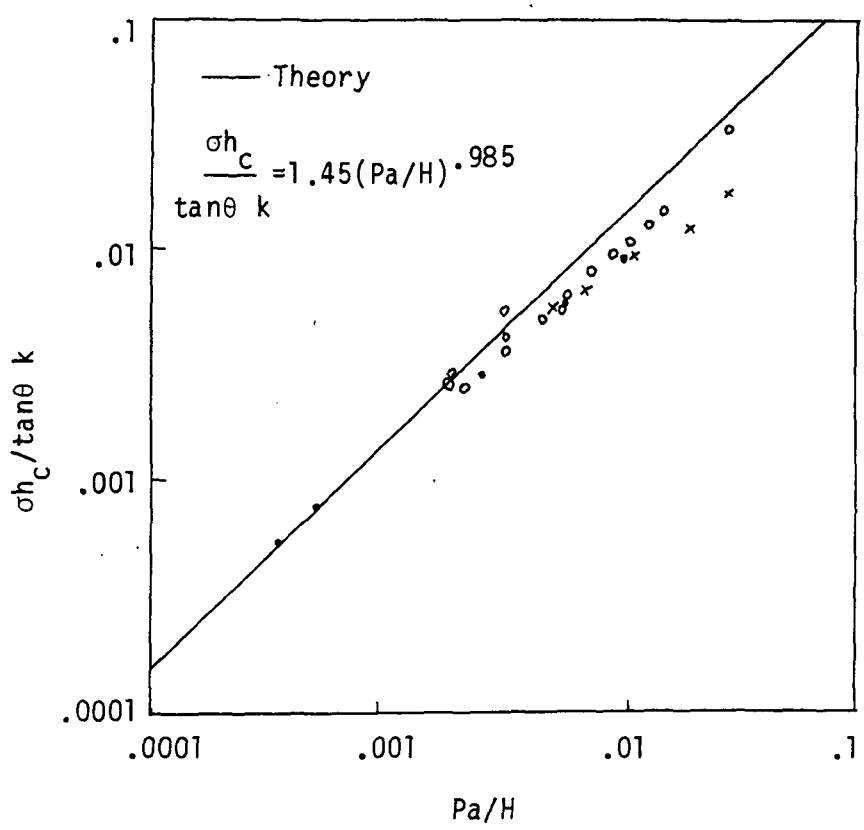

Fig. 2-5. Thermal contact conductance correlation (ref. 14).

good for $.0035 < P_a / H \leq .01$, but overpredicts h by 100% at high loads.

A better fit is given by (15)

$$h = 0.55\ k\ m(P_a / H)^{0.85} / s \qquad (2.18)$$

with m being the rms slope of the contacting asperities and the other terms defined as above.

Given the number of complicating factors in contact resistance, these correlations must be used with care, so as to remain in regions where they are valid.

An interesting experimental case has been reported by Cuthrell and Tripping (18). The resistance vs load behavior of Au contacts in air and sputter cleaned in an ultra-high vacuum is shown in Figs. 2-6 and 2-7. The region of negative load indicates the formation of a cold weld. Note that the dependence is less steep for Au contacts in air-presumably due to adsorbed gas layers. Another property common to small contacts at low load is featured in Fig. 2-8 (19). The decrease in contact resistance vs time is attributed to dislocation creep (18,19), resulting in an increase contact area. Film covered contacts show the same behavior, although contact growth proceeds at a slower rate.

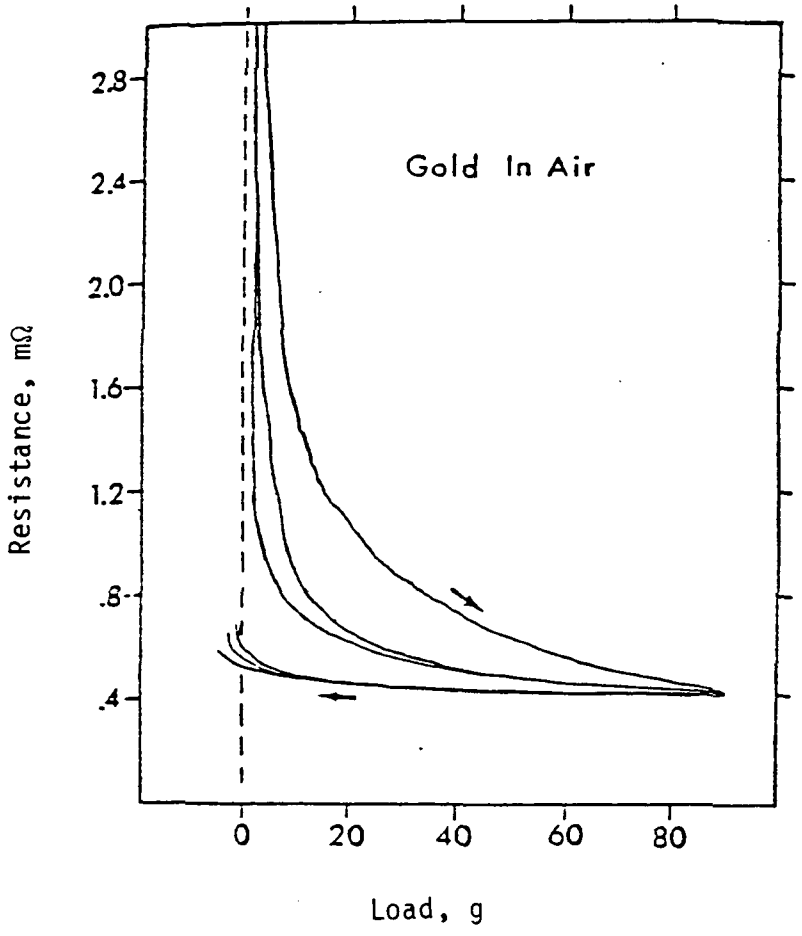

Fig. 2-6. Electrical contact resistance vs load for Au contacts in air (ref. 18).

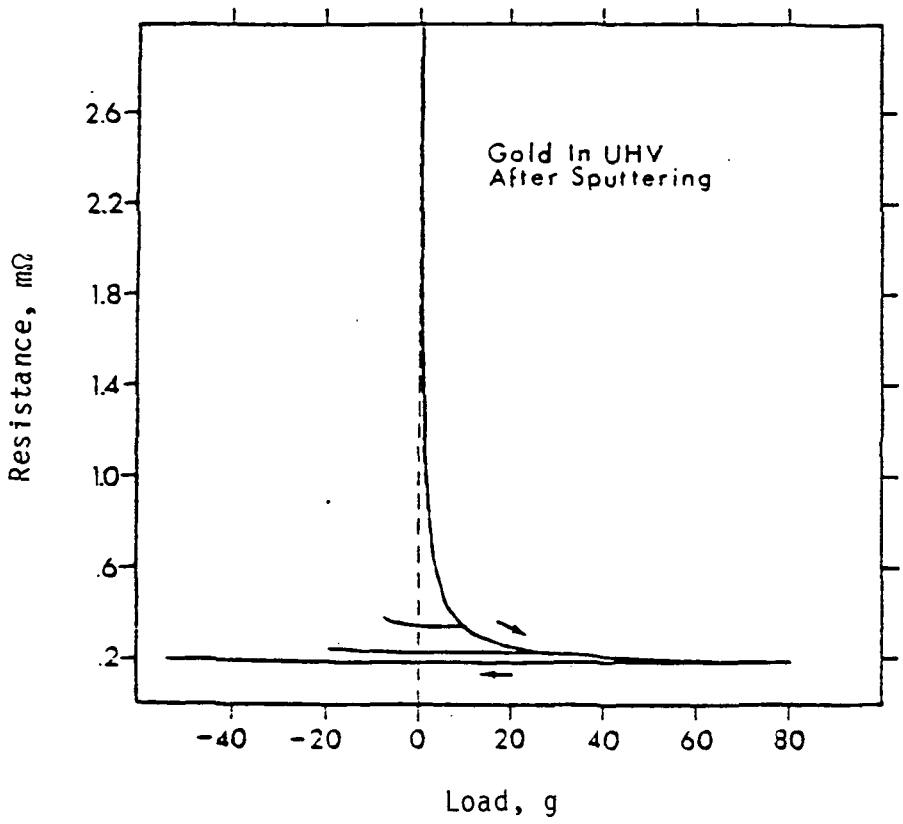

Fig. 2-7. Electrical contact resistance vs load for Au contacts in an UHV (ref. 18).

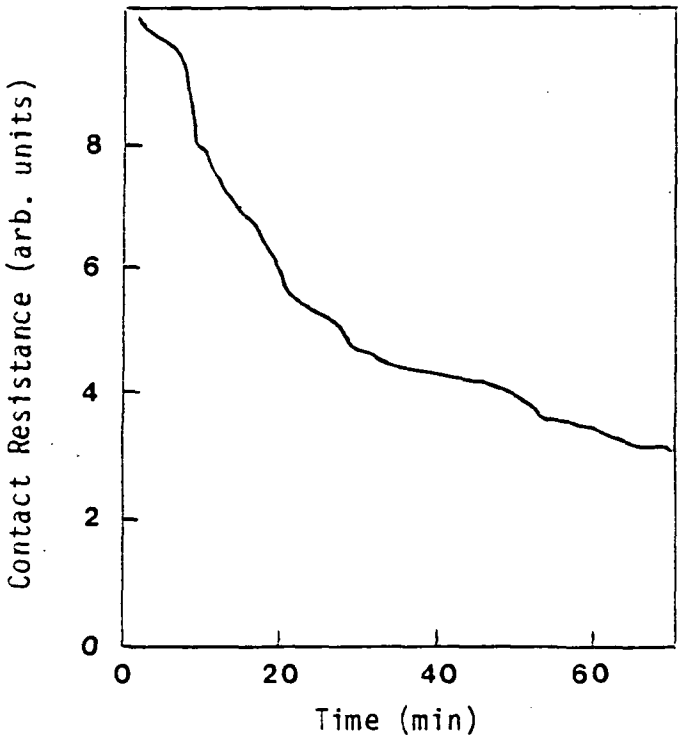

Fig. 2-8. Electrical contact resistance vs time for Al contacts in air (ref. 19).

2.2.2 EFFECTS OF SURFACE FILMS

Real metals under ordinary circumstances are always covered with some type of surface film. The nature of the film varies, it may be a native oxide or a tarnish layer, depending on the chemical environment of the surface. Prediction of contact resistance is complicated by the mechanical behavior of the film and also by its transport properties.

Hisakado developed a critical penetration model (20) whereby metallic contact occurs only after asperities have penetrated a critical depth into the opposing contact surface. There is rough agreement between experiment and theory, which is better at higher load, as shown in Fig. 2-9. The variation of R_c with roughness is not clear here, but another report (21) shows an increase in R_c with decreasing roughness for tarnished Ag contacts, Fig. 2-10.

2.3 FILM CONDUCTION

Because surface films are in general poor electrical conductors, it is obviously important to understand electronic conduction processes so as to either modify the film or reduce its influence. Thermal contact conductance is not affected as much, due to the large thermal conductivity of these films at room temperature.

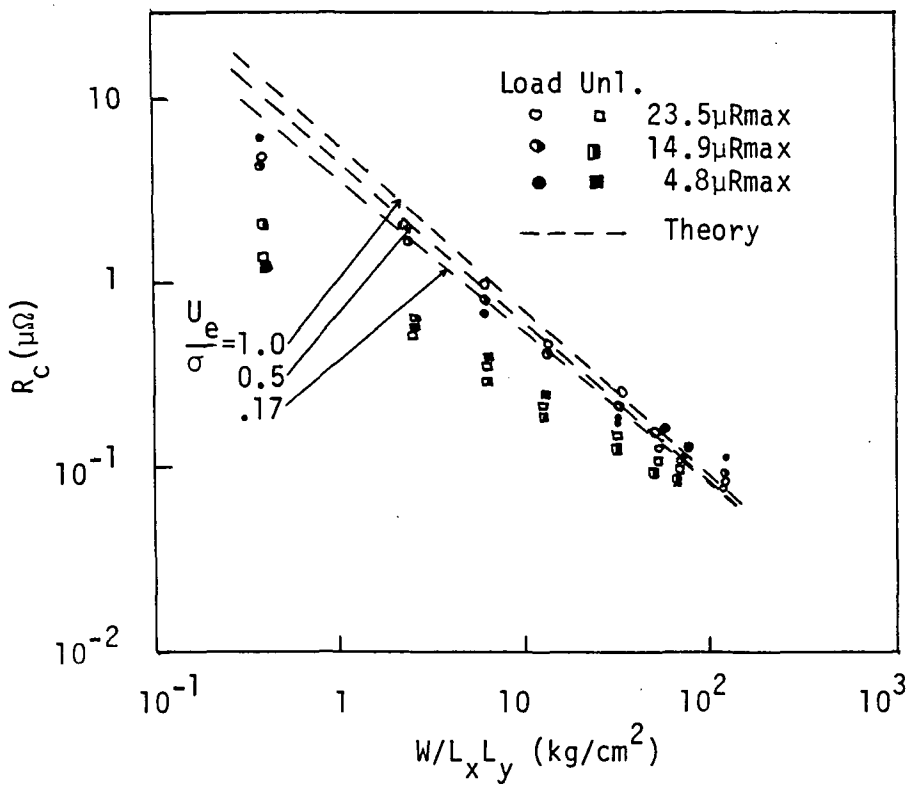

Fig. 2-9. Electrical contact resistance vs load for tarnished Ag contacts. - - - critical penetration model (ref. 20).

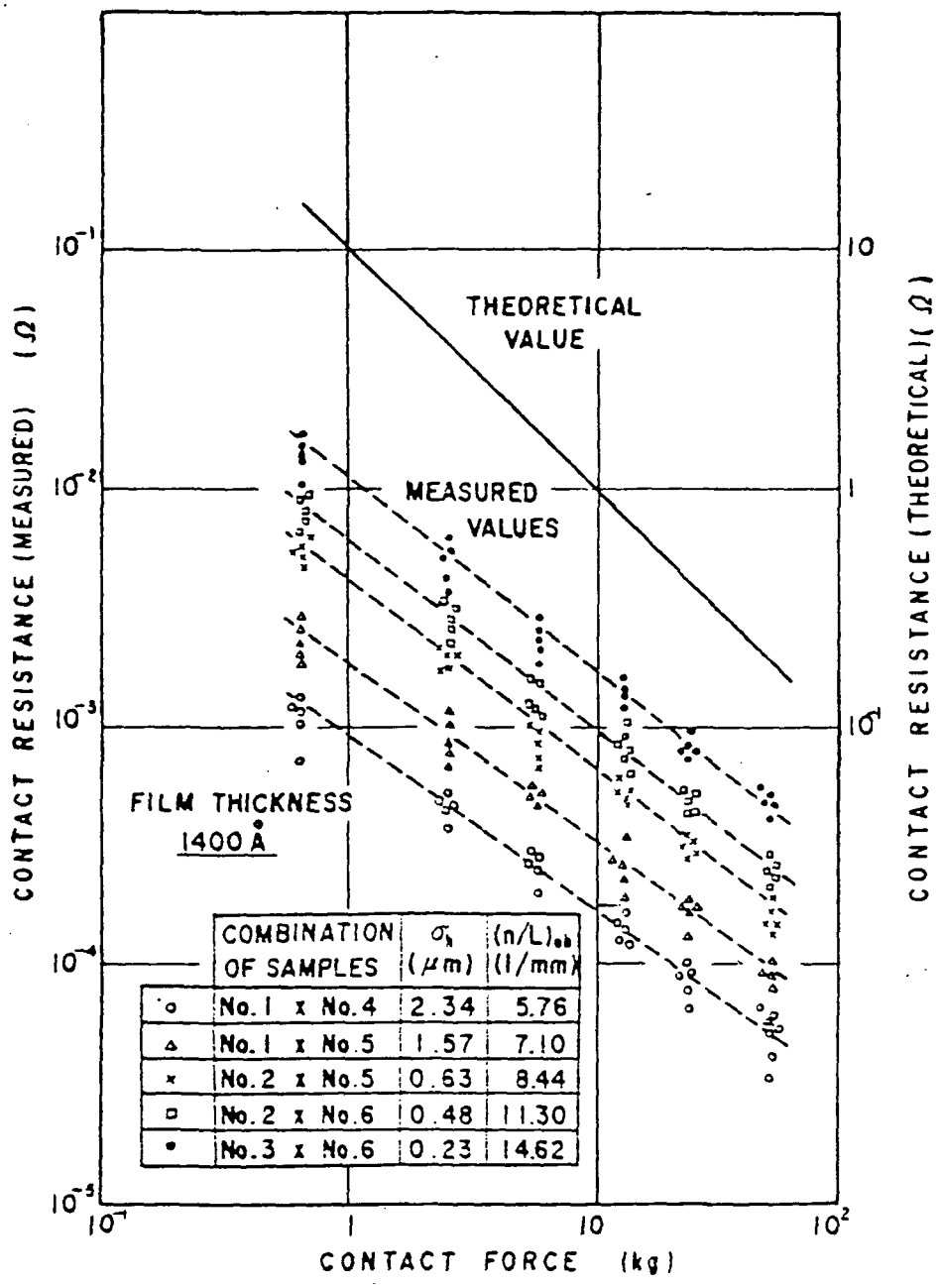

Fig. 2-10. Variation of contact resistance vs load for various surface roughnesses. (ref. 21).

Consider the situation shown in Fig. 2-11, a metal-insulator-metal contact. The Fermi levels on each side of the insulating layer line up, with a potential barrier in between. The barrier is due to the presence of the work function, ϕ, of the metal surface. Results from Simmons (22,23) make it possible to calculate tunnel and thermionic current densities as a function of voltage for any film thickness and barrier height. Results from Stepke (24) are shown in Figs. 2-12 and 2-13 for tunneling and thermionic mechanisms. It is possible to determine the dominant conduction mechanism from the resistance vs voltage curve. For Cu oxide films (50 A thick) at room temperature, tunneling dominates, while for thicker sulfide films (75 - 100 A thick) thermionic conduction dominates. The general trend of the experiment is predicted by theory.

Other methods for determining the dominant conduction mechanism include observing the temperature dependence of tarnished Ag contacts (25) and current-voltage curves as a function of temperature (26). One drawback to these experiments is the contact geometry (crossed wires or sharpened metal points) and load (tens of grams) do not reproduce technical environments very well. While these experiments are interesting from a physics point of view,

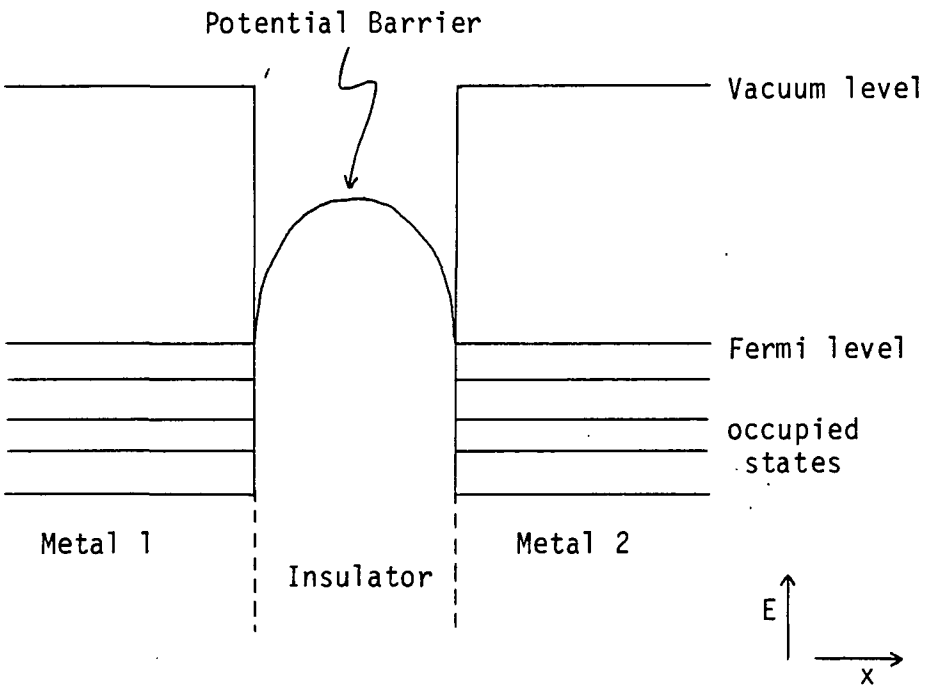

Fig. 2-11. Schematic representation of two metals in contact, separated by a thin insulating layer. A barrier exists due to the work function of each metal.

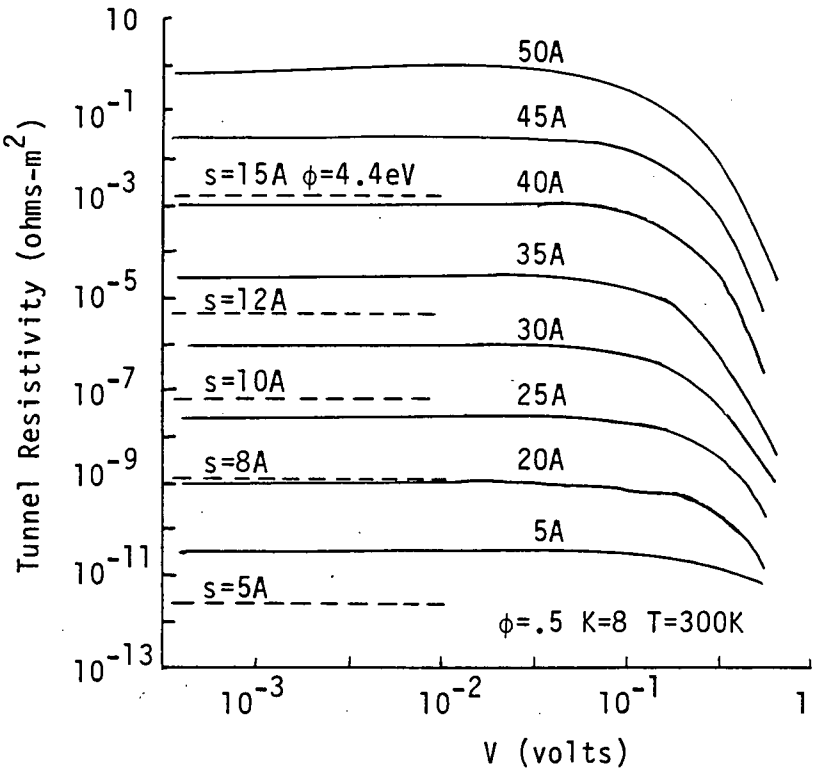

Fig. 2-12. Tunnel resistivity vs voltage for differing film thicknesses. —— Simmon's eqns. - - - Holm's eqns. (ref. 24).

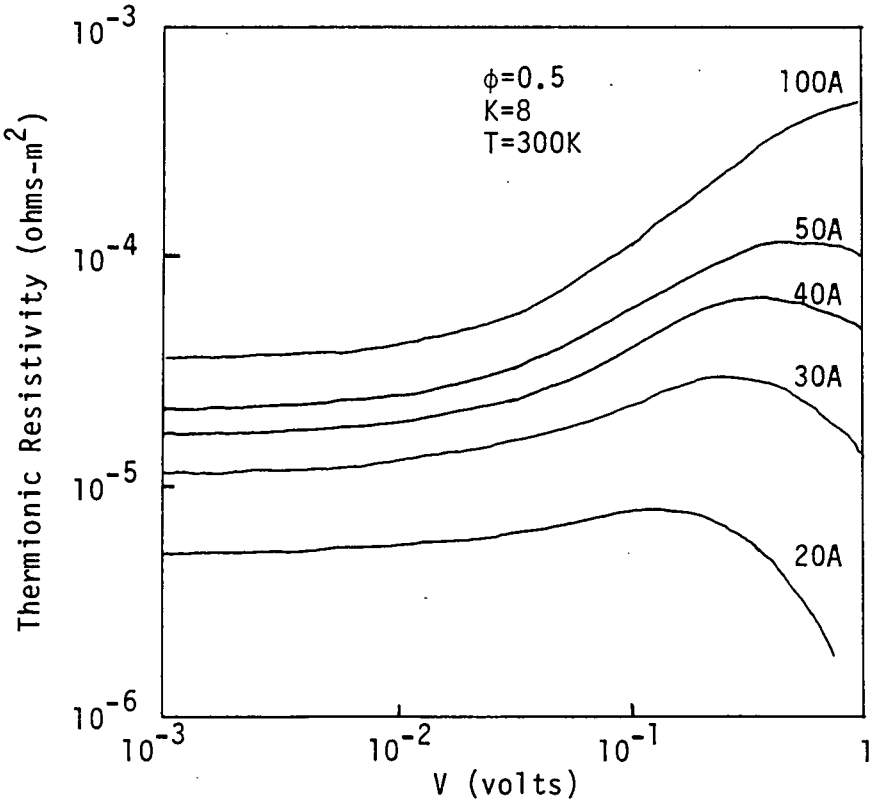

Fig. 2-13. Thermionic resistivity vs voltage for differing film thicknesses. (ref. 24).

it is unclear if film conduction plays an important role outside of these conditions.

2.4 LOW TEMPERATURE EFFECTS

The study of thermal and electrical contact resistance is important to a number of low temperature technologies. Examples include; space cryogenics, superconducting magnet systems and low temperature refrigeration systems. Space cryogenics is primarily interested in high thermal conductance joints independent of electrical conductance. Superconducting magnet designs need high electrical contact conductance to minimize current losses and high thermal contact conductance to ensure adequate magnet stability. Low temperature refrigeration systems often require mechanical joints, where the need for high thermal contact conductance (for T < 1K) is especially critical.

2.4.1 ELECTRICAL CONTACT

Figure 2-14 is a summary of low temperature electrical contact resistance versus pressure (27). There is considerable scatter in the data, ranging over 5 orders of magnitude. Also, oxidized contacts have a significantly higher resistance than un-oxidized contacts. The dashed line is a plot of

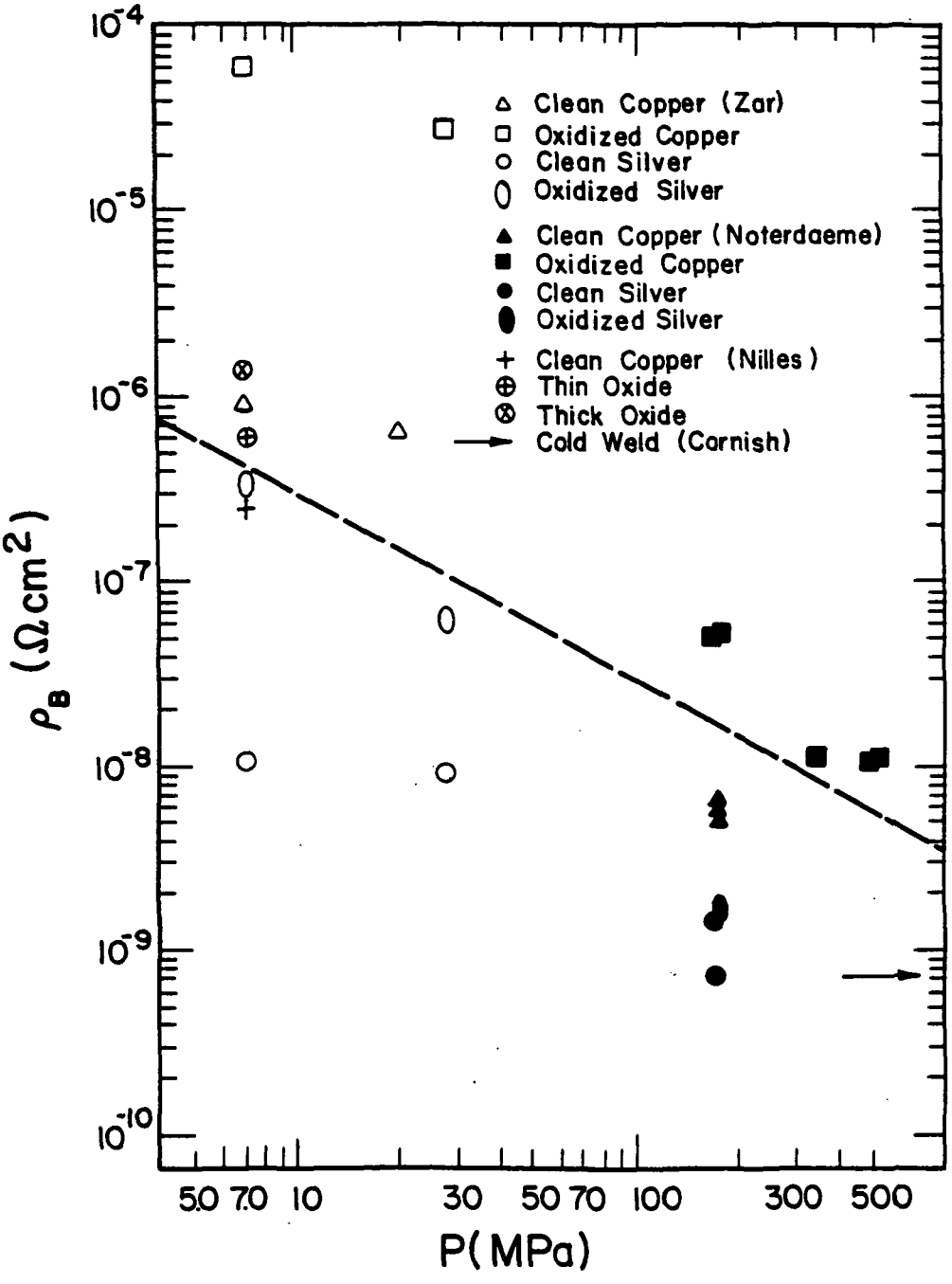

Fig. 2-14. Summary of low temperature electrical contact resistance data. ---- p = 3/P (ref. 27).

$$\rho_c = 3/P \qquad (2.19)$$

with ρ_c given in ohm-cm^2 and P is in Pa.

The temperature dependence has received little attention. Kawashima and Hoh (28) reported Cu contact resistances up to a factor of 100X greater at 77K than at room temperature. Tamai and Kawashima (26) also reported an increase in contact resistance with decreasing temperature. These results are very surprising since from eqn. (2.5), R_c should follow the bulk resistivity behavior. They conclude that thermal contraction reduces the contact area, competing with the reduction in resistivity as the temperature decreases. This effect is seen in Fig. 2-15. Tamai has extended this work (29) and included results for Au plated contacts and Nb contacts. For loads > 200g, his model predicts no effect, due to the relative size of the contact area. The contact geometry in these cases is crossed wires at low loads. Typical contact resistances are of the order of 1 ohm.

Holm and Meissner (2, sec. 26) attempted to measure a transition resistance, caused by the physical boundary between the two contact faces, as opposed to the constriction resistance. The constriction resistance was minimized by cooling the sample to 4K. A temperature independent resistance remained, which could be reduced by

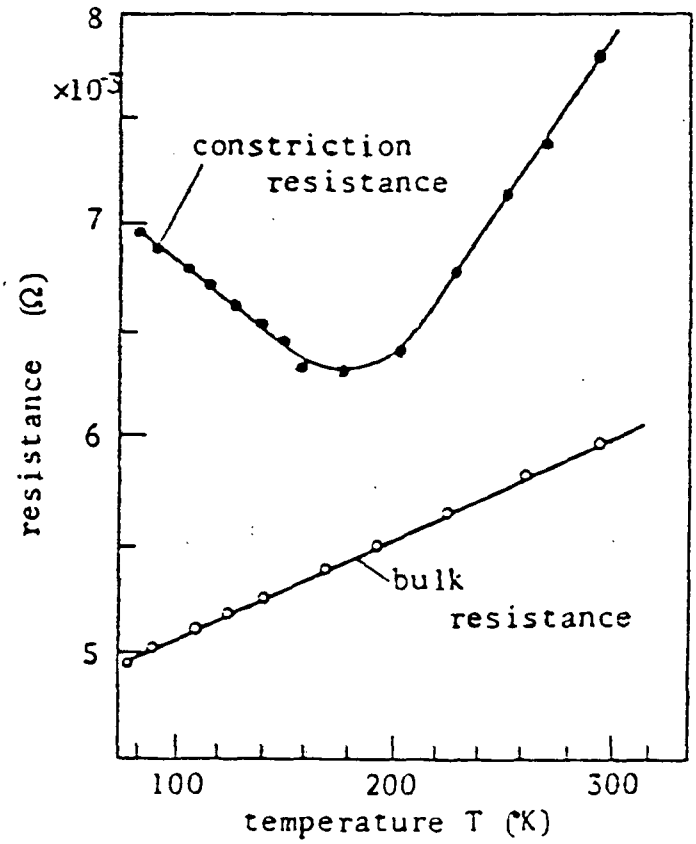

Fig. 2-15. Electrical contact resistance vs temperature for crossed rods at low loads. (ref. 26).

heating the contact to a high temperature in a vacuum. This feature was interpreted as a tunnel effect through thin adsorbed gas layers on the contact surface.

2.4.2 THERMAL CONTACT

Figure 2-16 shows in graphical form some low temperature thermal contact conductance data for metals as a function of temperature (27). As for electrical contact resistance, there is a large scatter in the data, over 5 orders of magnitude. Another comment is the low temperature ($T < 4K$) functional dependence follows a power law of the form

$$K_c = a T^n \qquad (2.20)$$

where a is a constant, K_c is the thermal contact conductance, T is temperature and $0.5 \leq n \leq 2.5$. Some data, curves 10-13, are for soldered contacts, while others, curves 14-16, are for joints with a soft metal foil inserted in between the contact faces. This temperature dependence contrasts with the linear behavior of bulk metal thermal conductivity.

More recent and extensive work by Salerno et. al. (34-36) for pressed-contacts in a variety of metals has been reported as a function of roughness and load. No systematic behavior for roughness can be seen, except for

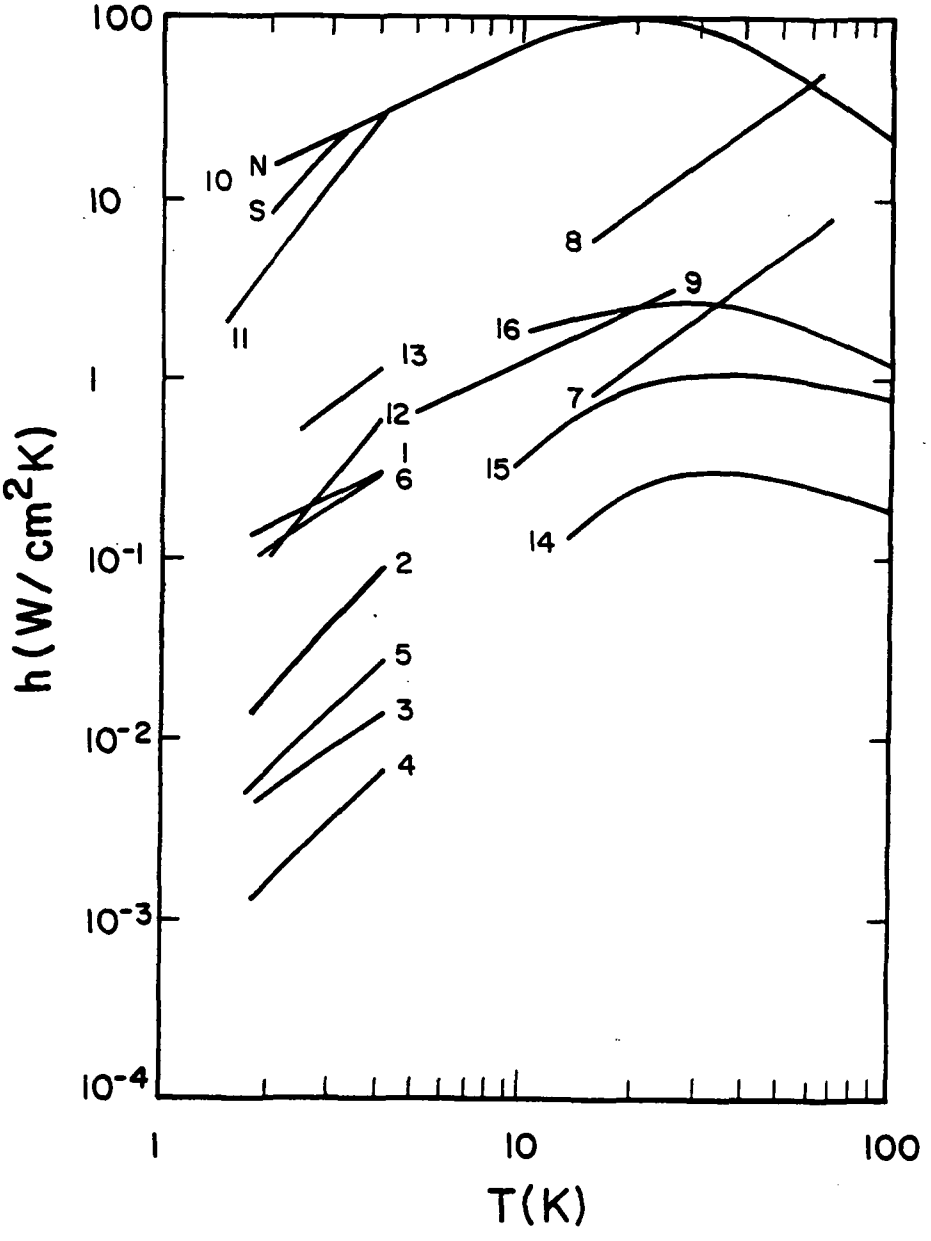

Fig. 2-16. Summary of low temperature thermal contact conductance vs temperature. See text for details.

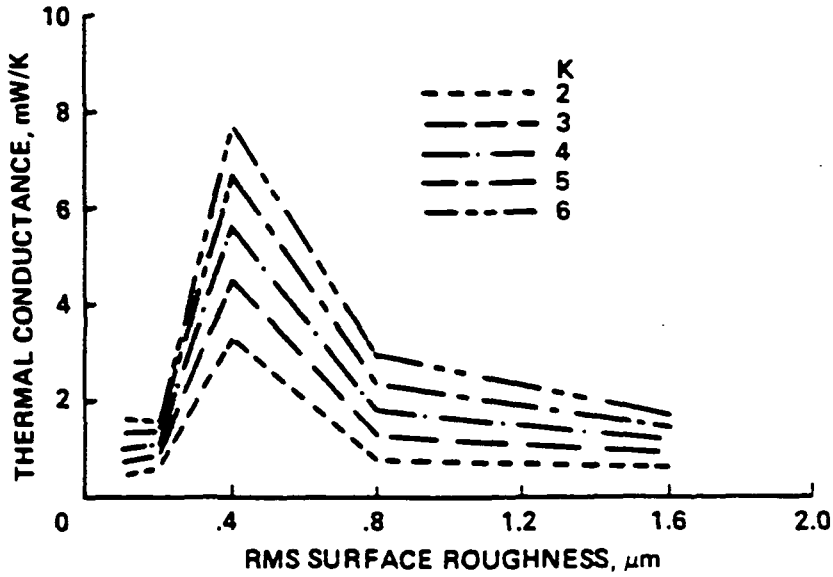

a)

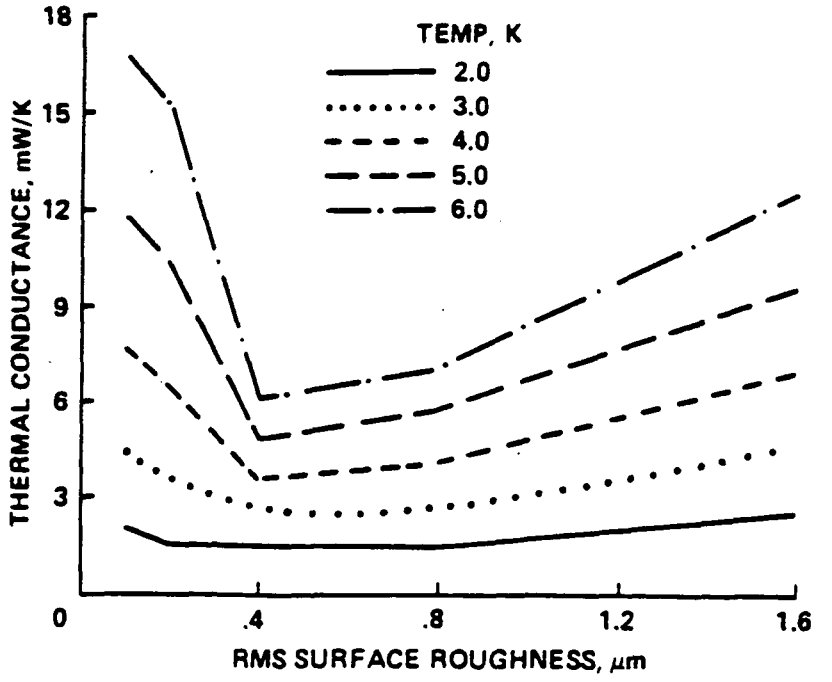

b)

Fig. 2-17. Thermal contact conductance vs roughness for a) stainlness steel and b) Al. (ref. 36).

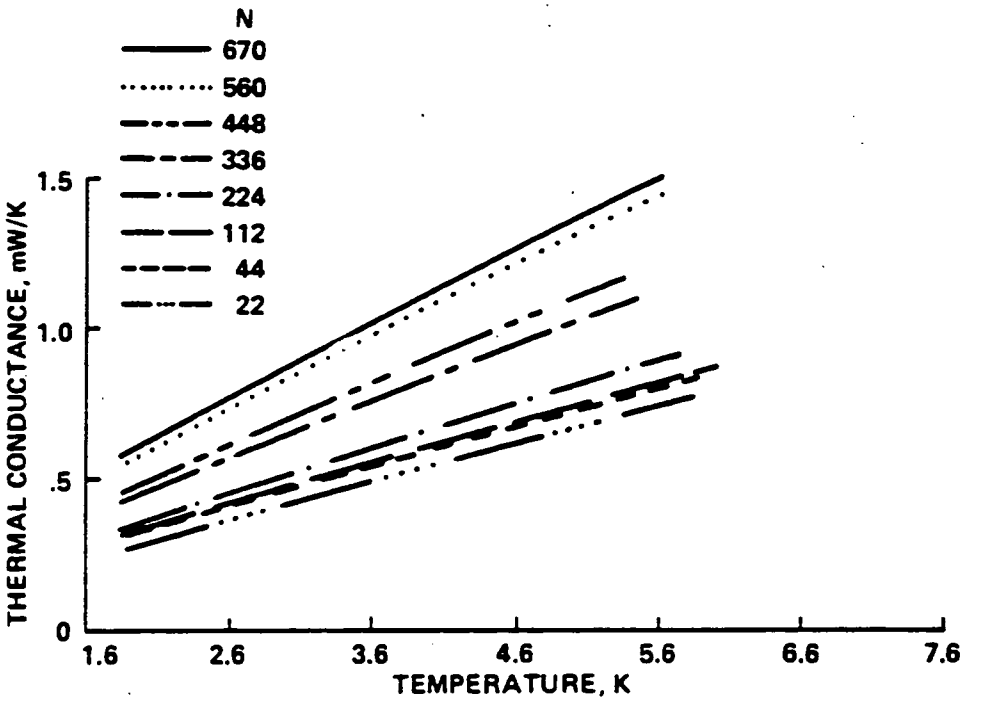

a)

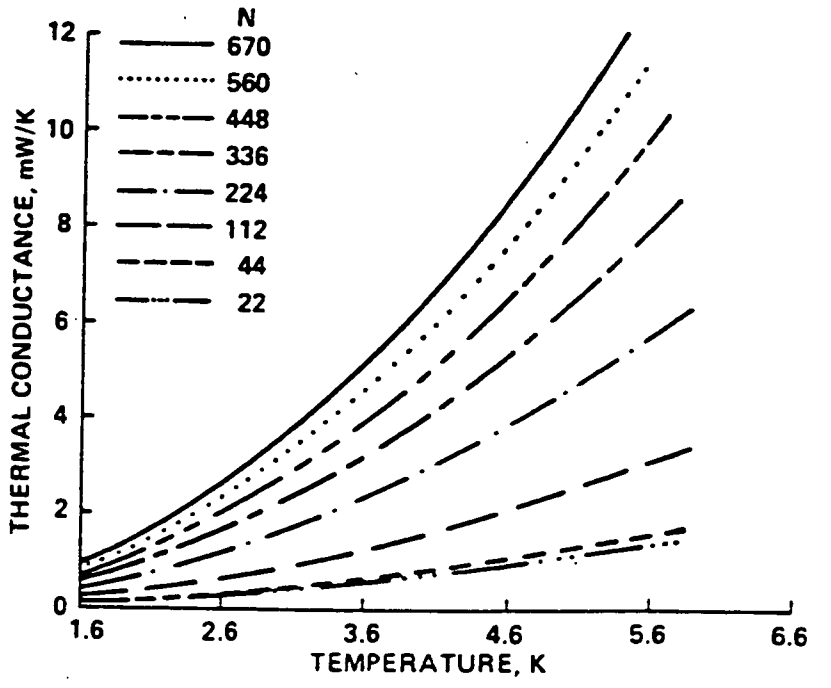

b)

Fig. 2-18. Thermal contact conductance vs temperature at different loads for a) stainless steel and b) Al. (ref. 36).

an anamoly at 0.4um roughness, Fig. 2-17. The thermal contact conductance follows a power law dependence, with the exponent ranging from 0.5 to 2.25. Conductance increases asymptotically with load, Fig. 2-18.

Berman (37,38) reported deviations from the Wiedemann-Franz-Lorenz (WFL) law, which states the ratio of the thermal conductivity to the electrical conductivity is proportional to temperature. He suggests that heat is flowing through electrically insulating regions of the contact.

2.5 SUMMARY

The preceding survey reveals several general characteristics about contact conductance. These are summarized below.

1) The general features of the load dependence are understood. Reasonable success in predicting contact conductance is possible only if detailed surface topography is known. Contact formation can then be treated in a statistical manner to estimate the actual contact area.

2) The presence of surface films introduces additional complexities. Mechanical behavior of the film will affect the area in metallic contact. Films also

affect electronic conduction by tunneling, semiconduction and thermionic mechanisms.

3) At low temperatures, the power law dependence of thermal contact conductance and the departure from the bulk WFL relation have been reported. A significant drawback in previous work is the lack of electrical and thermal contact conductance studies done on the same contact. The geometry employed for many electrical contact resistance studies are not typical for low temperature applications, i.e. crossed wires vs bolted joints.

CHAPTER 2 -- REFERENCES

1. J.C. Maxwell, A Treatise on Electricity and Magnetism, Dover (1891).

2. R. Holm, Electric Contacts, 4th ed., Springer-Verleg, New York (1967).

3. Y.V. Sharvin, Zh. Exsp. Teor. Fiz. 48, 984 (1965).

4. G. Wexler, Proc. Phys. Soc. 89, 927 (1966).

5. W.R. Smythe, J. Appl. Phys. 22, 1499 (1951).

6. J.C. Cooke, Quart. J. Mech. and Appl. Math. 16, 193 (1963).

7. M.M. Yovanovich, AIAA paper no. 71-80, 9th Aerosp. Sci. Meet., New York (1971).

8. T.N. Veziroglu and S. Chandra, Prog. Astro. and Aero. 21, 59 (1969).

9. R. Holm, Wiss. Veroff Siemens-Werken 7, 231 (1929).

10. J.A. Greenwood, Brit. J. Appl. Phys. 17, 1621 (1966).

11. J.F. Archard, Proc. Roy. Soc. A 243, 190 (1957).

12. J.A. Greenwood and J.B.P. Williamson, Proc. Roy. Soc. London 295, 300 (1966).

13. B.B. Mikic, Int. J. Heat Mass Transfer 17, 205 (1974).

14. T.N. Veziroglu, AIAA paper no. 67-317, AIAA Thermophysics Specialist Conf., New Orleans (1967).

15. C.L. Tien, Proc. 7th Thermal Cond. Conf., 775 (1968).

16. T.R. Thomas and S.D. Probert, ASME paper no 71-HT-AA.

17. M.G. Cooper, B.B. Mikic and M.M. Yovanovich, Int. J. Heat Mass Transfer 12, 279 (1969).

18. R.E. Cuthrell and E.W. Tripping, J. Appl. Phys. 44, 4360 (1973).

19. R.S. Tismit, Electrical Contacts, 79 (1979).

20. T. Hisakado, Wear 44, 345 (1977).

21. S. Harada and K. Mano, Electrical Contacts, 45 (1968).

22. J.G. Simmons, J. Appl. Phys. 8, 2472 (1964).

23. J.G. Simmons, J. Appl. Phys. 9, 2655 (1964).

24. E.T. Stepke, Electrical Contacts, 125 (1967).

25. J.H. Tripp, R.F. Snowball and J.B.P. Williamson, J. Appl. Phys. 38, 2439 (1967).

26. T. Tamai and K. Tsuchiya, Electrical Contacts, 151 (1977).

27. S.W. Van Sciver, M.J. Nilles and J. Pfotenhauer, Space Cryogenics Conf., 36, Berlin (1984).

28. A. Kawashima and S. Hoh, Cryogenics 14, 381 (1974).

29. T. Tamai, Electrical Contacts, 163 (1985).

30. J.M. Noterdame, D.B. Montgomery and L.M. Lindsky, Proc. 8th Symp. Eng. Problems of Fus. Res., 1797 (1979).

31. J.J. Winter, J.T. Breslin and G.K. Gaule, J. Appl. Phys. 43, 1226 (1972).

32. D.N. Cornish, D.W. Deis and J.P. Zbasnik, Proc. 7th Symp. Eng. Problems of Fus. Res., 1266 (1977).

33. K.T. Hartwig and S.W. Van Sciver, Proc. 8th Symp. Eng. Problems of Fus. Res., 1794 (1977).

34. L.J. Salerno, P. Kittel and A.L. Spivak, AIAA Journal, 22, 1810 (1984).

35. L.J. Salerno, P. Kittel and A.L. Spivak, 18th Int'l Thermal Cond. Conf., 184 (1984).

36. L.J. Salerno, P. Kittel, F.E. Scherkenbach and A.L. Spivak, 19th Int'l Thermal Cond. Conf., pre-print (1985).

CHAPTER 3 -- EXPERIMENTAL PROCEDURES

3.0 INTRODUCTION

The procedures and techniques employed in this study are described in detail in the present chapter. Emphasis is placed on the thermal conductivity measurement, due to the larger number of factors affecting the results. The first section focuses on some important instrumentation and the remaining sections detail techniques.

3.1 INSTRUMENTATION

3.1.1 CONTINOUS FLOW CRYOSTAT

A continous flow cryostat (1) provides the platform on which the temperature can be varied continously from 4K to 295K, Fig. 3-1. A flow of liquid helium is maintained during an experimental run, the flow rate manually adjusted by 1) a needle valve in the storage dewar and 2) a thermal impedance phase separator at the cryostat head. Typically, thermal stability achieved manually is within $\pm$0.1K. A 40 ohm heater, wound around the cold finger is used to regulate the temperature above 4K. Two Cu radiation shields surround the experimental enclosure to intercept room temperature thermal radiation and the whole assembly is evacuated to $< 10^{-5}$ torr to eliminate gas conduction heat leaks.

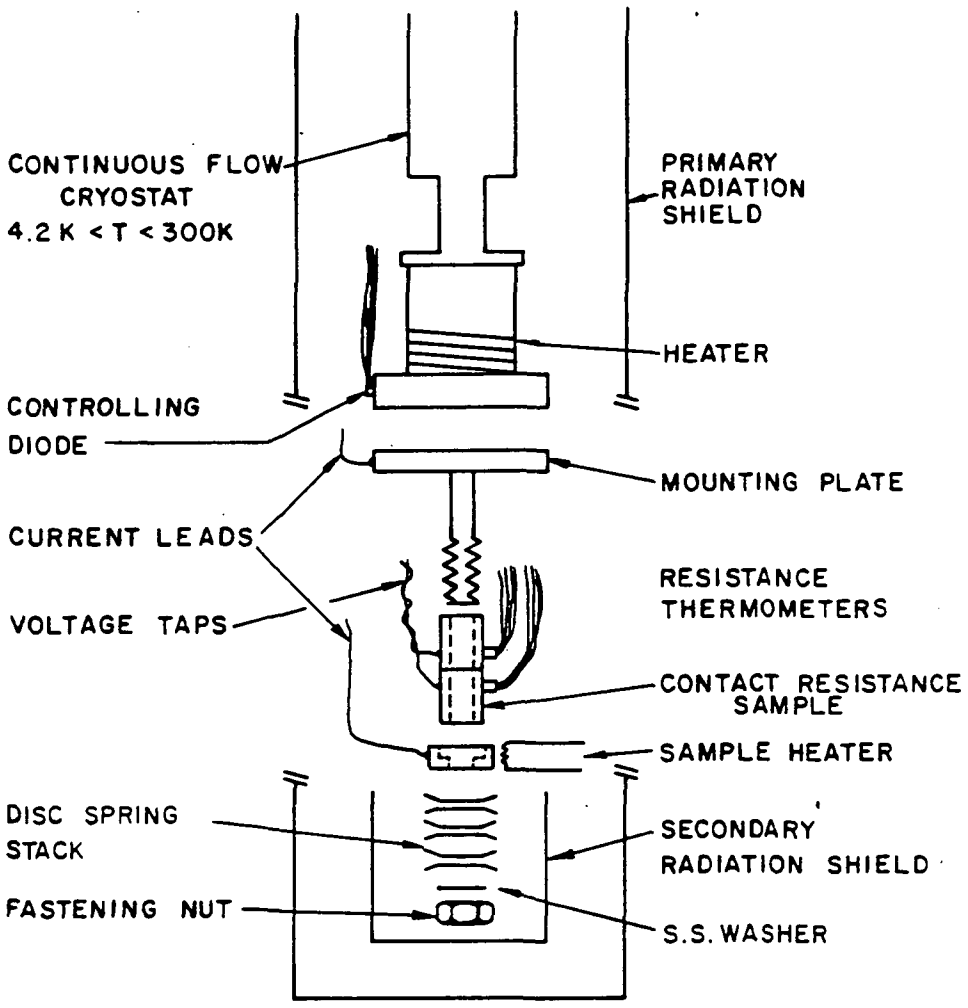

Fig. 3-1. Schematic of continous flow cryostat and sample arrangement.

3.1.2 TEMPERATURE CONTROLLER

Temperature stability achieved manually is inadequate for the thermal conductance measurements. An automatic temperature controller (2) which has the potential for $\pm$0.5 mK stability is required to achieve the desired temperature regulation. In practice, for T > 5K stability is within $\pm$1mK and for T $\leq$5K it is within $\pm$2mK, adequate for our purposes. The controller accepts a voltage input from a DT-500 series diode and compares it to an internal set point voltage. The voltage difference is processed to drive an external heater. An adequate thermal mass must be present at the cold tip, otherwise due to the high thermal diffusivity of metals for temperatures less than 30K, large temperature oscillations can occur due to the limited time response of the controller electronics. Care must also be taken with sensor placement and heat sinking of the experiment at the cold tip. Failure to do so can also result in temperature instabilities.

3.1.3 POTENTIOMETRIC CONDUCTANCE BRIDGE

Temperature sensors are read using a model PCB potentiometric conductance bridge from BTI Inc. (3). Instrument excitation is a 27.5 Hz square wave with a constant 300 uV rms voltage. The ac technique eliminates problems due to thermoelectric emfs and temperature

dependent contact resistances. Four output filters with time constants of 0.3, 1.0, 3.0 and 10.0 s help to average jitter at the display level. Constant voltage excitation is advantageous because sensor heating decreases as its resistance increases, while heating increases with constant current excitation. Self-heating can cause errors at low temperatures, due to inadequate heat transfer through the sensor package and resistance increase with decreasing temperature for germanium sensors. Nominal accuracy of the bridge is 0.1% after warmup.

3.1.4 NANOVOLTMETER

The material in this study, OFHC Cu, has a low resistivity, especially at low temperatures (the RRR = 110). For a current low enough, so that self-heating is negligible, the total voltage drop across the specimen is around 10 uV at 295K. Digital voltmeters are available with 1 uV resolution, however, time response is slow and thermal emfs complicate measurements. A Keithly model 147 nanovoltmeter does not have these problems (4). This is a null detector, hence thermal emfs can be zeroed out before measurement. Instrument response time is reasonable (about 2s) so zero point drift is not a

problem. Typical voltage levels encountered are 300 nV at 4K and 7 uV at 295K. Accuracy is $\pm$2% of full scale.

3.1.5 AUGER ELECTRON SPECTROSCOPY (AES)

AES is a surface sensitive technique used to identify the atomic composition of films existing on the contact surface. The Materials Science Center operates a PHI 548 Auger electron spectrometer. The system employs a double pass cylindrical mirror analyzer allowing analysis of either Auger or photoemitted electrons. The excitation source for the AES is a 0-5 kev, 0-40 uA electron gun producing 100 um diameter electron beam. It is also equipped with an Al or Mg x-ray source and suitable electronics for electron spectroscopy for chemical analysis (ESCA).

All surface analysis is done in a high vacuum. The system routinely operates at 10^{-9} torr using sorption and ion pumps. Sputtering can be done to determine film thickness. Auger spectra are collected with a primary electron beam energy of 3 kev and a current of 40 uA.

3.1.6 SCANNING ELECTRON MICROSCOPY (SEM)

The SEM in the Materials Science Center is a JSM 35-C. The SEM provides excellent contrast and improved depth of field over an optical microscope. Surface features

down to 1000 Å can be resolved. The system operates in a moderate vacuum of 10^{-6} torr with a primary electron beam energy of 25 kev.

3.2 SAMPLE FABRICATION

3.2.1 INITIAL PREPARATION

The sample geometry is a thick-walled tube of OFHC Cu. The nominal cross-section as specified by the supplier (5) is .1002 cm^2. Subsequent measurements performed by measuring the mass of water displaced from a volumetric flask and length measurements of the sample resulted in a calculated area of .09619$\pm$.00009 cm^2. Samples are cut from tubing to an overall length of about 3 cm, the ends faced off on a lathe and two grooves machined 1.6228$\pm$.0005 cm apart and .0025 cm deep. The grooves facilitate accurate placement of knife-edge clamps holding thermometers and voltage taps so as to maintain a constant separation from sample to sample, while the groove dimensions have negligible effect on bulk transport properties in that region. In an ultrasonic cleaner, specimens are cleaned in acetone, distilled H_2O and methanol and then annealed in a vacuum furnace for 2 h at 800C. The samples emerged bright and shiny from the furnace, so oxygen contamination is not a problem. They are stored in air at room temperature.

3.2.2 CONTACT SURFACE PREPARATION

The contact surface is subjected to various treatments in order to correlate their effects on the resulting measured contact resistance. These treatments are described in this section

A sample is sectioned approximately mid-way between the two grooves with a diamond saw. After ultrasonic cleaning in acetone, the contact faces are ground on silicon carbide paper. The paper grit is selected to provide the appropriate roughness. Each section is inserted into a grinding jig, which maintains the contact face perpendicular to the axis of the tubing. It is ground until the contact face is uniformly covered with grinding marks. The jig is rotated with respect to the grinding direction frequently, so as not to bevel the contact face. The section is removed and then cleaned in methanol. Length measurements before and after contact preparation determine the material lost during grinding. Loss is usually around 1.5%. Surface roughness is measured with a Tencor Alpha-step 200 profilometer (6). Output from the device includes: rms roughness and a profile of the surface topography, Fig. 3-2. Several traces are taken and the roughness is averaged over all traces.

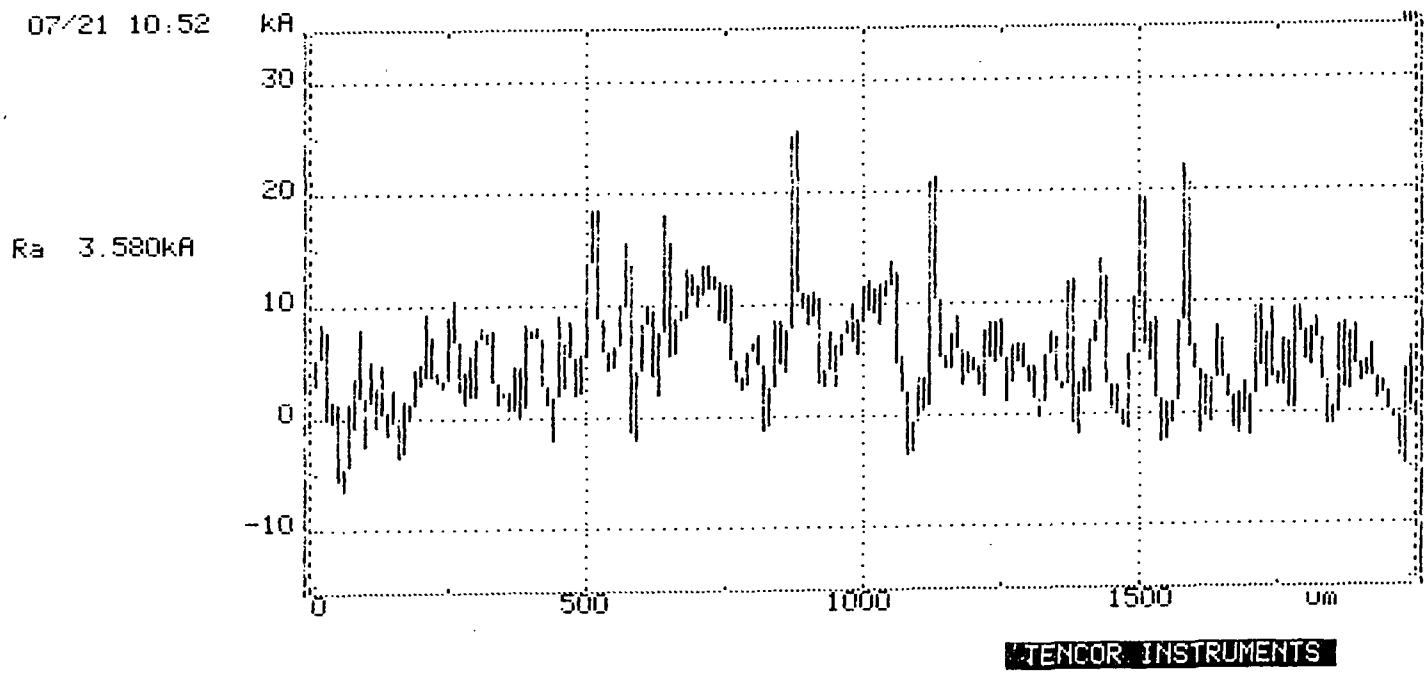

Fig. 3-2. Tencor profilometer output. Ra is the rms average surface roughness. 1kA = 0.1um

If desired, contacts are oxidized. Each section is placed in a jig, a piece of Cu sheet that holds each section upright in a quartz tube furnace. The furnace temperature is set to 200C and is open at both sides to laboratory air. The sample is inserted to the mid-point of the furnace and oxidizes for the desired length of time, usually 15 or 30min. The sample is removed from the furnace and allowed to air cool. At this particular temperature, the oxidized contacts have a shiny, uniform yellow color, looking remarkably like brass. It was in fact thought that the furnaces were contaminated, subsequent analytical work did not reveal the presence of either Sn or Zn on the oxidized contacts.

In one case, it was attempted to protect the contact faces from exposure to air. All assembly, i.e. grinding, cleaning, soldering and mounting onto the cold tip assembly took place under an inert N_2 atmosphere contained in a glove bag (7). A positive pressure of N_2 was maintained at all times, although no monitoring of O_2 partial pressure or of other contaminants was performed. Results to be discussed later, indicate at least partial success with this method.

Assembly of the contact section onto the mounting block takes approximately 40 minutes (2 h for the glove bag). A stainless steel threaded rod is wrapped with

teflon tape for thermal and elecrical insulation. It is this rod, which is silver brazed to the mounting block, that supports the load applied to the contact faces. The bottom contact section is soldered to the Cu block with Wood's metal (assumed composition is $Bi_{.48}$ $Cd_{.13}$ $Pb_{.26}$ $Sn_{.13}$), to ensure good heat sinking of the sample. The contact face is flooded with dry nitrogen to impede further oxidation during this operation. Knife-edge clamps holding thermometers and voltage taps are attached to each contact half. The heater cap is attached, the two sections mated together, on top of which is stacked Nomex paper (electrical insulation), a stainless steel washer, the spring stack and the nut and washer assembly. The spring stack is compressed by slowly turning the top nut until it abuts the spacer. Firmly grasping the knife-edge clamp on the top section prevents slipping of the contact section at this point. The assembly is then mounted to the cold finger of the continous flow cryostat.

3.3 LOAD APPLICATION

As discussed previously in chap. 2, the load dependence of contact resistance has received the most attention in previous studies, with

$$R_c = aL^{-0.85} \qquad (3.1)$$

where R_c is contact resistance, a is a constant and L is the applied load. The principal aim of this study is observing the temperature dependence of both thermal and electrical contact resistance, although the load must be approximately constant and be estimable for these results to be useful to the general community.

3.3.1 DISC SPRINGS

The above criteria are satisfied by Cu-Be disc springs (8). The springs have several advantages for low temperature work, including:

1) lack of a ductile-brittle transition between 4K and 295K
2) small size
3) force vs displacement curve that is digressive, i.e. $dF/dx < 0$
4) Young's modulus changes little with temperature (10%)

One disadvantage is a large spring constant. This can be offset by stacking springs in series so as to effectively reduce the total spring constant of the stack. Figures 3-3 and 3-4 show the force vs displacement data as supplied from the manufacturer and a set of springs stacked in series. The F vs x data were fitted to a

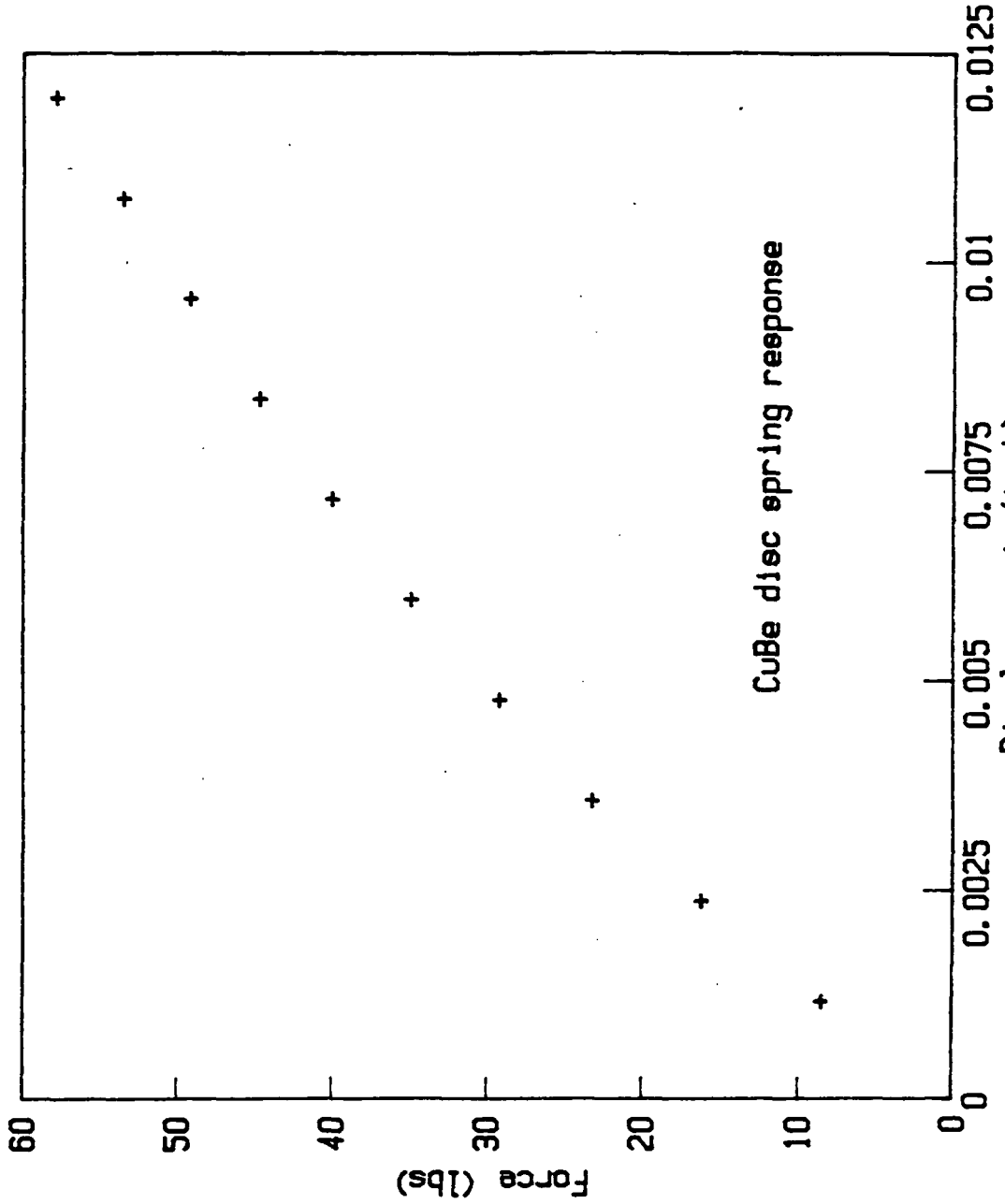

Fig. 3-3. Force vs displacement of CuBe disc springs.

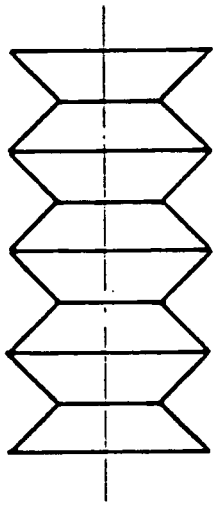

Cu-Be Disc Spring Stack

Fig. 3-4. Eight disc springs stacked in series to reduce the effective spring constant of the stack.

polynomial of order 3 with the coefficients as shown in Table 3-1 below.

Table 3-1: Fit coefficients; Be-Cu spring F vs x data

$$F = a_0 + a_1 x + a_2 x^2 + a_3 x^3 \qquad (3.2)$$

$a_0 = -.030763561$

$a_1 = 7562.12396$

$a_2 = -353170.823$

$a_3 = 10375748.2$

[F] = lb [x] = .001 inch

For this study, a stack of 7 springs is used. To ensure the same load from sample to sample, this spring stack must be compressed the same each time. A stainless steel guide, which fits inside the springs, of length 0.164" is used. A nut and washer assembly compresses the spring stack until it abuts the spacer. The intial stack height is .200" and from the resulting compression and using the above fit coefficients, a calculated load of 33 lb (137 N) is applied to the contact face.

3.3.2 THERMAL CONTRACTION

An estimate of the total differential thermal contraction is important to determine to what degree the load applied by the disc spring stack is constant. This

problem is helped somewhat by the digressive behavior of the F vs x curve of this particular type of disc spring. Because Cu contracts more than the stainless steel, differential thermal contraction acts to reduce the applied load. Figure 3-5 shows dimensions of the various components comprising the sample assembly.

Table 3-2: Integrated thermal contraction for relevant materials from 295K to 4K.

material	% contraction (9)
Be-Cu	.284
Cu	.294
301 stainless	.231

Carrying out the calculation shows 0.5% change in the disc spring stack compression upon cool down to 4K, which is small enough to be neglected.

3.4 THERMOMETRY

3.4.1 SENSOR SELECTION

Critically important to this study is the need for accurate and sensitive thermometry. A wide range of different sensors is available, including Si and GaAs diodes, carbon-glass, Ge and Pt resistance thermometers. In preliminary investigations, it was thought that carbon-glass sensors would provide the needed accuracy and

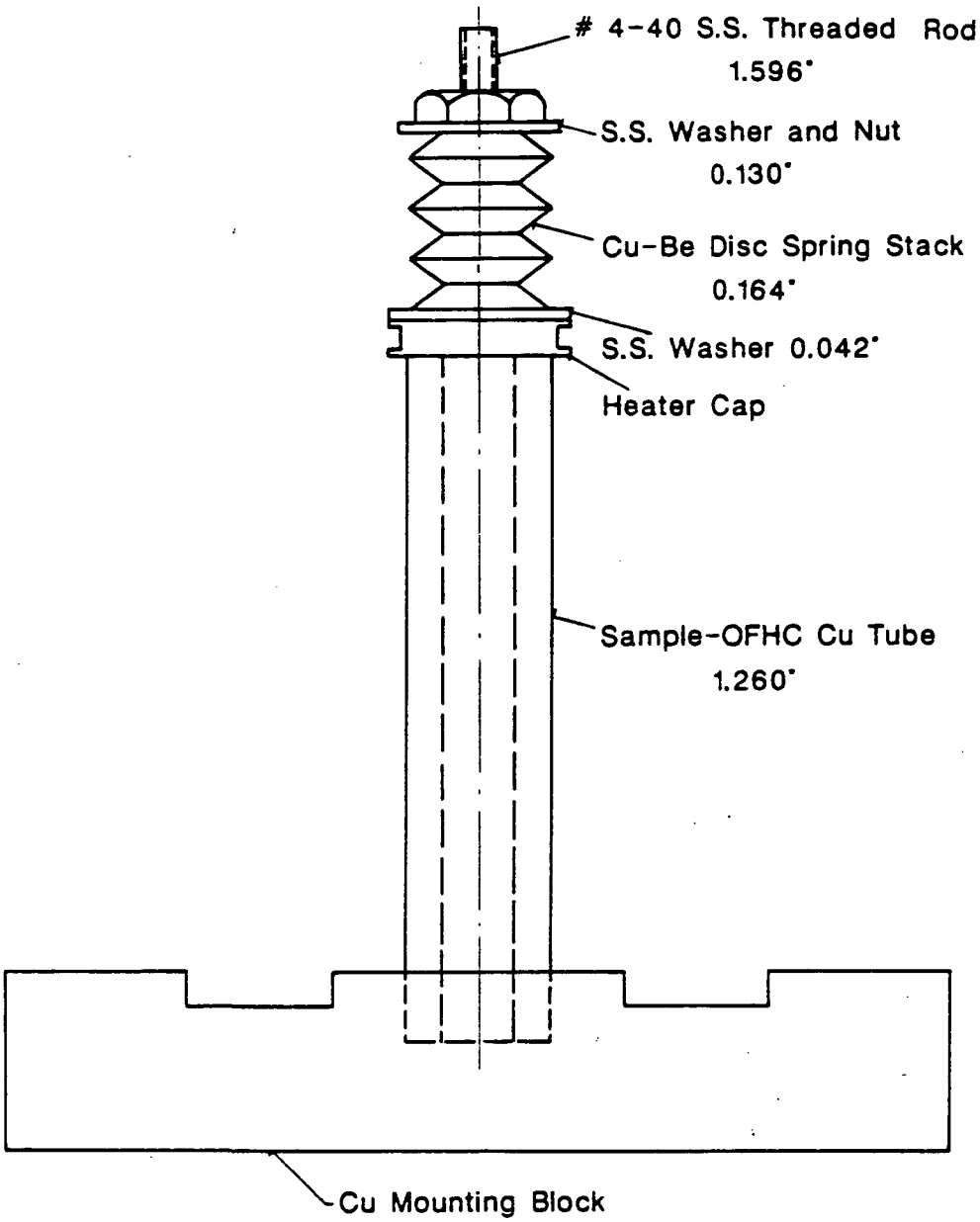

Fig. 3-5. Dimensions of sample assembly used in thermal contraction estimate.

sensitivity. Our work showed, however, there was a shift in calibration upon repeated thermal cycling and also the sensitivity above 100K was inadequate.

The only sensors adequate for our needs were a combination of Ge and Pt resistors. Diodes were ruled out, since their stability upon thermal cycling is questionable (within 50-100 mK), whereas Ge and Pt sensors have an excellent reputation for long term stability (10). Since the temperature is measured at two points along each sample, this necessitates a total of 4 thermometers, respectively labeled Ge-1, Pt-1, Ge-2 and Pt-2. Thermometer Pt-2 was calibrated by the manufacturer (11). Thermometers Ge-1 and Ge-2 were obtained from another vendor (12). Over the course of this study, two Ge thermometer elements shattered, and another had internal leads detach twice. This necessitated recalibrating the thermometer each time, with its ensuing inconvenience.

3.4.2 CALIBRATION

The Ge sensors were each calibrated individually against a Si diode, model DT-500 FP-HRC-7 which in turn was calibrated by the manufacturer (10). The diode was soldered to the knife-edge clamp near the Ge sensor with Wood's metal. Previous attempts to attach the diode with a mixture of silver paint and GE-7031 varnish resulted in

faulty calibrations, owing to poor thermal contact between the diode (which is potted in epoxy) and the clamp. The knife-edge clamps are designed to attach firmly in a groove on the sample and to provide adequate heat sinking for thermometers and sensor leads. Sensor bodies are cemented with silver paint into OFHC Cu tubes which had been silver brazed to the Be-Cu body of the knife-edge clamp, Fig. 3-6. The resulting data are then fit to a polynomial of the form

$$\ln (C) = a_0 + a_1 (\ln T) + \ldots + a_n (\ln T)^n \qquad (3.3)$$

where T = temperature and C = thermometer conductance in mmhos and n = 11 or 12, using a least squares method. In order to maintain accuracy, the data are broken into three temperature ranges as shown in the table below. The fit tolerance is within $\pm$10 mK, as shown in Fig. 3-7.

Table 3-3: Temperature regions for calibration fits

regime I	4K < T < 12K
regime II	12K < T < 20K
regime III	20K < T < 32K

Pt-1 is calibrated against Pt-2 in the configuration used when measuring the bulk thermal conductivity of the Cu tubing. There is a possibility for temperature gradients when calibrating in this manner, however, as

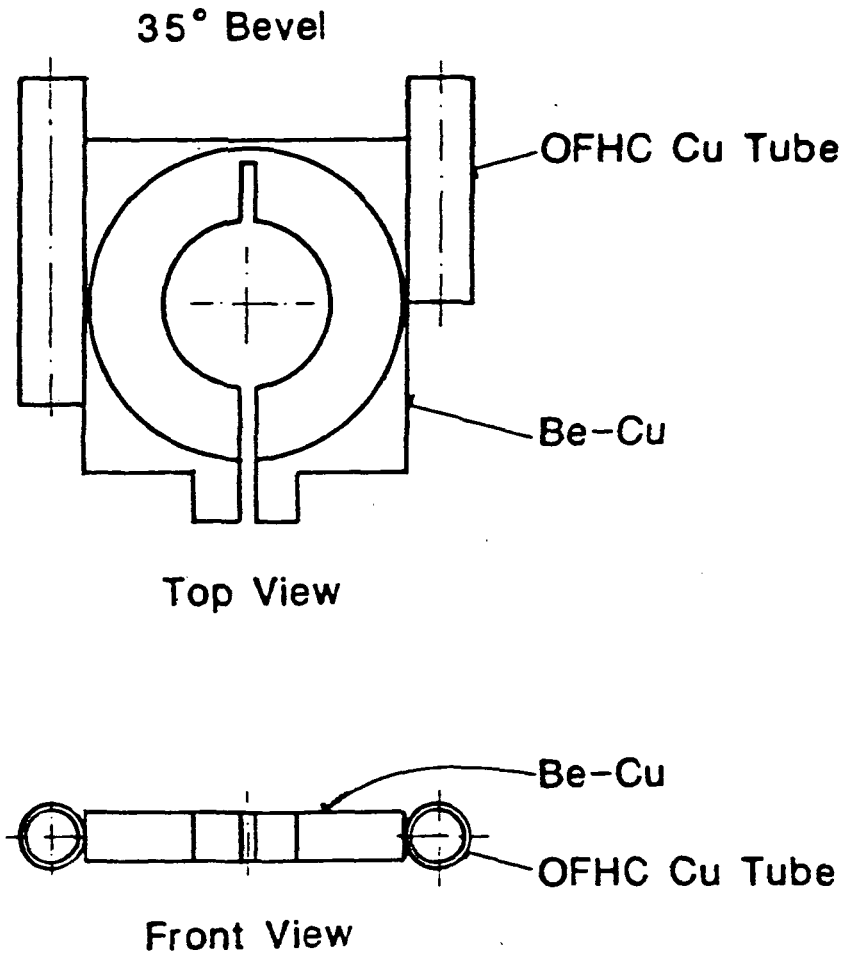

Fig. 3-6. Schematic of knife-edge clamps. Temperature sensors are glued into the OFHC Cu tubes.

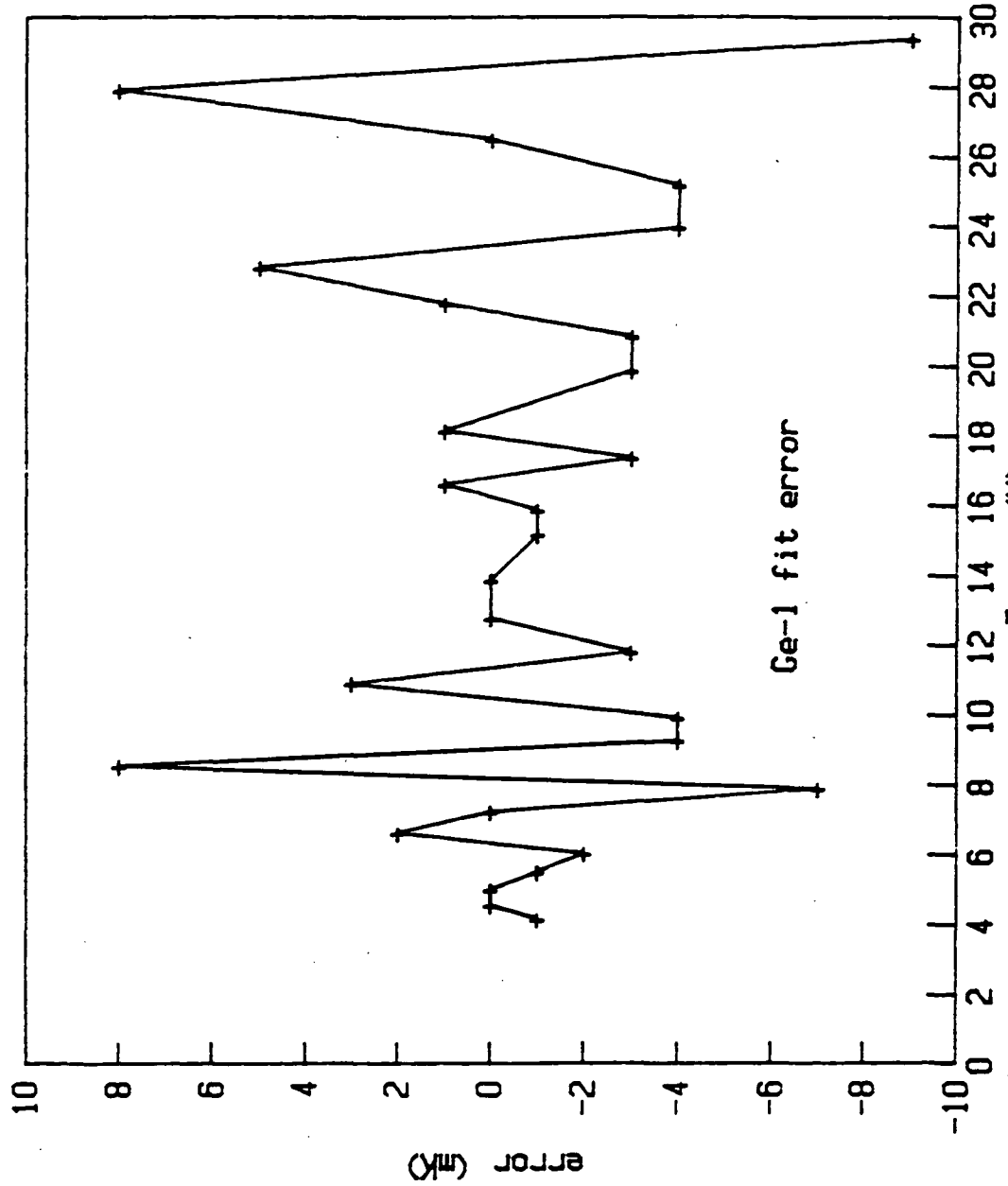

Fig. 3-7. Plot of fit error vs calculated temperature for thermometer Ge-1.

will be shown in a later section, results obtained for bulk thermal conductivity of Cu are in excellent agreement with published values. Therefore, if thermal gradients are present, they are small enough to be inconsequential. Also, the disagreement between Pt-2 and Ge-1 in regime III, where the calibrations overlap, is about 50mK, within the error bounds for calibration accuracy. The platinum thermometer calibration data are interpolated using a cubic spline.

3.5 EXPERIMENTAL METHODS

The contact resistance measurements performed in this work do not involve extrapolating voltage or temperature gradients to the contact face. Instead, having measured bulk thermal and electrical conductances of the sample material, the same measurement is repeated with a contact resistance specimen. This reduces instrumentation complexity and avoids uncertainties associated with extrapolation (13). The measured resistance is then corrected for the bulk contribution, with the remainder due solely to the presence of the contact.

We attempted to repeat subsequent measurements on contact resistance samples at the same temperature as the original bulk data. This provides a consistent set of

data and helps reduce interpolation errors of bulk data. Target temperatures are shown in Table 3-4.

Table 3-4: Target temperatures for data collection

Temperature	T Increment
$4K \leq T \leq 30K$	2K
$30K < T \leq 45K$	3K
$45K < T \leq 100K$	5K
$100K < T \leq 295K$	10K

3.5.1 ELECTRICAL CONTACT RESISTANCE

A 4-wire DC method is used for the electrical contact resistance measurement. At the desired temperature, the nanovoltmeter offset is zeroed, a current is passed through the sample and the resulting voltage drop is detected with the nanovoltmeter. The current level is varied so the voltage signal is easily resolved while ohmic heating in the sample is negligible, as determined by the thermometer response. Typical current density is $2.5\ A/cm^2$. The voltage drop across a 10 ohm, 100 watt power resistor is recorded to calculate the current in the sample. The data gathered consist of nanovoltmeter voltage, shunt voltage and thermometer conductance, either Ge-1 for $T < 30K$ or Pt-2 for $T \geq 30K$.

Automatic temperature control is employed for T < 70K for two reasons. The signal level is low, with temperature drift resulting in changing thermal emfs that are significant (at least 10% of signal level) and the drift rate is very high, around 1K/min. Above 70K, the helium flow is turned off and the sample is allowed to warm up. Owing to the low thermal diffusivity, dT/dt is about 10K/h, translating to a 30 mK temperature change during the measurement, which is acceptable. The signal level is larger, with the background offset essentially constant during the measurement.

The sample-mounting block assembly is electrically isolated from the cryostat by paper and teflon-tape wrapped brass screws, isolation is > 20Mohms. Nylon screws shear owing to their large thermal contraction upon cooldown. Electrical isolation is very important as electrical contact to the cryostat results in ground-loops to the nanovoltmeter, which produce large voltage offsets at the nanovoltmeter. A permanent (epoxy-coated block) is more desirable, however, it is necessary to remove the insulation for thermal conductance measurements, due to low heat transfer through the insulation. This allows the use of the same sample for both types of measurements and eliminates sample to sample variation in joint

conductance, between electrical and thermal experimental runs.

3.5.2 THERMAL CONTACT CONDUCTANCE

A steady-state longitudinal heat flux method is used for thermal contact conductance experiments. Target temperatures are the same as mentioned in the previous section. At the desired temperature, with the heater power off, the thermometer readings are recorded at equilibrium. The heater is turned on and after steady-state is reached, thermometer readings, along with heater voltage and heater current are recorded. A differential output on the back side of the PCB helps determine when steady-state is reached. This output (full scale = 10V, where full scale is 10% of PCB reading) is monitored with a strip chart recorder as a function of time. Constant output (flat line) indicates an steady-state condition. The heater power level is set to obtain a temperature difference across the sample of about 1% T, where T = (T1 + T2)/2. The point of keeping ΔT this small is to obtain a differential measurement of the thermal conductance. Some typical heater powers and ΔTs are shown below in Table 3-5 for bulk OFHC Cu.

Table 3-5: Thermal conductance heater powers

Q (mW)	T (K)	ΔT (K)
3.5	4.2	.034
117	20	.173
217	70	.348
285	100	1.073
301	200	1.276

The heater is manganin wire wound on a Cu cap that attaches snugly to the end of the sample and has a resistance of 44 ohms. Indium foil inserted under the cap prior to assembly improves thermal contact between the heater cap and the sample. The heater power is calculated from the heater voltage (4-wire measurement with a HP 3465A DMM) and the heater current (measured with a Keithly 197 microvolt DMM in the ammeter mode).

Sensors Ge-1 and Ge-2 are used for $T < 20K$, Pt-1 and Pt-2 for $T \geq 30K$ and both sets are averaged together for $20K < T < 30K$.

A possible source of error, given the experimental configuration, is the parallel heat leak through the disc spring stack and down the to heat sink through the stainless steel rod that supports the load. However, there are a total of 10 pressure contacts between the heater cap and the stainless support rod. An estimate of the heat leak along this path, shows it can be neglected.

Radiation losses were calculated from an equation which estimates the radiation loss between two concentric cylinders (14)

$$\dot{Q} = \frac{A_1 s \left(T_1^4 - T_2^4 \right)}{\frac{1}{e_1} + \frac{A_1}{A_2}\left[\frac{1}{e_2} - 1\right]} \qquad (3.4)$$

where Q is the radiation heat transfer, A is the surface area of the individual cylinder, T is temperature, e is emissivity, s is the Stefan-Boltzmann constant and the subscripts 1,2 refer to the inner and outer cylinders respectively. Because of the T^4 dependence, radiation losses, if significant, are usually only important above liquid nitrogen temperature. Table 3-6 shows some estimates of radiation losses calculated from eqn. (3.4), assuming a 5K temperature difference between the sample and the inner radiation shield.

Table 3-6: Radiation heat transfer estimate

T1	T2	$\dot{Q}$ (mW)
270	260	0.6
220	215	0.3
200	195	0.2
180	175	0.2
150	145	0.1
100	95	.04

Typical heater power for these temperatures is around 230 mW. Also, the assumed 5K temperature difference between the sample and inner radiation shield is likely to be an overestimate. The temperature drop across the sample is typically 1.2K. Radiation losses are a small enough fraction of the heater input (< .2%), so they can be neglected.

Results on the the thermal conductivity of bulk OFHC Cu, reported in a later section, agree very well with published values, indicating the validity of neglecting the various heat leaks. Therefore, no corrections need be applied to our experimental data.

One final point needs to be discussed, concerning the conductance bridges. The nominal accuracy is 0.1% of full scale. Near the low end of the range, this translates to 1% of the actual value. The electronics can drift somewhat and still be within the accuracy rating of the instrument. This results in offset errors between the two thermometers that change from day to day. This problem is best illustrated by an example. At 110K, Pt-1 has a conductance of 2.949 mmhos. The temperature resolution is .028K. If the two bridges drift in opposite directions by 1 digit, a change in offset of .056K results. Since the desired ΔT across the sample is about 1.0K, this drifting causes a 6% error in the measured thermal conductance. In

practice, this example is conservative. Offsets changing by a factor of 2 have been observed, and the actual ΔT is more likely to be .7% of T for T > 100K. This offset problem is eliminated by recording the ΔT before the heater is turned on and after. The measured ΔT is then corrected for the offset error.

3.6 DATA ANALYSIS

3.6.1 ELECTRICAL CONTACT RESISTANCE

Raw data from this experiment are in the form of conductance from one thermometer (Ge-1 or Pt-2) vs nanovoltmeter voltage and shunt resistor voltage. The conductance data are converted into temperature, either using a polynomial approximation for Ge-1 or a cubic spline interpolation for Pt-2. Resistance is calculated from

$$R = \frac{V_n}{V_s} \cdot R_s \qquad R_s = 9.906\,\Omega \tag{3.5}$$

where R is the total resistance, V_N is the nanovoltmeter voltage and V_s is the shunt resistor voltage.

These data, R vs T, are input to a data reduction program which for a given T, calculates the corresponding bulk resistance with a cubic spline interpolation of the bulk data, subtracts this value from the measured total resistance correcting for material loss and prints out the

remaining resistance. This remainder is due to the presence of the contact and is called the electrical contact resistace of the sample, R_c.

3.6.2 ERROR ANALYSIS -- ELECTRICAL RESISTANCE

The principal source of uncertainty is the 2% accuracy of the nanovoltmeter. The current passing through the sample is monitored with the shunt resistor. Resolution of the HP 3465A DMM is $\pm$0.1%. The shunt resistor value was measured to 9.906 $\pm$.005 ohms. This value is slightly dependent on the ambient temperature in the laboratory. The observed variation was less than 0.1%. In the following analysis, the uncertainties in shunt resistance and shunt voltage are neglected because their contribution to the overall uncertainty is an order of magnitude less than the contribution due to the nanovoltmeter. The emphasis is placed on the nanovoltmeter resolution and the relative sizes of the bulk resistance vs the contact resistance. From eqn (3.5), the uncertainty in the measured resistance R is

$$\delta R^2 = \left(\frac{V_n}{V_s}\right)^2 \delta R_s^2 + \left(\frac{R_s}{V_s}\right)^2 \delta V_N^2 + \left(\frac{V_N R_s}{V_s^2}\right)^2 \delta V_s^2 \qquad (3.6)$$

with the terms defined as above. The contributions of the first and last terms are ignored, as explained previously. Equation (3.6) can be simplified as

$$\delta R = \frac{R}{V_N} \cdot \delta V_N \qquad (3.7)$$

where δV_N is 2% of the full scale voltage range of the nanovoltmeter.

The electrical contact resistance, R_C, is the difference of the total resistance, R_T, and the bulk resistance, R_B. Thus,

$$\delta R_c^2 = \delta R_T^2 + \delta R_B^2 \qquad (3.8)$$

with the individual δR given by eqn. (3.7).

At this point, we note that the voltage levels encountered are very similar from one run to the next. This simplifies the error estimate by letting V_N be the same for both bulk and total resistance measurements. By factoring V_N out, the uncertainty in R_C becomes

$$\delta R_c = \frac{\delta V_N}{V_N}\left[R_T^2 + R_B^2 \right]^{1/2} \qquad (3.9)$$

3.6.3 THERMAL CONTACT CONDUCTANCE

Data are in the form of thermometer conductances, with and without heat flux, heater voltage and heater current. Heater power is calculated from the voltage-current product. Thermometer conductances are converted into temperatures as described in the section on electrical contact resistance. The temperature difference

ΔT is defined as (T1 - T2) where T1 is calculated from Ge-1 or Pt-1 and T2 is from Ge-2 or Pt-2. Sensors Ge-1 and Pt-1 are located closest to the heater cap, so $\Delta T \geq 0$. the measured temperature difference is corrected for offset and a thermal conductance is calculated from

$$K = \dot{Q} / \Delta T \qquad (3.10)$$

where K is the measured thermal conductance, $\dot{Q}$ is the heater power and ΔT is the corrected temperature difference.

These data, K vs T, are input to a data reduction program. A correction is applied to this data to account for the bulk contribution, interpolated from the bulk K vs T data, and the thermal contact conductance, K_c, is output.

3.6.4 ERROR ANALYSIS -- THERMAL CONDUCTANCE

The thermal contact conductance, K_c, uncertainty is primarily due to the PCB resolution. Heater power is determined through simultaneous measurement of current and voltage. The combined uncertainty of these measurements $\pm$0.1%. The PCB sensitivity results in a resolution of the temperature drop of 40mK at room temperature to 2mK at 4K. While nominal accuracy of the PCB is $\pm$0.1%, the resolution ranges from $\pm$.005% at the high end of the scale to $\pm$.05%

at the low end. When the temperature sensor conductance necessitates a change in scale, the uncertainty in the resulting temperature drop takes a corresponding jump. As one decreases the temperature, the K_c uncertainty decreases smoothly until a change in bridge scale is required. The uncertainty then jumps discontinously and then decreases as before.

The uncertainty in thermal conductance as determined from eqn. (3.8) is

$$\delta K^2 = \left[\frac{1}{\Delta T}\right]^2 \delta \dot{Q}^2 + \left[\frac{\dot{Q}}{\Delta T^2}\right]^2 \delta \Delta T^2 \qquad (3.11)$$

The first term is neglected as explained previously. This equation simplifies to

$$\delta K = \frac{K}{\Delta T}\, \delta \Delta T \qquad (3.12)$$

As in the case for R_c, K_c is the difference between the total thermal resistance and the bulk thermal resistance. We have

$$\frac{1}{K_c} = \frac{1}{K_T} - \frac{1}{K_B} \qquad (3.13)$$

The uncertainty in K_c can be put in the form (after some algebra),

$$\delta K_c = K_c^2\, \frac{\delta \Delta T}{\Delta T} \left[\frac{1}{K_T^2} + \frac{1}{K_B^2}\right]^{1/2} \qquad (3.14)$$

There are two terms which dominate the overall uncertainty. They are the PCB resolution and the ratio of K_c to K_T. At high temperatures, K_c is large compared to the bulk and ΔT is also large. At 290K, a typical uncertainty in K_c is $\pm 25\%$. At low temperatures, K_c is saml1 compared to K_T and ΔT is small, the typical uncertainty in K_c is about 3%.

3.6.5 COMMENT ON OVERALL UNCERTAINTY

If the contact resistance followed the bulk behavior, as might be expected from eqn (2.5), the uncertainty would be constant as a function of temperature. This is not the case. For example, electrical contact resistance changes only by a factor of about 2 for $4K \leq T \leq 273K$, while the bulk changes by a factor of 110. At room temperature, $\delta R_c/R_c$ is around $\pm 20\%$, due to a large bulk resistance and a small contact resistance. At 4K, the bulk resistance has decreased considerably and $\delta R_c/R_c$ is near $\pm 3\%$, basically limited by the nanovoltmeter resolution. This is also true of the K_c, i.e. low temperature contact conductances are more precise than the room temperature values. This aspect of the experiment is also reflected in the scatter of the data at higher temperatures.

CHAPTER 3 -- REFERENCES

1. Janis Research Co., Inc., 2 Jewel Drive, P.O. Box 696, Wilmington, MA 01887.

2. Model DTC-500SP, Lake Shore Cryotronics Inc., 64 E. Walnut St., Westerville, OH 43801.

3. BTI, Inc., 4174 Sorrento Valley Blvd., San Diego, CA 92121.

4. Keithly Instruments Inc., 28775 Aurora Rd., Cleveland, OH 44139.

5. Judson A. Smith Co., P.O. Box 563-T, Boyertown, PA 19512.

6. Tencor Instruments, 2400 Charleston Road, Mountain View CA 94043.

7. Instruments for Research and Industry, P.O. Box 159 P, Cheltanham, PA 19012.

8. Bauer Springs, Inc., 509 Parkway View Drive, Pittsburgh, PA 15205.

9. Handbook of Superconducting Machinery and Materials, Metals and Ceramics Information Center, Battelle Columbus Labs, 505 King Ave, Columbus, OH 43201.

10. L.G. Rubin, B.L. Brandt and H.H. Sample, Cryogenics 22, 491 (1982).

11. Lake Shore Cryotronics, Inc., 64 E. Walnut St., Westerville, OH 43081.

12. Cryo Cal, Inc., 2457 University Ave., St. Paul, MN 55114.

13. T.R. Thomas and S.D. Probert, Int. J. Heat Mass Transfer 13, 789 (1970).

14. J.R. Howell and R. Siegel, Thermal Radiation Heat Transfer, NASA SP-164, 1969.

CHAPTER 4 -- RESULTS AND DISCUSSION

4.0 INTRODUCTION

This chapter reports on measurements of electrical contact resistance and thermal contact conductance from $4K \leq T \leq 290K$ as a function of oxidation state and surface roughness. Oxidation ranges from "clean", i.e., contact face ground and assembled in air while attempting to minimize exposure time, to oxidation times at 200C of 15 min and 30 min. In addition, one sample was prepared in an inert N_2 atmosphere contained in a glove bag. Three surface finishes of 0.4um, 0.2um and 0.1um were prepared for each oxidation state. Finally, an In foil was inserted into a contact to observe the effect of soft metallic bonding materials on the overall contact resistance.

4.1 BULK OFHC Cu

Figures 4-1 and 4-2 show values for the electrical resistance and thermal conductance of an OFHC Cu sample, which is the basic material used to form contacts. There are several notable features present in these figures which are typical for pure metals. At low temperatures ($T < 20K$ for Fig. 4-1) the resistance is independent of temperature. Electron scattering is

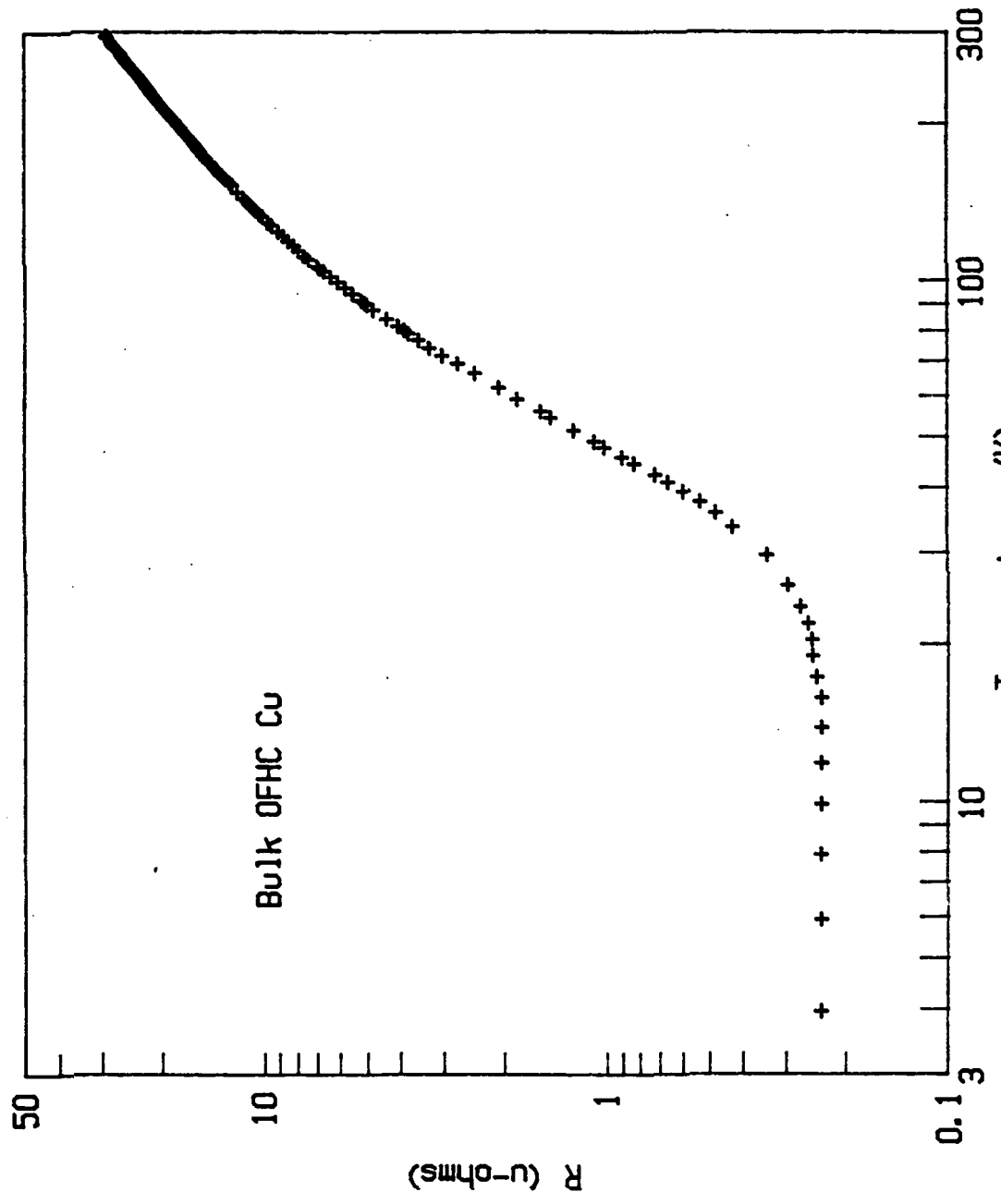

Fig. 4-1. Measured electrical resistance of bulk OFHC Cu vs temperature.

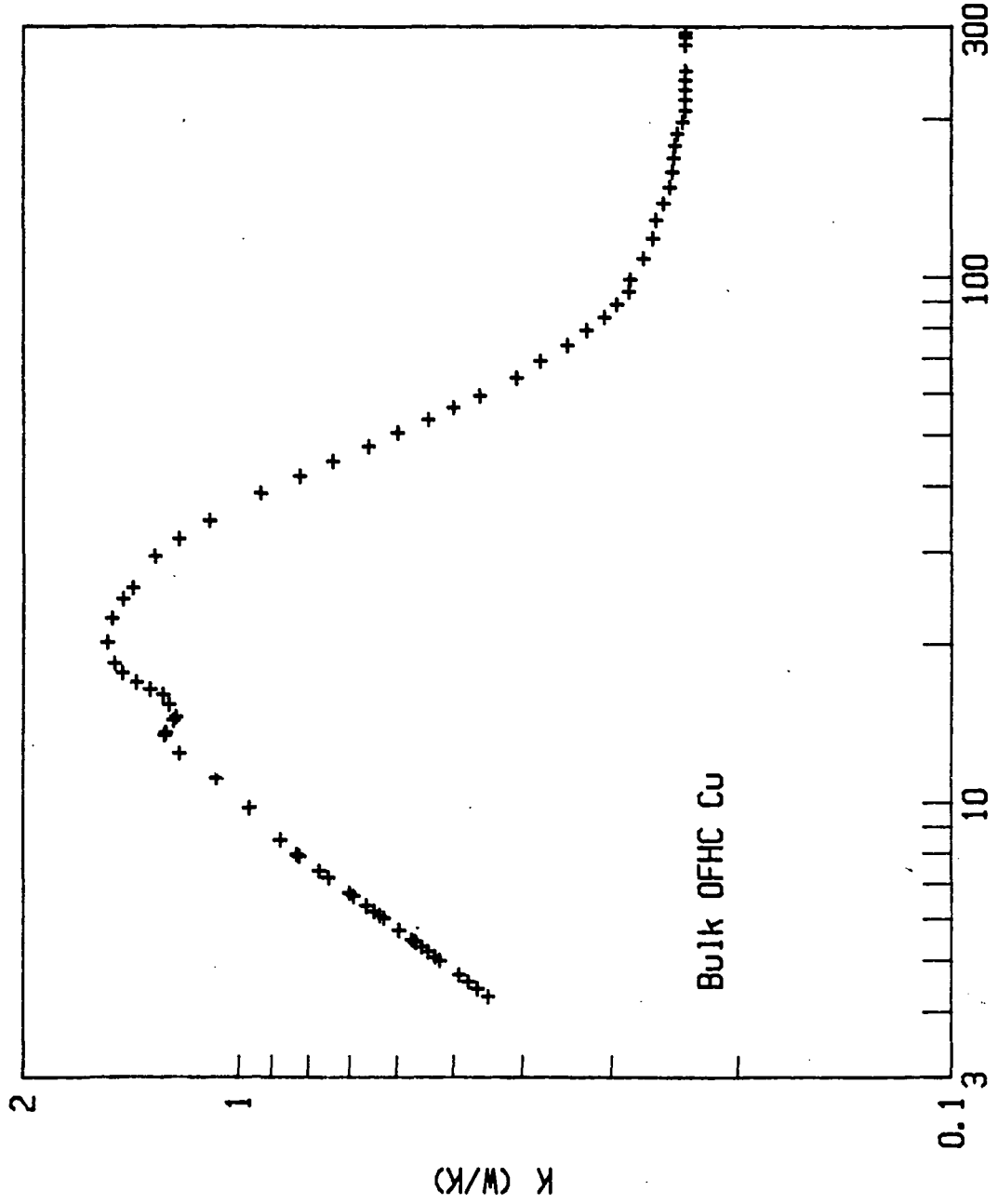

Fig. 4-2. Measured thermal conductance of bulk OFHC Cu vs temperature.

dominated by defects and impurities present in the material. As the temperature increases, the average phonon energy increases along with the phonon density. The temperature at which phonon scattering becomes apparant depends on concentration of impurities, i.e., a large impurity concentration results in a large low temperature resistance and a constant resistance that spans a larger temperature range than a purer material. For temperatures near room temperature, phonon scattering dominates, which results in a resistance that is a linear function of temperature. The residual resistance ratio (RRR), defined as

$$RRR = R(273\,K) / R(4\,K) \qquad (4.1)$$

is an indication of the purity of the metal. For very pure metals, such as Al, RRRs can range up to 10,000. The RRR for the OFHC Cu used in this study is 112.

The behavior for the thermal conductance is the complement of the resistance behavior. Near room temperature, the thermal conductance is constant, while for low temperatures ($T < 22K$ in Fig. 4-2) a linear dependence is seen. This behavior is a result of the competition between the specific heat of the primary transport carrier (electrons in the case for pure metals) and the mean free path. For electrons, the specific heat

is proportional to temperature. Thus at low temperatures, with defects causing a temperature independent mean free path, the thermal conductance is proportional to T. Near room temperature, with phonons scattering resulting in a mean free path inversely proportional to T, the thermal conductance is constant. The peak in the thermal conductance curve at about 22K comes at a temperature where phonon scattering is as effective as defect scattering, with the thermal conductance decreasing with increasing T from that point on.

A striking feature of Fig. 4-2 is the dip in the curve for $11K \leq T \leq 17K$. This feature is reproducible and remains even after re-calibrating the Ge thermometers against the same Si diode standard. There appears to be a drop in sensor sensitivity in this range, resulting in a lower measured ΔT than one would otherwise expect. This effect is small. A 10% increase in the measured ΔT would eliminate the dip.

This feature is unlikely to be a generic problem of Ge temperature sensors (1). However, according to Gerber and Sellmyer (2), Si diodes have shown anamolous behavior for $11K \leq T \leq 16K$, Fig. 4-3. The size and temperature range of this anamolous behavior varies among differing diodes.

Assuming our Si diode standard has a similar problem, the following scenario accounts for the dip in the thermal

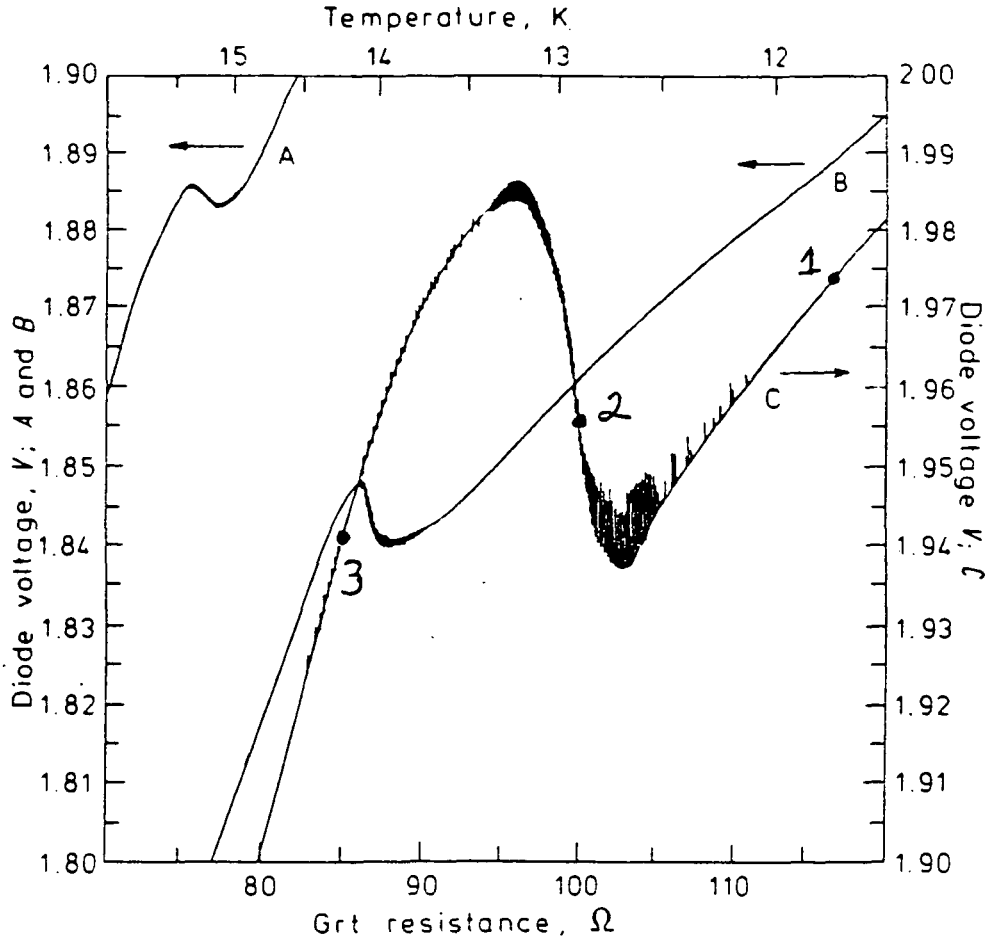

Fig. 4-3. Anamolous temperature dependence of Si diode voltage for three different diodes. (ref. 2).

conductivity curve. The Ge thermometers are calibrated against diode voltage on a point-to-point basis. Owing to the scaling employed for fitting the Ge conductance vs temperature data, the Ge conductance values are choosen to be evenly spaced on a log scale. When the desired value is reached during the calibration, it is recorded along with the resulting diode voltage. If the calibration points follow points 1-3 as shown in Fig. 4-3, a decrease in sensitivity results. Outside of this range, the sensitivity increases to its correct value. Thus, for a given change in conductance, a lower ΔT is measured for $11K \leq T \leq 16K$. It is a very small effect. A 10mK increase in the measured temperature difference would eliminate the dip. The exact temperature range and dropoff in sensitivity is diode dependent, however, this qualitatively accounts for the observed behavior.

The anomaly in the thermal conductance of the bulk material would be a problem if this were the final measurement. However, in this study, the bulk contribution is a background effect that is subtracted from subsequent measurements on contact samples. As will be shown, thermal contact conductance results are only slightly affected by this thermal anomaly problem.

Figure 4-4 shows a plot of Lorenz number vs temperature. The Lorenz number is defined as

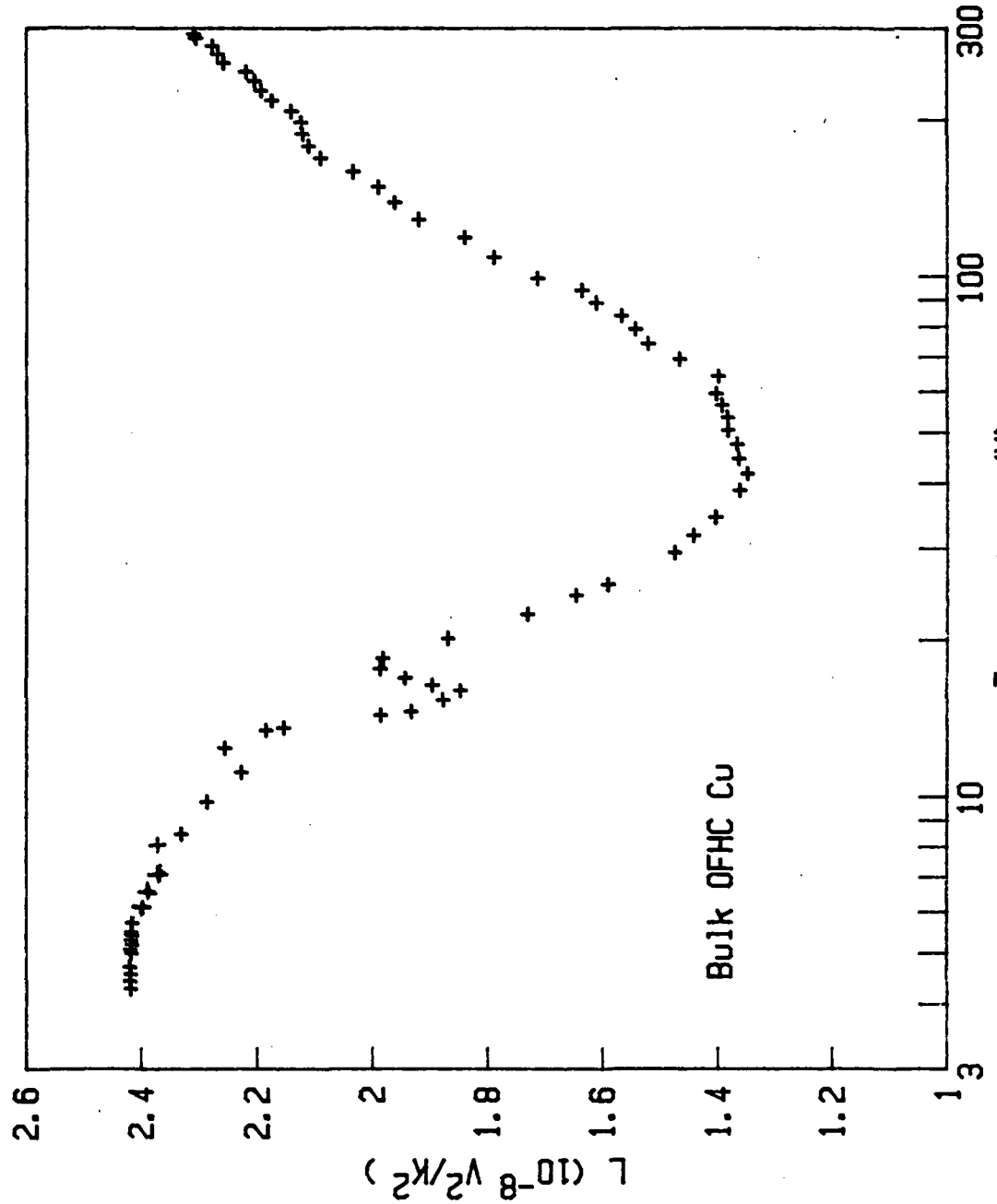

Fig. 4-4. Lorenz number for bulk OFHC Cu, calculated from L=K*R/T.

$$L = R \cdot K / T \qquad (4.2)$$

where R is resistance, K is thermal conductance and T is temperature. The anamoly present in the thermal conductance curve is readily apparent here also. With this one exception the curve follows the expected shape and compares well with previous reports (3).

Some transport property values, calculated from experimental data are compared to "accepted" values for OFHC Cu (4) in Table 4-1. The l/A ratio for the speciman is 16.87 cm^{-1}.

Table 4-1: Comparison of experimental with standard property values for OFHC Cu

property	T (K)	Expt	stnd
ρ (u-ohm)	273	1.55	1.56
k (W/cm-K)	273	4.04	3.98
L (10^{-8} V^2/K^2)	4	2.42	2.44

Because the 4K electrical and thermal conductances are very dependent on the impurity levels in the individual sample, a Lorenz number is calculated and compared to the Sommerfeld value. The Lorenz number is temperature independent at 4K, providing a convenient comparison among Cu samples with differing impurity levels.

4.2 CONTACT RESISTANCE RESULTS

A few introductory remarks, concerning the data presented below, are in order here. A wide variation in electrical contact resistance has been observed, under nominally the same preparation conditions. Typical sample-to-sample variation is around 40%, well above the uncertainty estimate at 4K. Figure 4-5 presents some preliminary data illustrating this variation. All three plots are for contacts prepared similarly. The variation is 50% centered on an average contact resistance of 1.5u-ohms. Improvements in grinding, cleaning and contact assembly have helped reduce this variation, but do not eliminate it.

The sensitive behavior of electrical contact resistance is evident when reading the literature. The phrases "averaged over many samples" or "contact was opened and closed until a stable value was reached" occur frequently. The variation does not reduce the usefulness of our results pertaining to low temperature applications in real systems, because a similar variation would be expected to occur.

For minor changes in procedure, such as rinsing the freshly ground contact face in methanol instead of ultrasonic cleaning, the electrical contact resistance can increase by a factor of 10, in the case of our "clean"

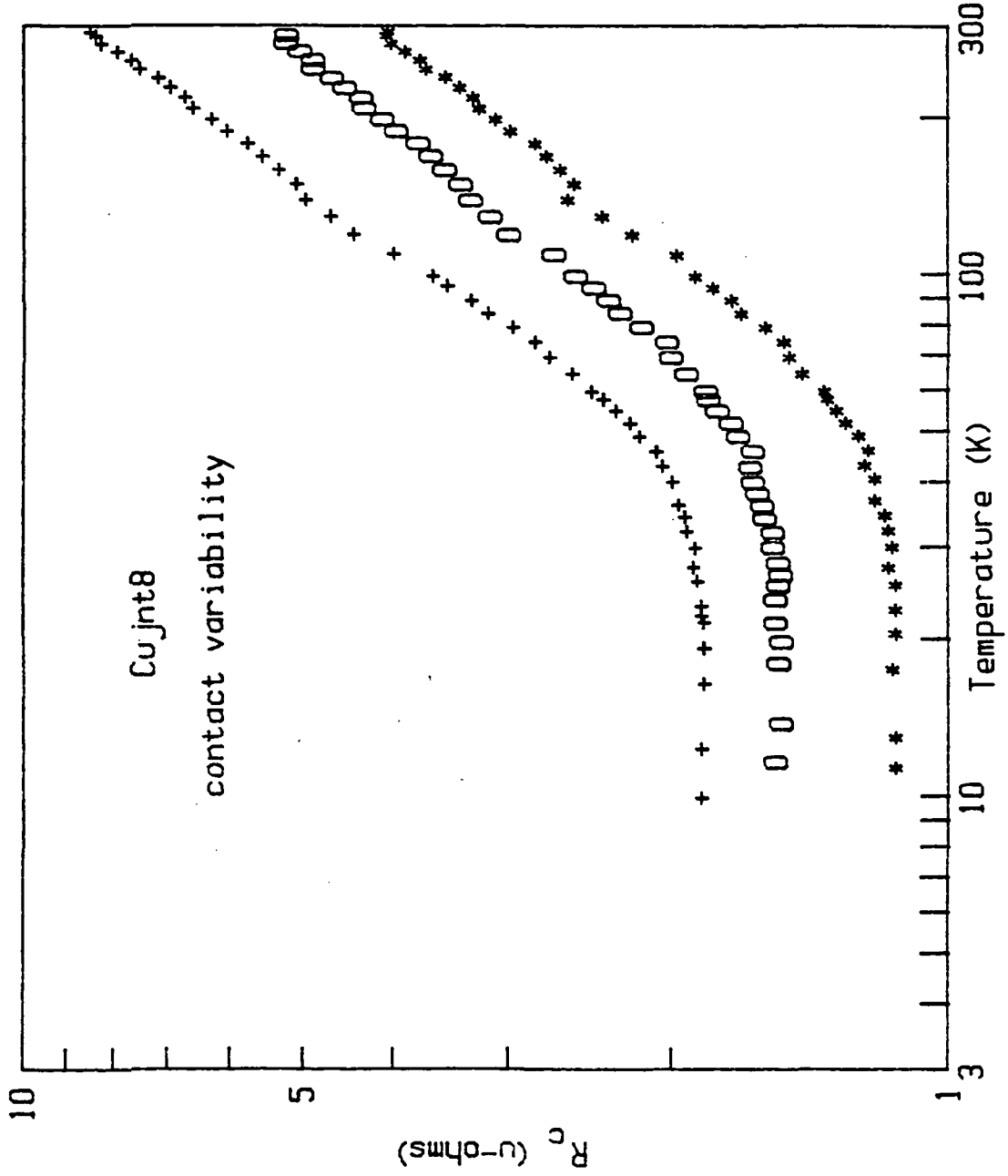

Fig. 4-5. Observed variation of electrical contact resistance for three identically prepared contact samples.

contacts. By contrast, thermal contact conductance measurements show much less variation.

Table 4-2 summarizes the sample number, oxidation state and surface roughness of the data to be presented.

Table 4-2: Summary of sample number, oxidation state and surface roughness.

Cujnt_#	Oxidation	Roughness_(um)
10	c	0.4
12	c	0.1
15	c	0.2
14	g.b.	0.1
18	15 min @ 200C	0.4
19	"	0.1
20	"	0.2
21	30 min @ 200C	0.4
22	"	0.1
23	"	0.2
24	c + .003" In foil	0.2

where c means "clean" and g.b. stands for the N_2 glove bag contact sample. Cujnt24 was prepared as a "clean" contact, but with the addition of a .003" In foil in between the contact faces. Results pertaining to this sample are discussed separately.

4.2.1 EFFECTS OF OXIDATION

Figure 4-6 shows the electrical contact resistance of 4 contact samples as a function of oxidation state. Surface roughness on all samples is 0.1um, except for Cujnt 20, which has a finish of 0.2um. The choice of Cujnt 20 over Cujnt 19 is related to the sample-to-sample variation in electrical contact resistance as discussed earlier.

The sample assembled in the glove bag, Cujnt 14, has the lowest 4K contact resistance of all other samples but a higher contact resistance than Cujnt 12 at room temperature. Table 4-3 summarizes these data. Note that the 4K electrical contact resistance spans 3 orders of magnitude.

Table 4-3: 4K and 273K electrical contact resistance (u-ohms) as a function of oxidation state.

Cujnt #	Oxidation	R_c (4K)	R_c (273K)	RRR
12	c	1.19	2.51	2.1
14	g.b.	.41	4.52	11
20	15 min	5.43	15.0	2.8
22	30 min	23.3	46.1	2.0

The most interesting result is the contrast between the RRRs of the contacts compared to the RRR of the bulk material. According to eqn (2.4) the only material

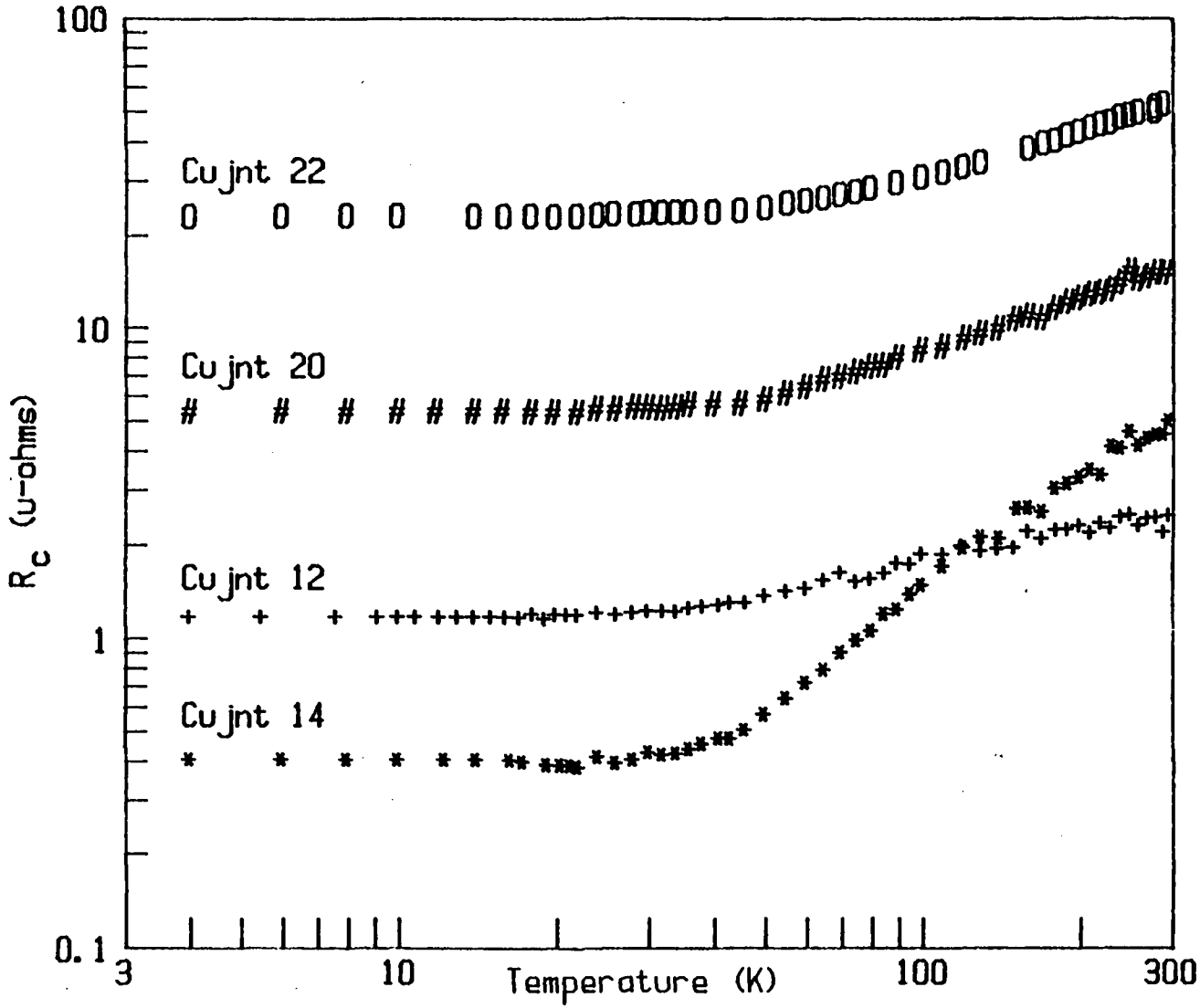

Fig. 4-6. Effect of oxidation on electrical contact resistance vs temperature. *-g.b., +-clean, #-15min at 200C and O-30min at 200C.

parameter contributing to the electrical contact resistance is the bulk resistivity. Therefore, the contact resistance should follow the bulk dependence. This is clearly not the case. The RRR for the contacts is independent of oxidation, with the exception of the glove bag sample which has a RRR of 11. It is interesting to notice that by preventing oxygen from contaminating the contact surface, one obtains a more metallic behavior, as evidenced by the RRR. Note also that while the $R_c(T)$ increases steadily with increasing oxidation time, the overall temperature dependence does not change.

For comparison, the thermal contact conductance at 4K varies only by a factor of 5 in these measurements as opposed to a 60-fold variation in R_c. Figure 4-7a presents K_c as a function of temperature for the same series of contacts as in Fig. 4-6. An interesting feature of this plot is that the K_cs for the two oxidized samples are equal, while their respective R_cs differ by a factor of 4. Figure 4-7b is a plot of K_c for Cujnt 14 only. A peak in the thermal contact conductance curve can be seen, followed by lower thermal contact conductance at higher temperatures, similar to the bulk behavior.

For $T \geq 100K$, the bulk electrical resistance and thermal conductance tend to dominate the measurement. Small random errors in measurements of the total signal,

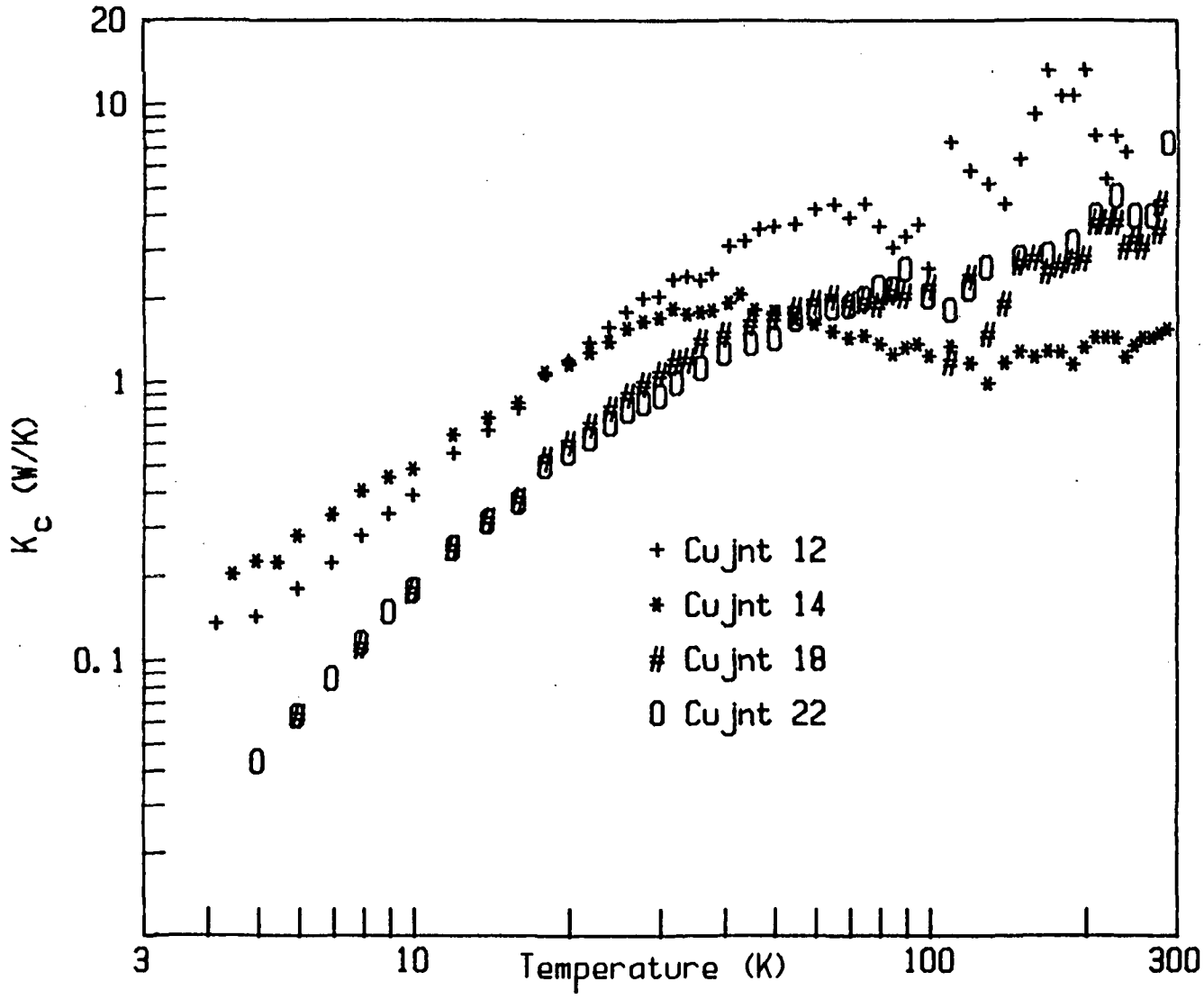

Fig. 4-7a. Effect of oxidation on thermal contact conductance vs temperature. *-g.b., *-clean, #-15min at 200C and 0-30min at 200C.

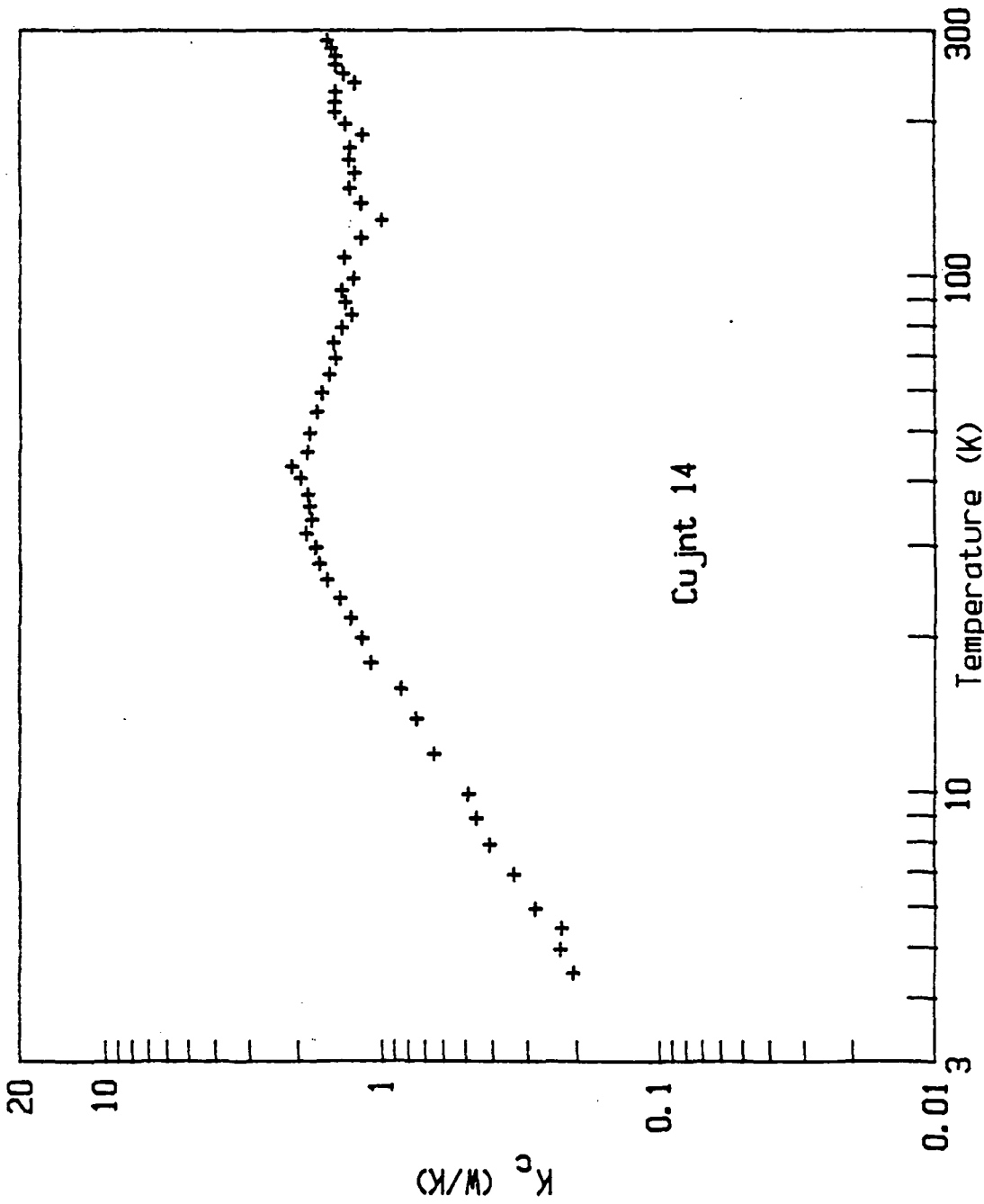

Fig. 4-7b. Cujnt 14 (g.b. sample) showing a peak in the thermal contact conductance, due to better metallic contact relative to other samples.

result in large fluctuations in contact values, especially for K_c. These fluctuations do not obscure the general trend of the data, but do cause scatter, as can be seen in the figures.

As discussed in chap. 3, the thermal contact conductance at low temperatures can be described as

$$K_c = aT^n \qquad (4.3)$$

where $n \cong 2$, generally. The present data were fit to this function for $T \leq 12K$ and for $T \leq 20K$. Results are shown in Table 4-4.

Table 4-4: Empirical fit to K_c data of the form, $K_c = aT^n$

Cujnt #	$T < 12K$	$T < 20K$
12	$16\times10^{-3}\ T^{1.4}$	$13\times10^{-3}\ T^{1.5}$
14	$32\times10^{-3}\ T^{1.2}$	$32\times10^{-3}\ T^{1.2}$
18	$1.7\times10^{-3}\ T^{2}$	$2.3\times10^{-3}\ T^{2}$
22	$1.7\times10^{-3}\ T^{2}$	$2.0\times10^{-3}\ T^{2}$

If pure electron transport dominated the thermal contact conductance, a linear relationship would exist between K_c and temperature. This is not the case. In fact, as one progresses from samples 14-12-18-22, which is associated with increasing oxide thickness, the exponent increases from almost linear (n=1.2) to quadratic. Pure lattice thermal transport would have a cubic dependence.

The origin of the T^2 dependence for K_c is unclear. Many amorphous solids have thermal conductivities at low temperatures showing a dependence ranging from $T^{1.5}$ to T^2 (6). Specific heat measurements on these materials at low temperatures indicate that not only is the specific heat larger that what one would calculate from elastic constants, but its temperature variation is slower that the Debye specific heat model. Impurities have been shown to appreciably affect the specific heat, but leave the thermal conductivity unchanged (7). Briefly then, there exist additional excitations in the lattice, the nature of which is unclear, which yield a linear contribution to the specific heat. A T^2 dependence then results from the scattering of phonons by the extra excitations.

The situation is unclear for amorphous solids. It is also questionable whether or not these results are relevant to our thermal contact conductance data. However, the T^2 behavior for low temperature K_c has been established by results from many experiments.

With both K_c and R_c as a function of temperature for each contact, we calculate the Lorenz number as in eqn. (4.2). These results are shown in Fig. 4-8. Note the log scale. Rather remarkable behavior is seen for samples where one would nominally expect mostly metallic contact. The dashed line is the Sommerfeld value for the free

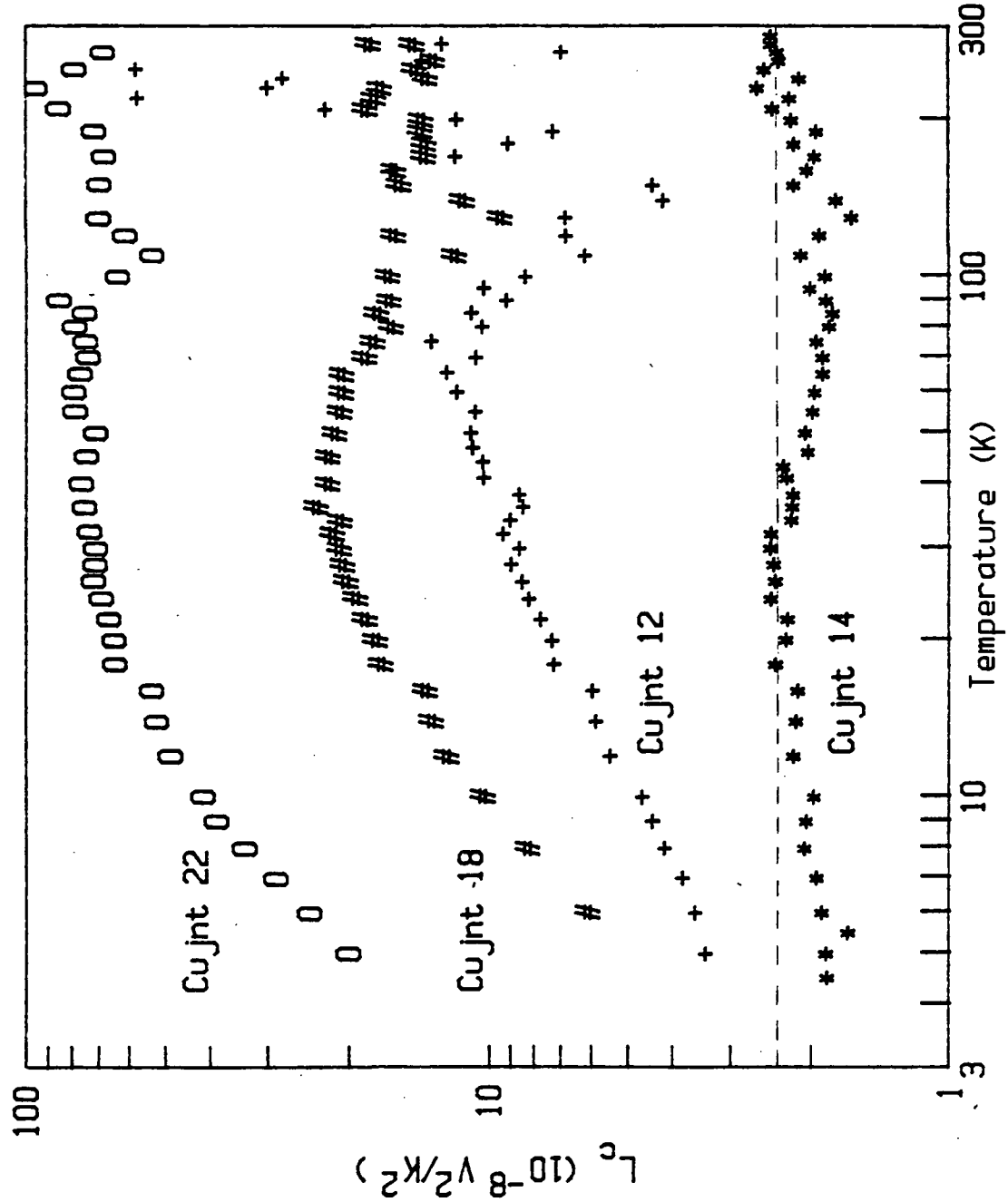

Fig. 4-8. Effect of oxidation on contact Lorenz numbers. *-g.b., +-clean, #-15min at 200C and 0-30min at 200C.

elctron model. This behavior contasts with Fig. 4-4 which shows the bulk dependence. Cujnt 14 (the g.b. sample) comes closest in terms of following the bulk behavior. It is puzzling to note that for T < 20K, the Lorenz number actually decreases below the Sommerfeld value for this sample. For Cujnt 12, which has only a very thin native oxide, the Lorenz number is always greater than the Sommerfeld value. Samples 18 and 22 display very large Lorenz numbers, with the same general behavior as Cujnt 12.

Lorenz numbers greater than the bulk value at a given temperature indicates that the lattice makes a sizable contribution to the measured thermal conductance. As seen in Fig. 4-8, the amount of lattice thermal conduction is very large, compared to that estimated from the Sommerfeld value and the electrical contact resistance. Table 4-5 compares thermal contact conductances estimated from the Sommerfeld value of the Lorenz number and R_c with experimental values at 4K. The difference is largest for oxidized contacts.

Table 4-5: K_c estimate from Lorenz number and R_c (4K)

Sample	R_c (u-ohms)	K_{est} (W/K)	K_{exp} (W/K)	K_c %diff
12	1.2	.080	.111	+39
18	5.9	.017	.027	+60
22	23.3	.004	.027	+575

Except for the glove bag sample, the temperature dependence of R_c and K_c for the three different oxidation states is remarkably similar. At first glance, the contact resistance behavior looks very similar to a heavily alloyed metal. Given the preparation conditions, this seems unlikely. The contacting asperities undoubtedly undergo plastic deformation and subsequent work hardening. Although not enough to change the RRR from 110 to 2. If the points are in metallic contact, then R_c and K_c should follow the bulk temperature dependence. Obviously, this is not the case. An important clue is provided by the difference between the glove bag contact and a "clean" contact. The native oxide, present on the contact surface due to its exposure to air, is about 10A thick (7). This oxide is not present on the glove bag sample, due to a protecting atmosphere of N_2, although a nitride film is probably present. We hypothesize that this oxide layer insulates the majority of the load bearing area, preventing true metallic contact. Transport of current across the contact then proceeds primarily by the tunneling mechanism.

The tunneling resistance depends on the barrier height and on the electrode separation. This resistance is constant at the voltage levels encountered in the present study (8). It is also independent of temperature. Figure

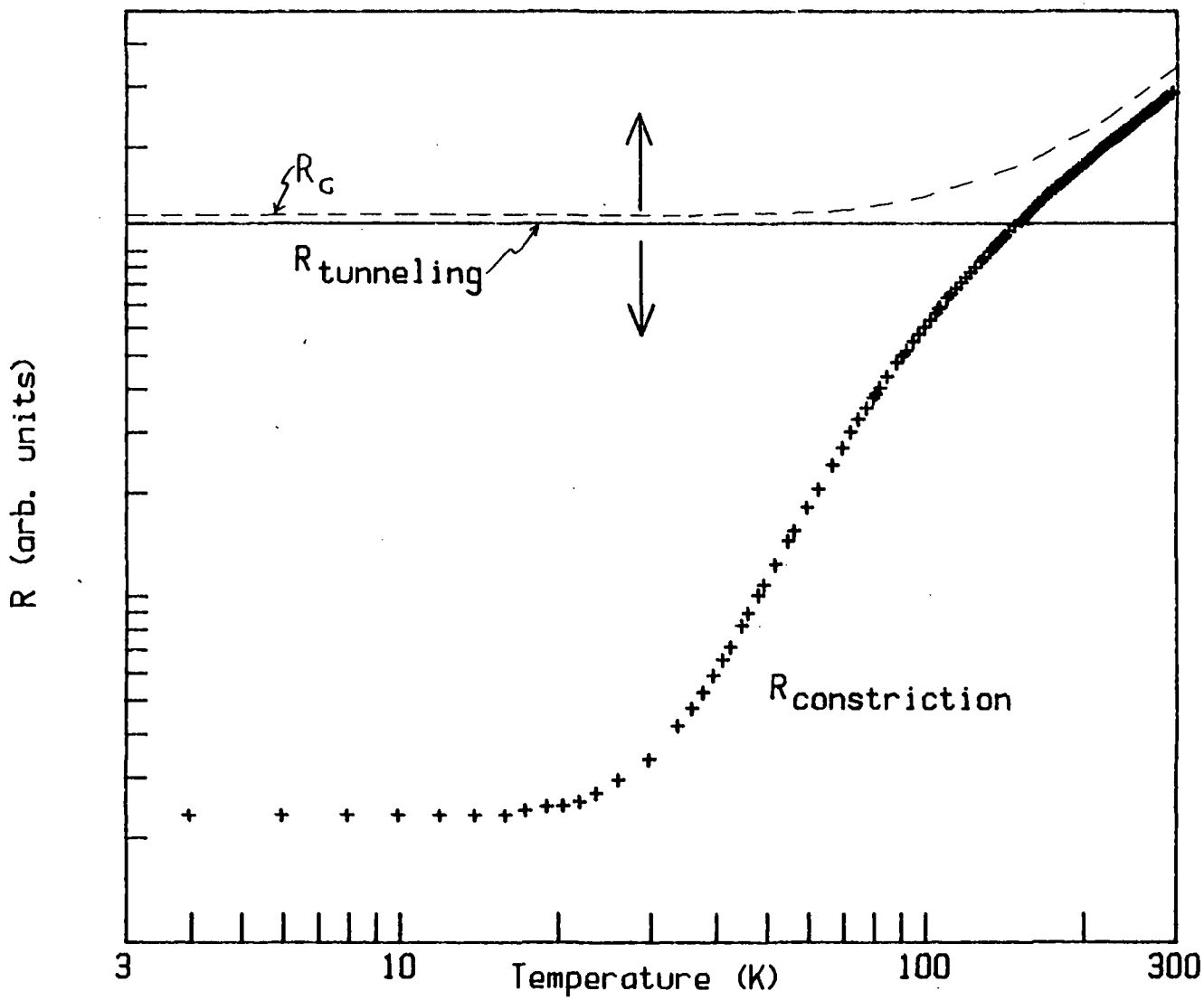

Fig. 4-9. Schematic plot of a tunneling resistance and a constriction resistance combining to give the observed contact resistance.

4-9 illustrates schematically how the tunneling resistance and constriction resistance combine to give the observed contact resistance. The tunneling resistance shifts up or down depending on oxide composition and thickness. The constriction resistance scales according eqn. (2.4), dependent on the area in metallic contact. This area in turn, depends on other parameters including oxide thickness, load, hardness and roughness. The sum of these two terms results in the measured contact resistance, the dashed line in Fig. 4-6. It is unclear why this behavior would lead to a RRR of 2, regardless of oxidation state of the surface. In other words, why does the tunneling resistance at 4K equal to the constriction resistance at 273K?

A similar argument holds for Cujnt 14, although the surface film is of a different composition. The behavior of R_c and K_c is more metallic-like than any other sample, although with a higher contact resistance at room temperature than the other samples. It could be argued that because of sample-to-sample variation, the room temperature contact resistance has a large uncertainty. Electrical contact resistance measurements were repeated twice, each time using a fresh sample, with essentially unchanged results. While samples 12, 20 and 22 had stable resistances over a period of one week, Cujnt 14 was seen

to have an increasing value of R_c at 4K. Its room temperature value of R_c also dropped at the same time, with the RRR changing from 11 to 7. After noticing this effect, a short thermal conductance measurement was performed. The 4K K_c had dropped slightly, the room temperature K_c had increased and the peak present in Fig.4-7b had disappeared. The sample was not disassembled during this time, but remained in the cryostat which remained partially evacuated to < 100 torr. No systematic investigation of the effect was carried out, but these observations indicate that the temperature dependence of these samples is dependent on the contact surface oxide coverage and composition.

4.2.2 EFFECTS OF ROUGHNESS: "CLEAN" CONTACT

Figures 4-10 and 4-11 present electrical contact resistance and thermal contact conductance data for a series of three contacts. The oxidation state of the contact is nominally clean, i.e., the contact surface was exposed to air for the minimum time required to assemble the sample, typically about 40 min. The contact surface roughness is given in Table 4-2. Cujnt 10 has a R_c about twice as high as the other two samples in this series. This difference is ascribed to sample-to-sample variation

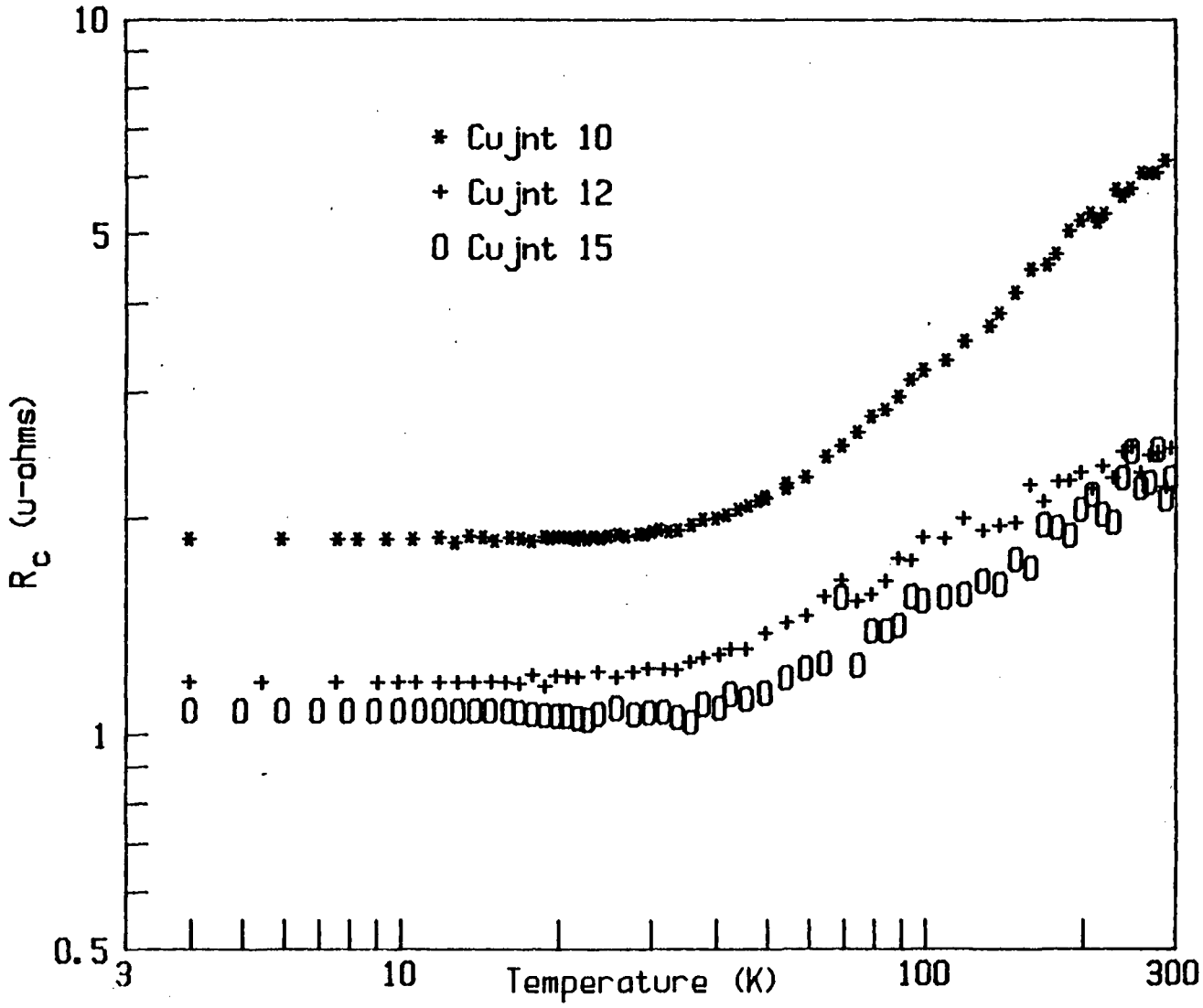

Fig. 4-10. Electrical contact resistance for various surface finshes. * - 0.4um, O - 0.2um and + - 0.1um rms roughness, clean contact.

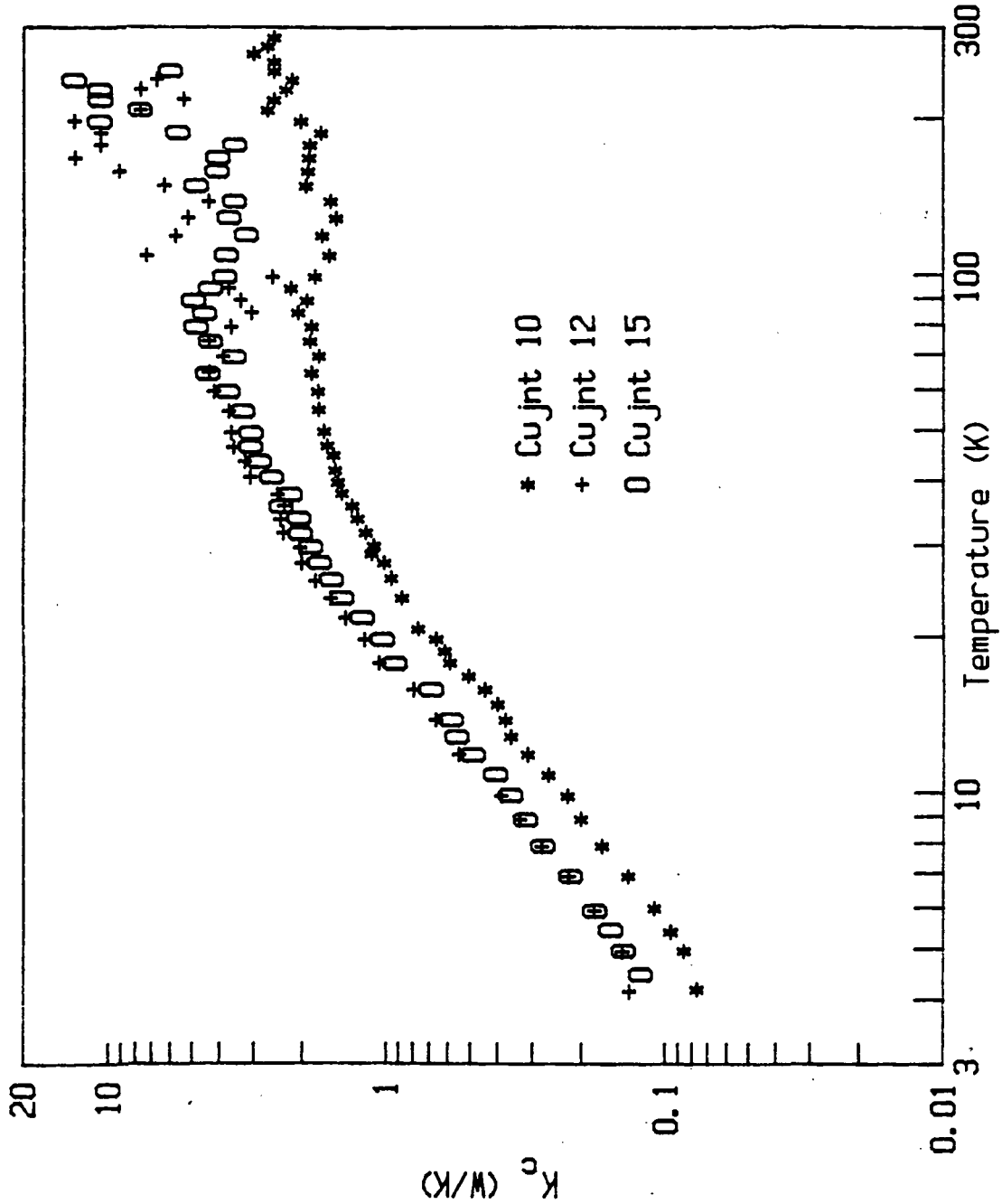

Fig. 4-11. Thermal contact conductance for differing surface finishes.
* - 0.4um, O - 0.2um and + - 0.1um rms roughness, clean contact.

as discussed previously. Table 4-6 lists the RRR for each contact

Table 4-6: R_c (u-ohms) and RRR for clean contacts.

Sample	Roughness (um)	R_c (4K)	R_c (273K)	RRR
10	0.4	1.88	6.1	3.2
12	0.1	1.19	2.51	2.1
15	0.2	1.08	2.36	2.2

The thermal contact conductance follows the electrical contact resistance. A slightly lower thermal contact conductance is seen for Cujnt 10 relative to the other two samples. Table 4-7 presents the best fit to the experimental data and the 4K thermal contact conductance.

Table 4-7: Empirical power law fit for clean contacts.

Sample	T < 12K	T < 20K	K_c (4K) (W/K)
10	$8.2\times10^{-3} T^{1.5}$	$8.2\times10^{-3} T^{1.5}$	.066
12	$16\times10^{-3} T^{1.4}$	$13\times10^{-3} T^{1.4}$	.111
15	$15\times10^{-3} T^{1.4}$	$14\times10^{-3} T^{1.4}$	.104

The Lorenz number as calculated from these data are shown in Fig. 4-12. The Lorenz number at 4K is about 3.1×10^{-8} V^2/K^2 and the agreement among these samples is within $\pm$10%.

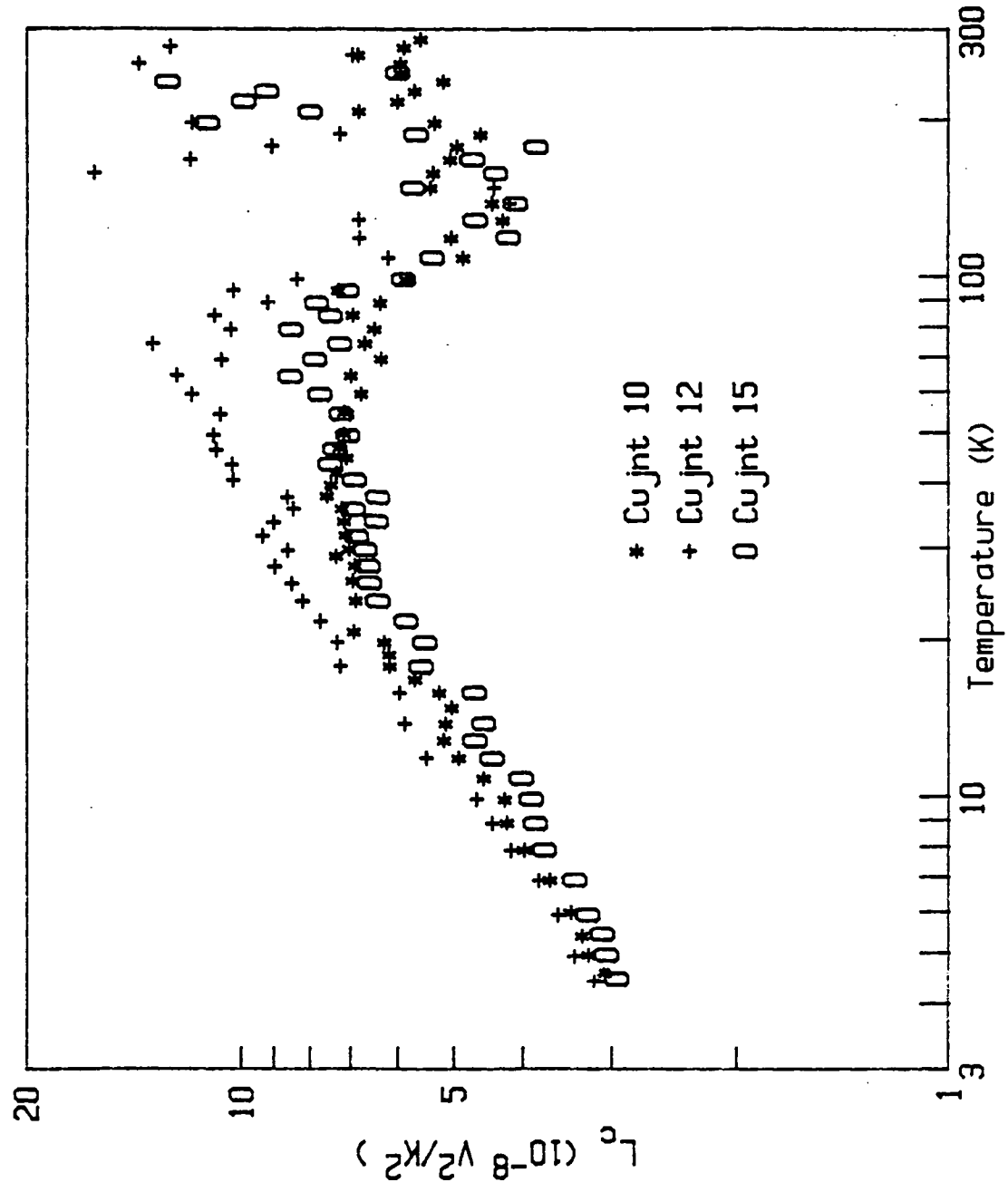

Fig. 4-12. Contact Lorenz numbers for differing surface finishes.
* - 0.4um, 0 - 0.2um and + - 0.1um rms roughness, clean contact.

4.2.3 ROUGHNESS: OXIDIZED 15MIN AT 200C

This series of contacts was oxidized for 15 minutes at a temperature of 200C in laboratory air. Table 4-8 summarizes these data.

Table 4-8: R_c (u-ohms) and RRR for oxidized contacts - 15min at 200C.

Sample	Roughness (um)	R_c (4K)	R_c (273K)	RRR
18	0.4	5.88	11.3	1.9
19	0.1	29.4	56.3	1.9
20	0.2	5.43	15.0	2.8

Sample 19 has a contact resistance a factor of 5 higher than the other two contact samples in this series, Fig. 13. Because Cujnt 19 has the smoothest surface, an oxide layer might prevent the contact asperities from breaking through the layer and making metallic contact, as in a model proposed by Hisakado (9). However, the thermal contact conductance, Fig. 4-14, for Cujnt 19 is exactly the same as Cujnt 18, which has the roughest surface, this can also be seen in Table 4-9.

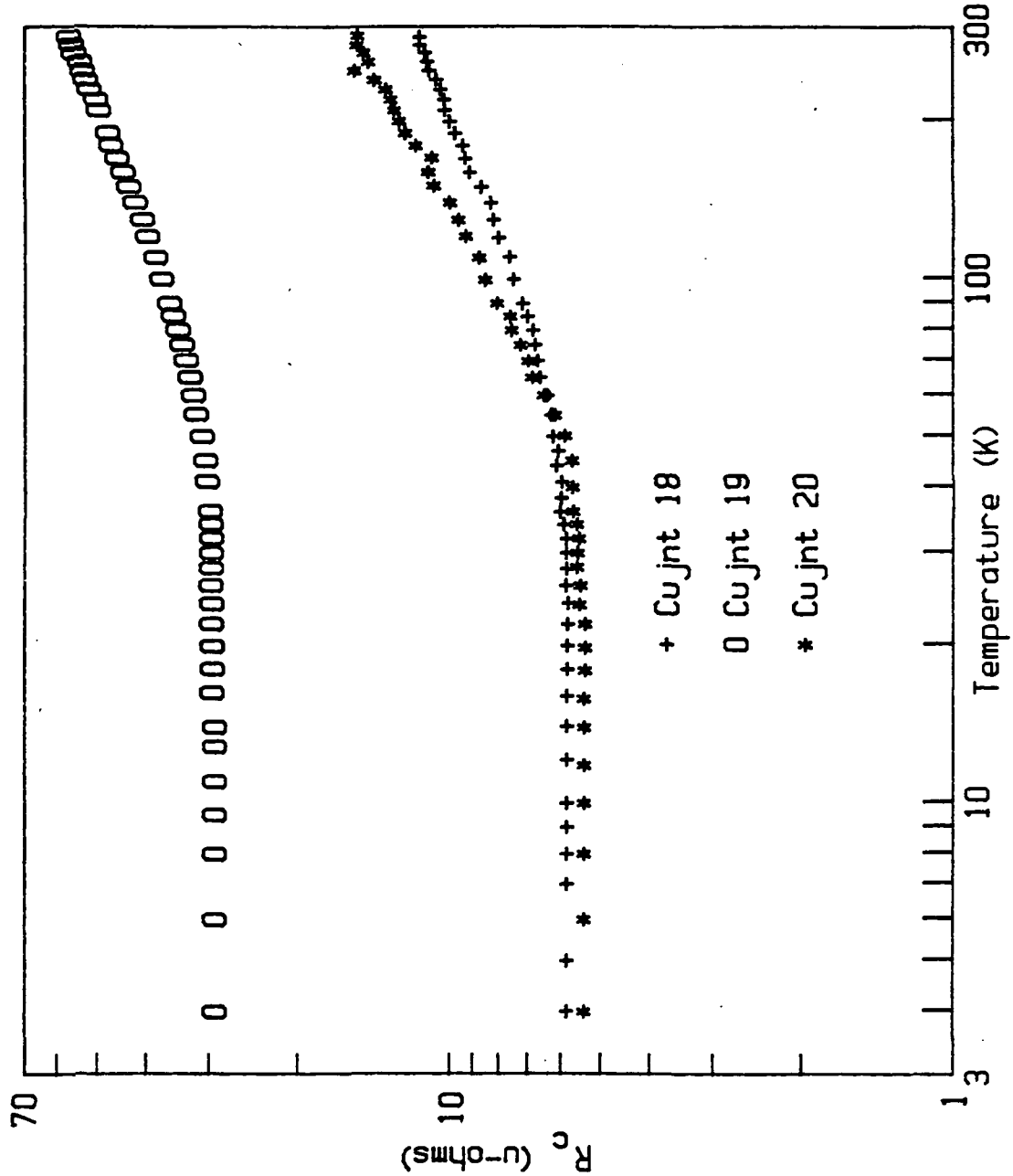

Fig. 4-13. Electrical contact resistance, differing surface finishes.
+ - 0.4um, * - 0.2um and 0 - 0.1um rms roughness. Oxidized 15min at 200C

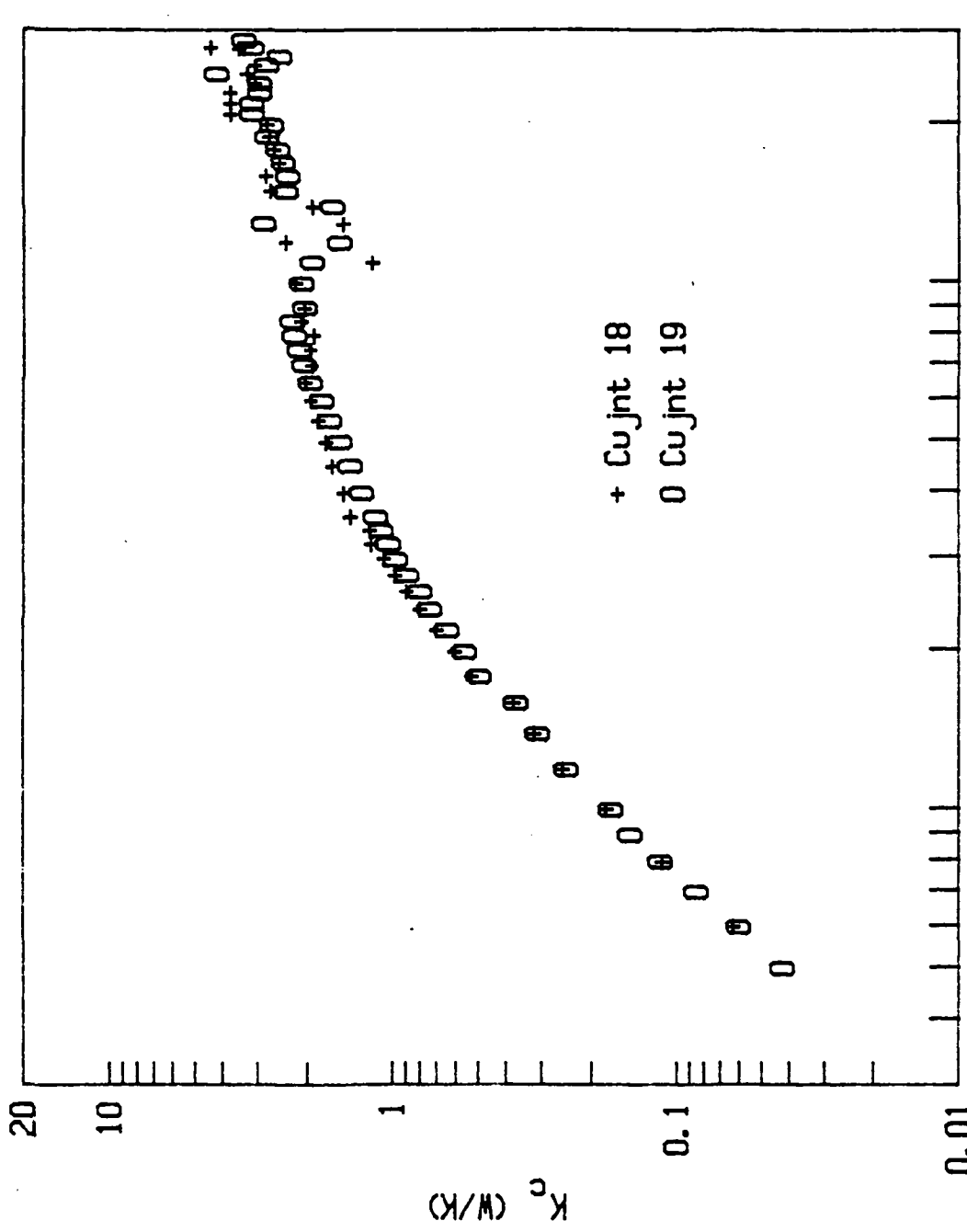

Fig. 4-14. Thermal contact conductance, differing surface finishes. + - 0.4um and O - 0.1um rms roughness. Oxidized 15min at 200C.

Table 4-9: Empirical power law fit for oxidized contacts - 15min at 200C.

Sample	T < 12K	T < 20K	K_c (4K) (W/K)
18	$1.7\times10^{-3} T^2$	$2.3\times10^{-3} T^{1.9}$	.027
19	$1.6\times10^{-3} T^2$	$2.2\times10^{-3} T^{1.9}$	.027

If penetration of the oxide layer were important for establishing contact, electrical contact resistance and thermal contact conductance would change in manner proportional to the area in metallic contact. A decrease in electrical contact resistance and an increase in thermal contact conductance would occur as more metallic contact took place. However, for R_c determined by tunneling, slight changes in the barrier height or width could easily account for this variation in electrical contact resistance while leaving K_c unchanged.

Figure 4-15 shows a plot of the Lorenz number for samples 18 and 19. The difference between the two samples is a reflection of the variation in R_c. In both cases the value for L_c is significantly larger than the Sommerfeld value.

4.2.4 ROUGHNESS: OXIDIZED 30MIN AT 200C

A similar series of contacts was oxidized for 30 min at 200C in laboratory air. As in the preceding series,

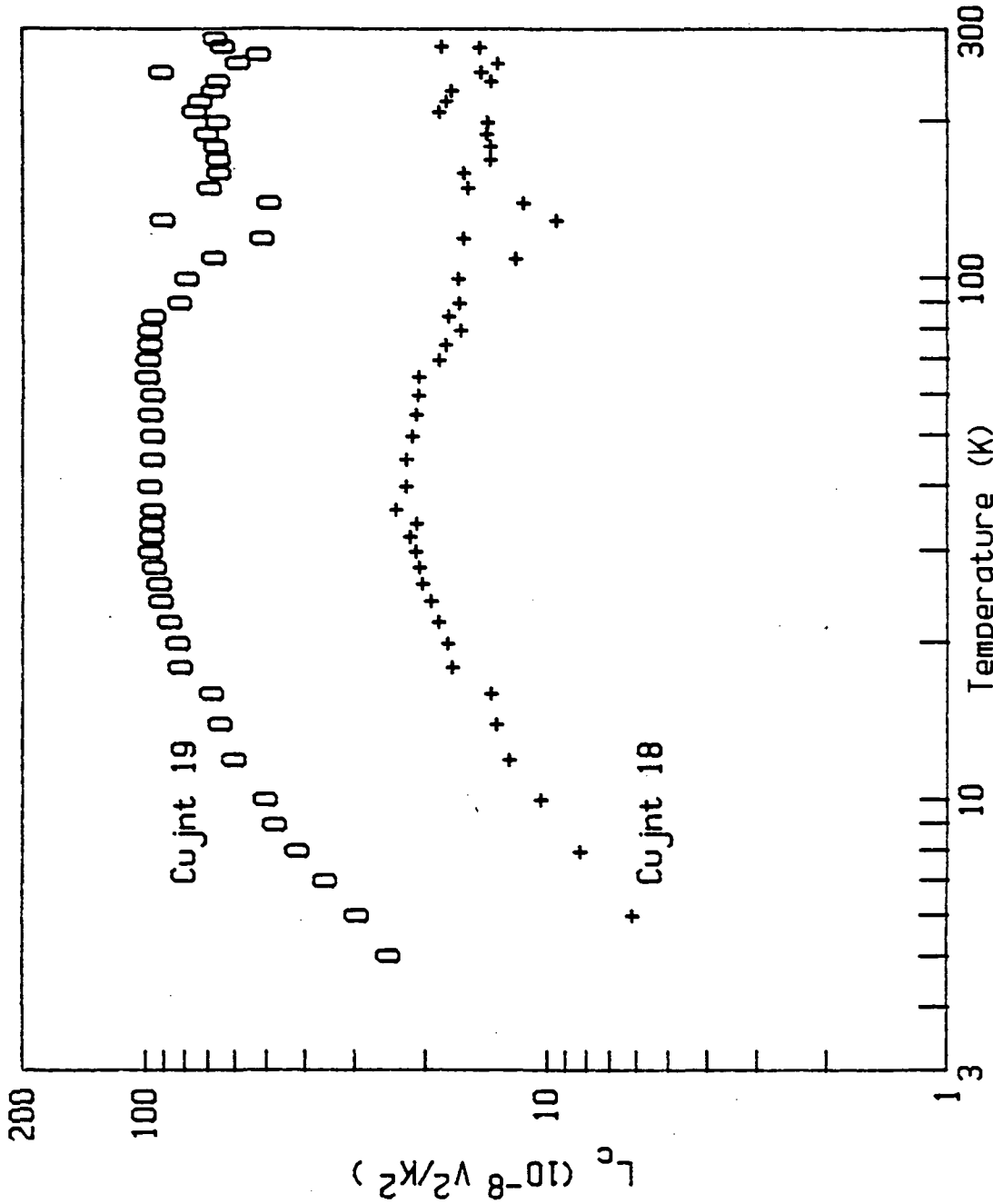

Fig. 4-15. Contact Lorenz number for contacts oxidized 15min at 200C.
+ - 0.4um and O - 0.1um rms roughness.

one sample has a notably higher contact resistance than the other two, Fig. 4-16 and Table 4-10.

Table 4-10: R_c (u-ohms) and RRR for oxidized contacts - 30min at 200C.

Sample	Roughness (um)	R_c (4K)	R_c (273K)	RRR
21	0.4	24.0	56.0	2.3
22	0.1	23.3	46.1	2.0
23	0.2	58.9	108	1.8

Thermal contact conductance results are shown in Fig. 4-17. A notable point is that while the R_c value at 4K of Cujnt 21 is a factor of 2 higher than the other two, its K_c is about the same as Cujnt 22, Table 4-11. This aspect is also reflected in the Lorenz number, Fig. 4-18.

Table 4-11: Empirical power law fit for oxidized contacts- 30min at 200C.

Sample	T < 12K	T < 20K	K_c (4K) (W/K)
21	$0.8\times10^{-3} T^2$	$1.1\times10^{-3} T^2$	.013
22	$1.7\times10^{-3} T^2$	$2.0\times10^{-3} T^2$	.027

4.2.5 In FOIL CONTACT

It is common practice to insert a thin soft metal foil inbetween the contact faces in order to improve the contact conductace of the joint. This improvement results

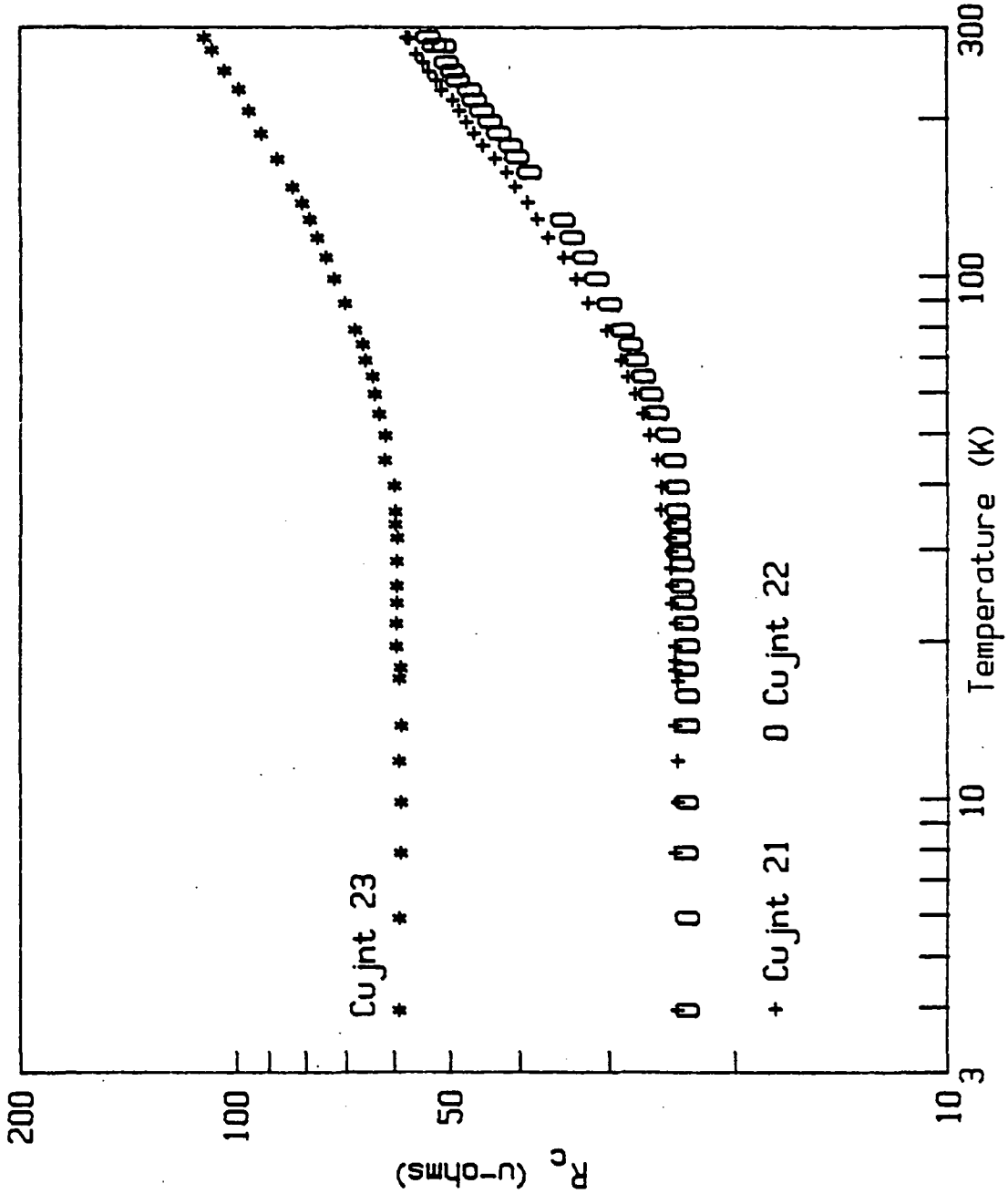

Fig. 4-16. Electrical contact resistance, differing surface finishes.
+ - 0.4um, * - 0.2um and O - 0.1um rms roughness. Oxidized 30min at 200C

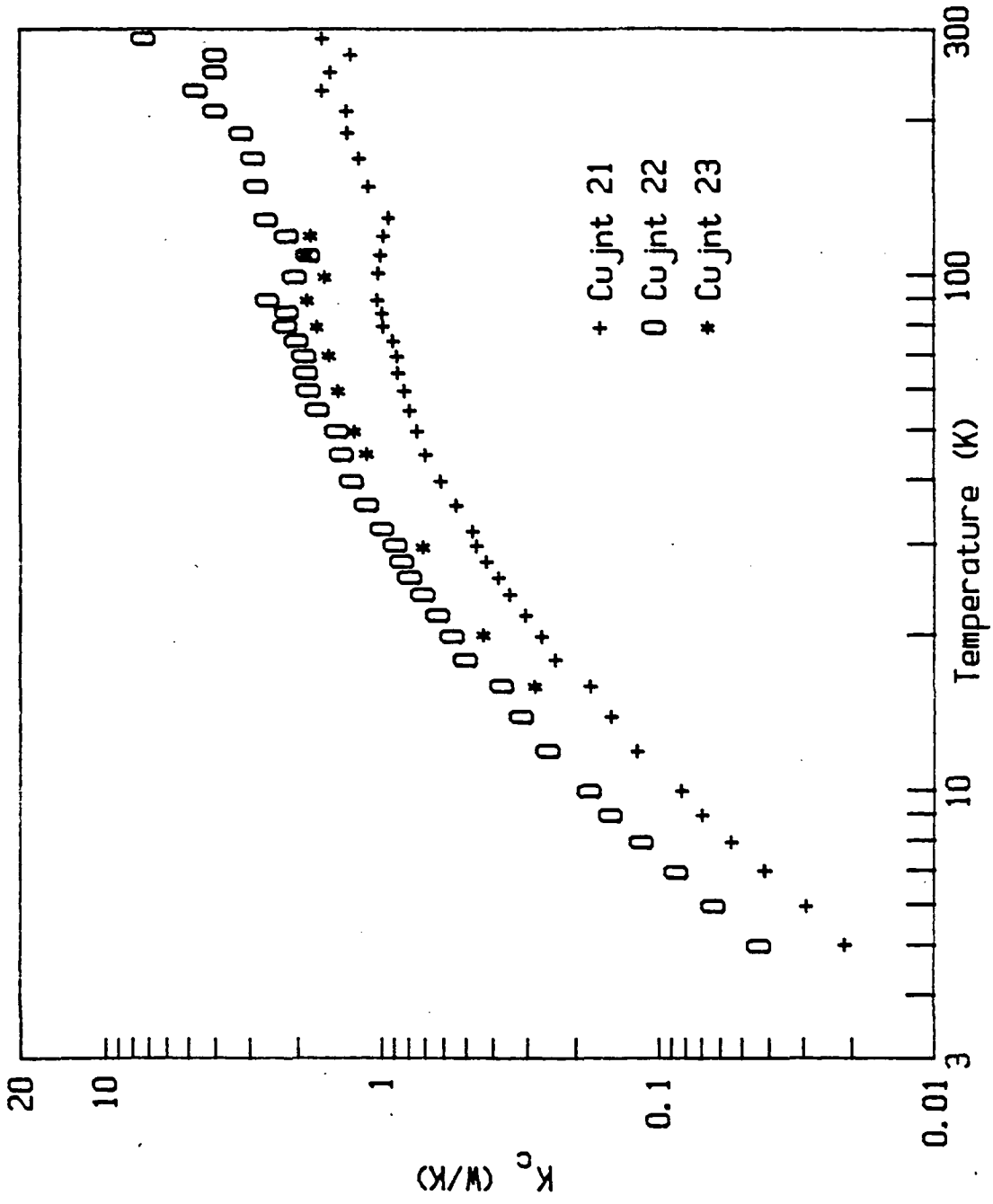

Fig. 4-17 Thermal contact conductance, differing surface finishes.
+ - 0.4um, * - 0.2um and O - 0.1um rms roughness. Oxidized 30min at 200C

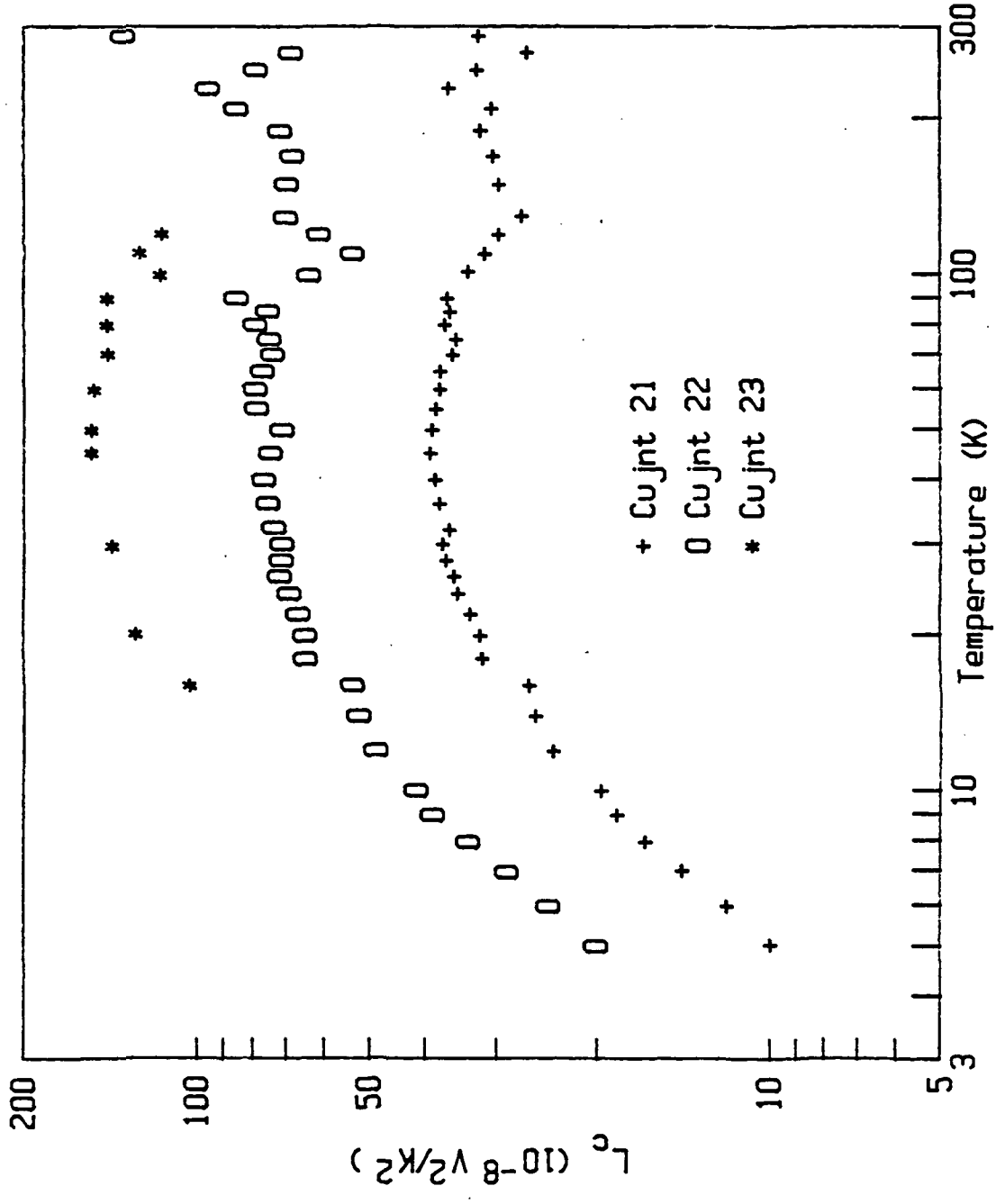

Fig. 4-18. Contact Lorenz number for contacts oxidized 30min at 200C. + - 0.4 um, * - 0.2um and O - 0.1um rms roughness.

from an increase in the surface area in contact, due to the deformation of the foil under load.

A .003" In foil was placed between two contact faces of 0.2um roughness, equivalent to Cujnt 15. Electrical contact resistance and thermal contact conductance data are shown in Figs. 4-19 and 4-20 respectively. The R_c(4K) is 0.18 u-ohms, a 5-fold decrease versus the clean contacts. Because of this very low contact resistance, a large scatter is seen for T > 70K. The nanovoltmeter accuracy is $\pm$2% and near room temperature R_c is <1% of the total measured resistance. Thus, R_c is beyond the measurement resolution. Similarly for the thermal contact conductance near room temperature, the temperature difference across the sample length is much larger than the temperature drop at the contact. From the error estimate, the uncertainty in the measured contact conductance is 120% of K_c. The improvement in K_c(4K) is a factor of 8 over Cujnt 15 as shown in Table 4-12. The effect of the bulk conduction through the In foil has been neglected.

Table 4-12: Empirical power law fit for In foil contact

Sample	T < 12K	T < 20K	K_c(4K) (W/K)
24	$.088T^{1.6}$	$.099T^{1.5}$	1.81

Two results stand out from the measurement. The

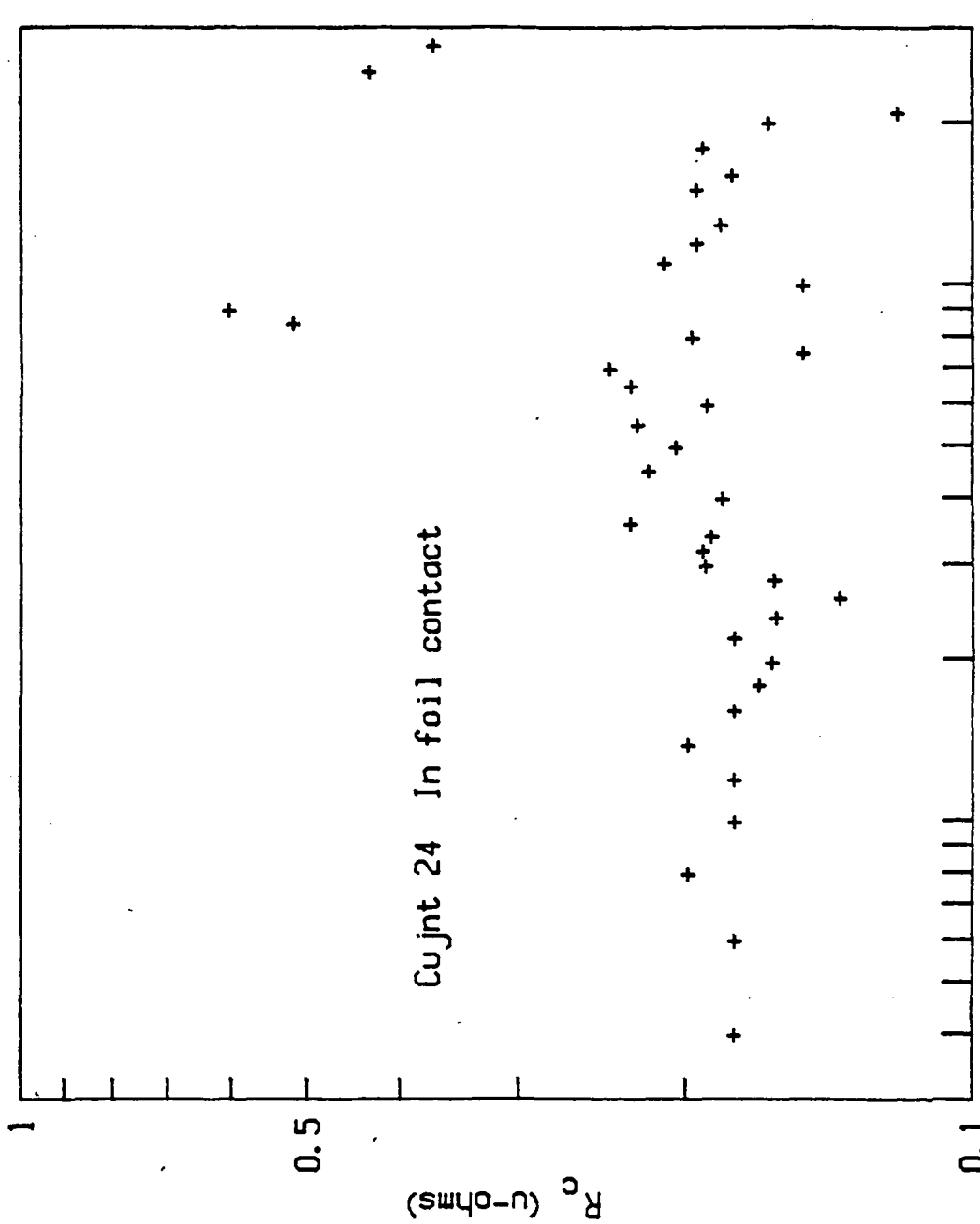

Fig. 4-19. Electrical contact resistance for In foil contact. Note the vertical scale in comparison to the preceeding graphs.

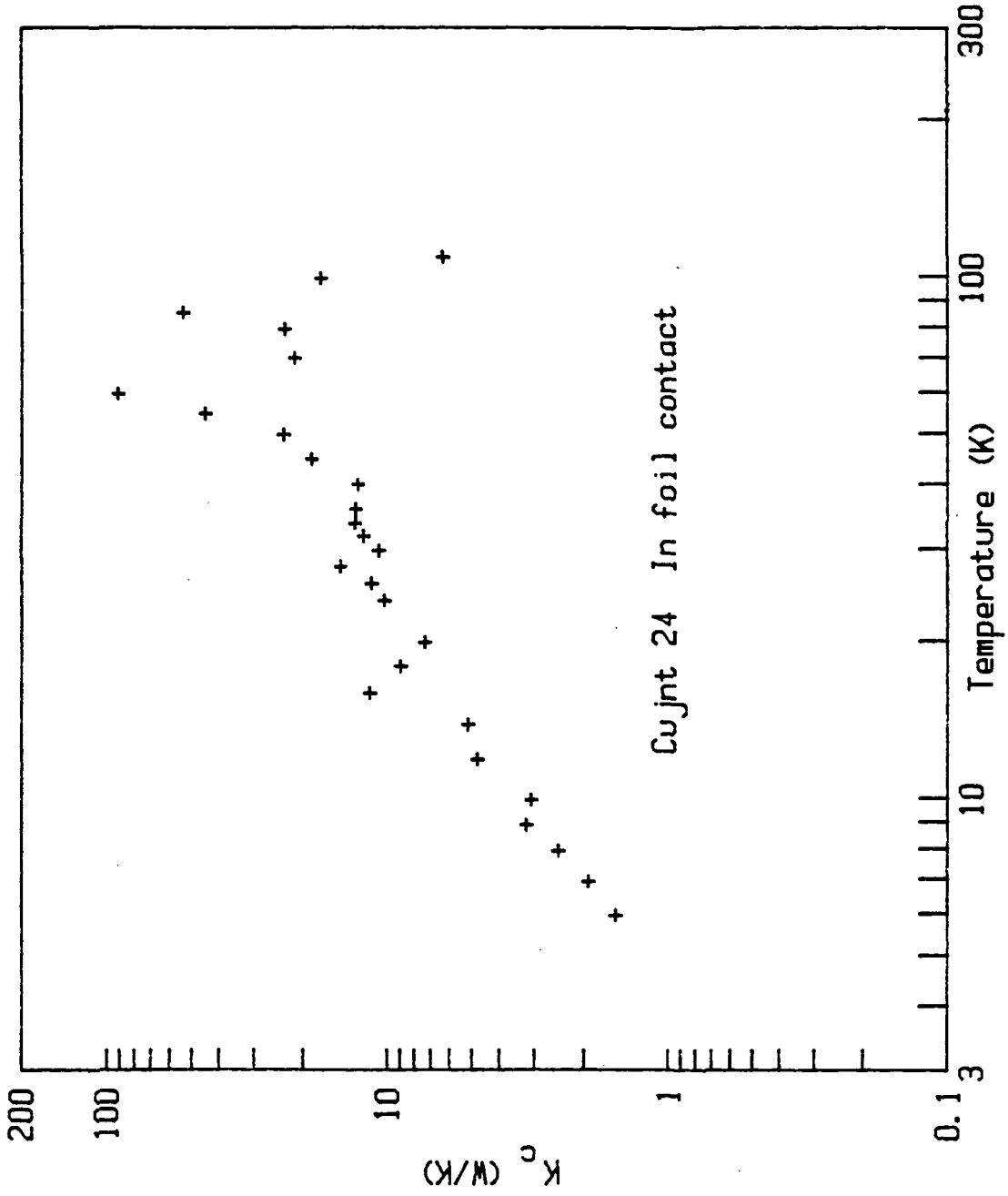

Fig. 4-20. Thermal contact conductance for In foil contact.

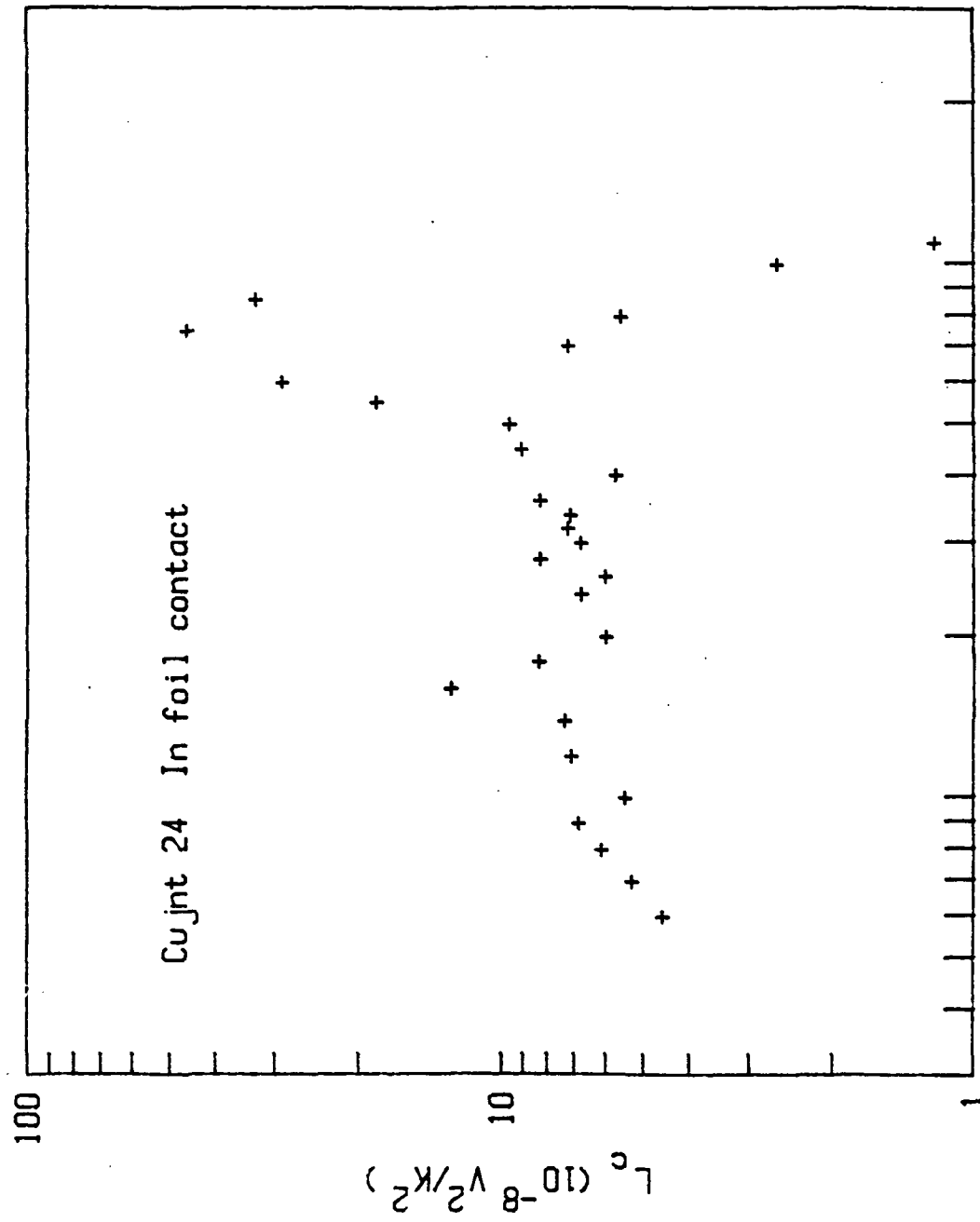

Fig. 4-21. Contact Lorenz for In foil contact. This plot follow the clean contact Lorenz number variation very closely.

temperature dependence of K_c is not linear. Also, as can be seen in Fig. 4-21, the Lorenz number follows the clean contact results very closely in terms of temperature dependence and magnitude. Clearly then, the transport mechanisms are the same in both cases.

4.3 AUGER ELECTRON SPECTROSCOPY (AES)

AES is a surface sensitive technique which provides information on elemental surface composition. Combined with inert ion sputtering, one can measure the composition of surface films as a function of sputter time. If thin films of known thickness and composition are available as standards, the sputter time can be converted to depth and film thicknesses information can be obtained. This technique thus provides a means of characterizing the contact surface and the oxides present on it.

AES measurements were performed on 3 foils which were subjected to identical oxidations as the contact samples. The foils were formed by rolling the OFHC tubing to a thickness of .025". The foils were degreased in Freon and the top surface was ground with #600 grit silicon carbide paper, leaving a surface roughness of 0.1um. Auger analysis includes elemental composition of the surface and depth profiling in an attempt to measure the oxide thickness. No standards were available at the time of the

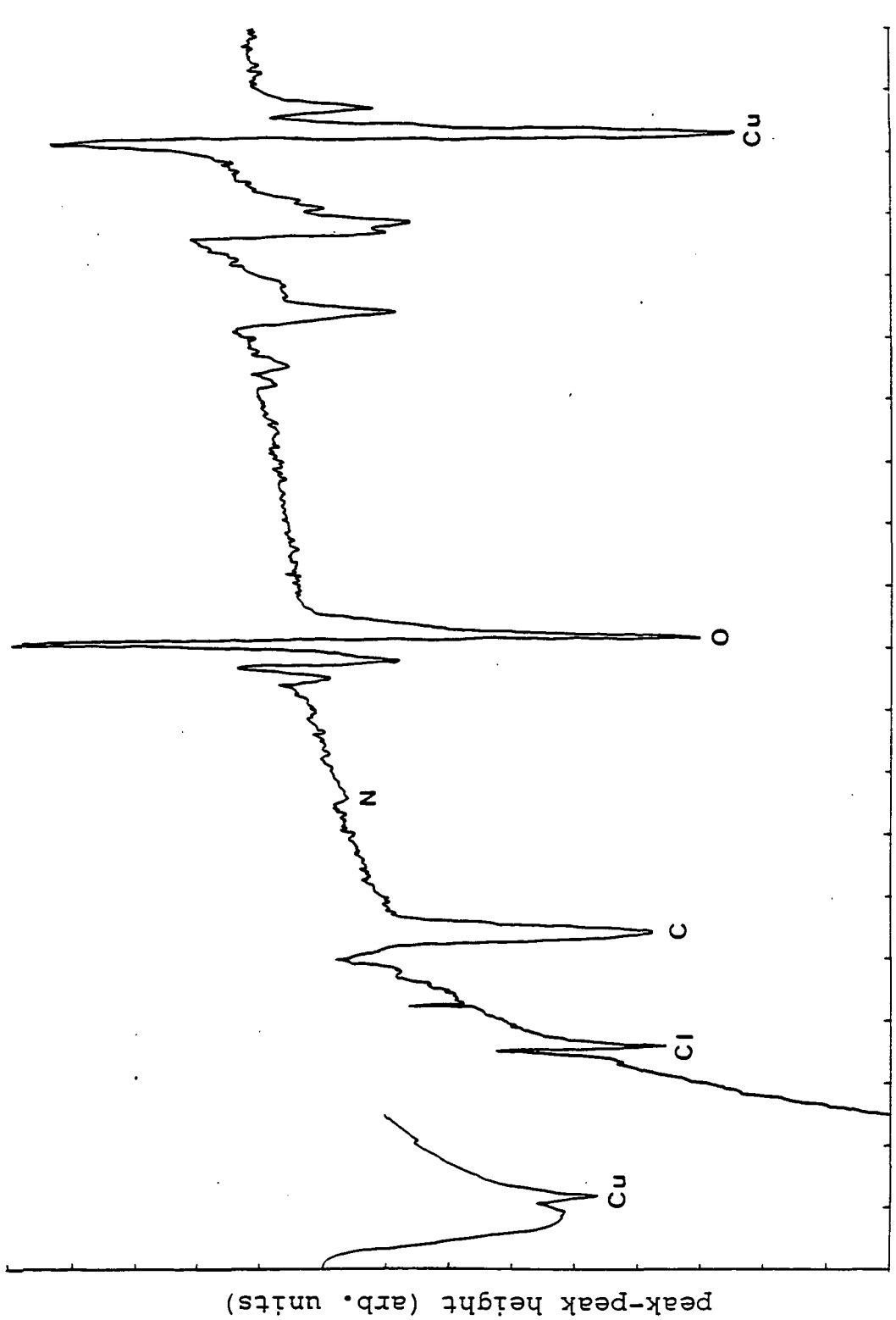

Fig. 4-22. Auger surface scan of an oxidized 15min at 200C contact.

measurements, so the sputter time cannot be converted to a film thickness accurately. The oxide thicknesses are estimates based on previous work and the sputter rate of pure Cu.

Figure 4-22 shows a surface scan of a foil that had been oxidized in air for 15min at 200C. The elements detected are indicated on the figure. The source of Cl, which was detected on all samples, is unknown. Freon and methanol were the only solvents in contact with the samples. The Cl could not be a contanimant in the Auger system. After sputtering the Cl away and waiting, the Cl signal did not increase over a period of 30 minutes.

The surface composition of each of the foils and time required to reduce the original O signal 50% are summarised in Table 4-13. The Cl and C present on the surface are removed in the first minutes of sputtering.

Table 4-13: Surface composition and oxide depth from AES.

surface treatment	% composition Cu	O	C	Cl	N	oxide depth (A)
clean	52	5	31	12	--	10
15min at 200C	50	22	25	3	--	375
30min at 200C	40	21	35	4	--	474

The oxide composition is Cu_2O as expected. Taking the ratio of the sputter times for the two oxidized samples, the longer oxidation time results in a 25% increase in

oxide thickness. Comparing this to the electrical contact resistance data, a 25% thicker oxide increases the R_c (4K) value by a factor of 4. If the contact resistance were dominated by the oxide resistivity, thrn from eqn. (2.11) R_c would scale as the film thickness, d_f. This clearly does not occur. A more likely mechanism is tunneling, which has an exponential dependence with respect to the electrode separation. Although only two different oxidations will not clearly establish an exponential dependence, the data do rule out an Ohm's law behavior for the electrical contact resistance.

4.4 SCANNING ELECTRON MICROSCOPY (SEM)

SEM was performed on each of the 3 grades of surface roughness. Thin sections were cut from contacts after contact formation and compared to freshly ground samples in an attempt to identify areas of plastic deformation resulting from the applied load. A total of six samples were examined. They were arranged in three groups, one group for each grade of roughness. Each group contained two contact samples; one freshly ground and the other having been part of an actual contact resistance speciman.

Visual observation of the microscope image and micrographs of selected areas of the contact surface constituted the procedure for comparing loaded and

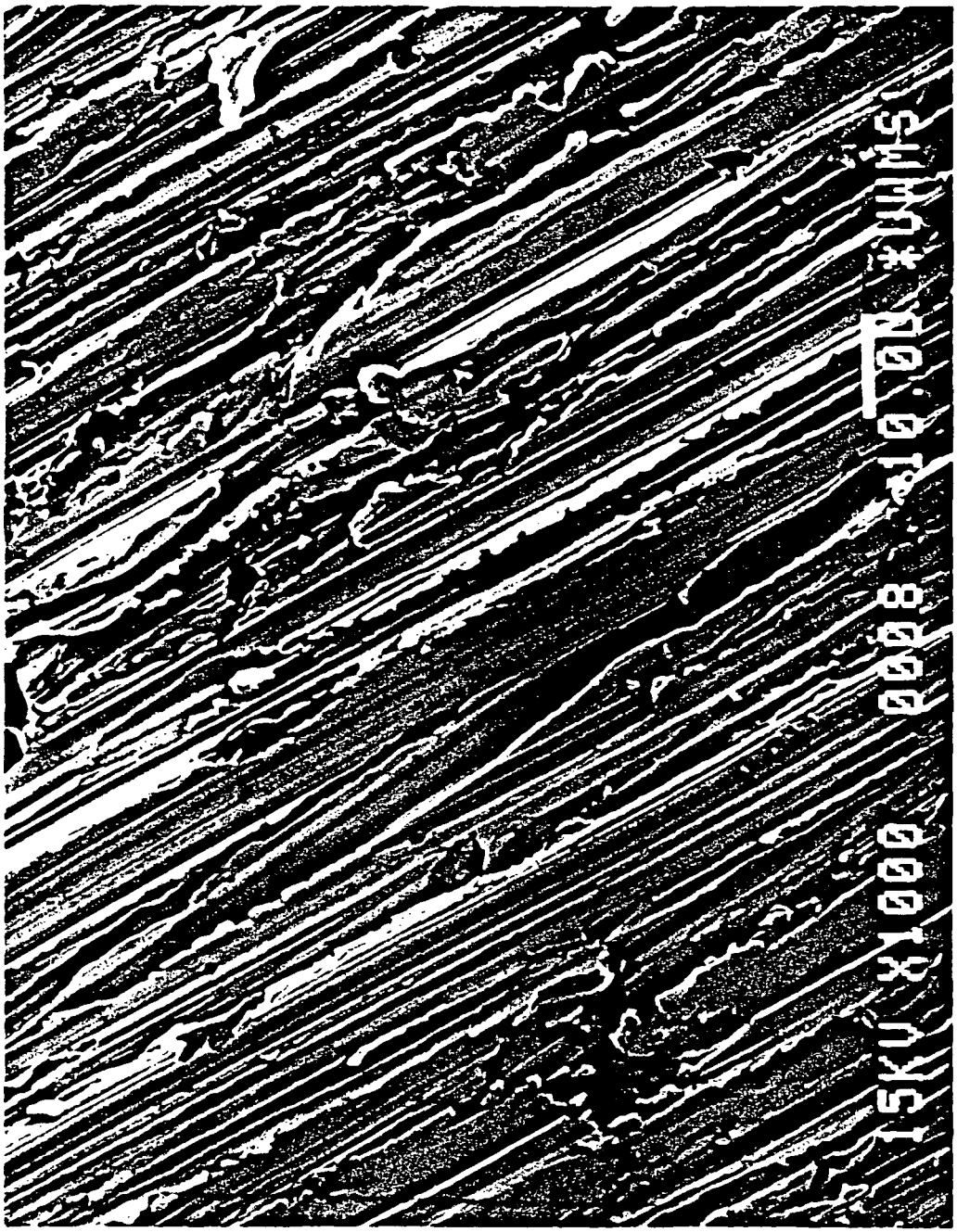

Fig. 4-23. Scanning electron micrograph of a 0.4um rms rough clean contact before loading. No difference was seen after loading.

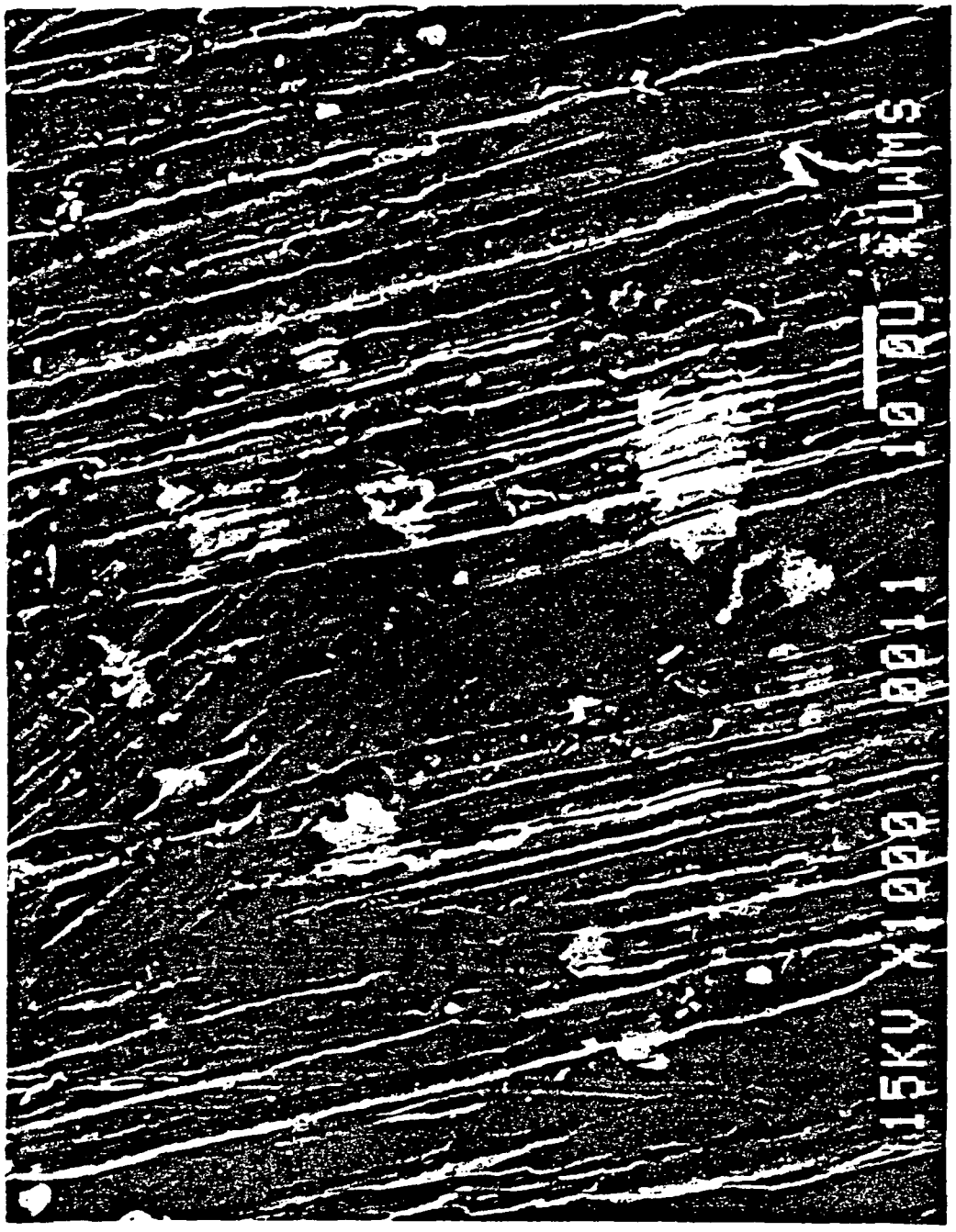

Fig. 4-24. SEM micrograph of a 0.1um rough oxidized contact. Light areas are assumed to result from film rupture during loading.

unloaded specimans. As seen in Fig. 4-23, a 0.4um unloaded contact sample, the surface is covered with many fine scratches running parallel to each other, a result of the griding operation. It was hoped that SEM would be able to resolve regions of plastic deformation on the loaded contact specimans. These would show up as deformed areas on the surface. No regions could be indentified. Both loaded and unloaded contact surfaces were very similar in appearance.

There was one exception. A 0.1um sample that had been oxidized for 30min at 200C and had a load applied to it is seen in Fig. 4-24. A number of light regions are apparent. These regions were present only on this oxidized sample. Damage from the 25kev electron beam was observed on this sample, appearing as a darkened rectangle in the middle of the viewing screen when the magnification was reduced. However, the contrast between the light and dark areas in the figure remained. We hypothesize that the oxide film has been ruptured at the light regions due to local surface deformation, either plastic or elastic, thereby allowing more secondary electrons to escape and resulting in increased contrast with the undamaged film around it. An estimate of the area thus covered by the light regions is 3%. Note that this micrograph is of an area that has a larger concentration of the light colored

regions that other parts of the contact surface. Whether or not these spots result from local deformation is not clear, but the estimated contact area is in reasonable agreement with previous work on the actual contact area (10-12).

4.5 SUMMARY

Data have been presented on electrical contact resistance and thermal contact conductance as a function of temperature from 4K to 290K. For the surface roughnesses covered in this study, no systematic variation with respect to roughness can be seen. Oxidation of the contact surface increases the electrical contact resistance and decreases the thermal contact conductance, as would be expected. However, the relative increase in R_c is not the same as the relative decrease in K_c. This is also seen as an increase in the value of the contact Lorenz number, L_c. The RRR of the contacts contrast very strongly with the bulk material, with RRR_{bulk} =112 and RRR_c ~ 2. The K_c increases with temperature up to roughly 100K and levels off. This increase covers three order of magnitude. No peak in the thermal conductance curve is seen, which is in direct contrast to pure metals. The Lorenz number variation of the contacts indicates a marked fraction of heat transfer is occuring by mechanisms not

involving electrons. An In foil contact showed a much higher contact conductance at low temperatures, with the Lorenz number variation strikingly similar to the clean contacts in magnitude and temperature variation. The deformation of the In foil under load results in greater contact area, hence an decrease in contact resistance. Because the Lorenz number of the foiled contact is the same as the clean contacts, the mechanism responsible for the measured contact resistance is similar, although with a larger total area in contact. Owing to the large conductance, data on this sample are unreliable above 80K.

AES and SEM provide further information about oxide composition and surface morphology. The oxide composition is Cu_2O. Scanning electron microscopy was unsatisfactory in observing plastic deformation, with the one exception of an oxidized contact. Light areas were observed on this one sample, the only oxidized contact examined with SEM, which if assumed to result from oxide film damage due to deformation, give a reasonable estimate of the total area in contact, about 3% of the nominal contact area.

CHAPTER 4 -- REFERENCES

1. L.G. Rubin, B.L. Brandt and H.H. Sample, Cryogenics 22, 491 (1982).

2. J.A. Gerber and P.J. Sellmyer, Cryogenics 18, 619 (1978).

3. J.G. Hust and L.L. Sparks, NBS Tech. Note 634, (1973).

4. Mateials at Low Temperatures, ed. R.P. Reed and A.F. Clark, ASME (1983).

5. R. Berman, Thermal Conduction in Solids, Chap. 9, Oxford, (1979).

6. R.B. Stephens, Phys. Rev. B 13, 852 (1976).

7. M.R. Pinnel, H.G. Tompkins and D.E. Heath, J. Vac. Sci. Technol. 16, 161 (1979).

8. E.T. Stepke, Electrical Contact Seminar, 125 (1967).

9. T. Hisakado, Wear 44, 345 (1977).

10. M.J. Edmonds, A.M. Jones, P.W. O'Callaghan and S.D. Probert, Wear 50, 299 (1978).

11. R. Holm, Electric Contacts, 4th ed. Springer-Verleg, New York (1967).

12. J.A. Greenwood and J.B.P. Willaimson, Proc. Roy. Soc. London 295, 300 (1966).

CHAPTER 5 -- CONCLUSIONS

We have carried out a series of experiments to measure electrical contact resistance and contact conductance in OFHC Cu pressed contacts fro 290K. The contact surface roughness and oxidation were varied in order to observe their effects o contact resistance. A unique aspect of these exper is measurement of both thermal and electrical cc resistances on the same contact sample. Our conclu are based on the evidence supplied by both types measurements. The load applied to the contacts is constant.

Variations in electrical contact resistance w observed, sometimes increasing by a factor of 10 over m typical values. These variations are seemingly inher in contact formation, due to the large number of variab influencing the process of contact formation. The cont resistance variations are also extremely dependent on exact procedures used to fabricate contact resista samples. Because of this variation, no firm conclusi can be drawn as to the effect of surface roughness contact resistance.

The temperature dependence of electrical cont resistance shows one very surprising feature. The RRR each contact which had been exposed to air was alw

between 2 and 3. The RRR of the OFHC Cu tubing used in making contact resistance samples is 112. Assuming metallic contact, the contact resistance would also have a RRR near 112. This is not the case. For low resistance contacts ($R_c \leq$ 1u-ohm) one can see a temperature dependent resistance contributing to the overall contact resistance at around 25K. This is the same temperature where the bulk resistance starts to exhibit a temperature dependence. So there is clearly some contribution due to the bulk dependence, although a very small one. A simple model that can qualitatively account for the observed behavior is to assume a thin insulating layer between the contact points. The layer exists because of the native oxide present on all metal surfaces exposed to air. The oxide forms a tunneling barrier, the resistance of which is temperature independent. Assuming a small fraction of the load bearing area is in real metallic contact, these two terms combine to give a total contact resistance that has a small temperature dependent component and a large temperature independent component. It is not clear why the temperature dependent component at 273K must equal the tunneling resistance at 4K, which is necessary for a RRR=2. Further work would be required, including investigating the load variation of RRR, to resolve this effect.

The thermal contact conductance shows some interesting behavior also. K_c increases by almost three orders of magnitude when going from 4K to room temperature for oxidized contacts. In the low temperature limit, the thermal contact conductance exhibits a power law behavior. The exponent varies between 1.5 - 2 depending on the oxidation treatment. A similar dependence has been observed at low temperature for the thermal conductivity of amorphous solids. Pure electronic transport would give a linear dependence while pure phonon transport would give a cubic behavior. This temperature dependence apparantly results from the oxide present on the contact surface. For example, the glove-bag sample, assembled under dry nitrogen, had an exponent = 1.2. As one progressed from this sample to the clean sample and then to the two oxidized contact samples, the exponent increased gradually from 1.2 to 2.

Also, the variation of thermal contact conductance among similar samples is much less than for electrical contact resistance. There is also less variation among different oxidized samples. At room temperature, the thermal contact conductance for clean contacts is about a factor of two better than the oxidized contacts. At 4K, however, the difference between the two sets of contacts is about a factor of 5.

The temperature variation of the Lorenz number provides further information on this subject. The bulk temperature dependence, as shown in Fig. 4-4 behaves as expected at low temperatures, i.e. the Lorenz relation is valid. This is clearly not true for contacts. Not only is L_c a function of temperature where L_{Bulk} is not, but it increases as the temperature is raised whereas L_{Bulk} decreases. Thus heat transfer by phonons becomes even more important at higher temperatures.

The variation of the electrical contact resistance and the thermal contact conductance points to the oxide layer as playing an extremely important role in determining the transport properties of the contact. This is true even for the clean contacts, which have a very thin oxide present. It is surprising that this layer is effective in preventing metallic contact between the contacting surfaces. Only the glove-bag sample comes close to the bulk in terms of its overall behavior.

If similar experiments of this type could be repeated in an ultra-high vacuum, so that the metal contact surfaces could be sputter cleaned or degassed at high temperature, the influence of the oxide layer on transport across the contact could be clearly resolved.

Of obvious interest is the behavior of other metals, such as Al, brass or stainless steel. Does the oxide

layer affect the contact resistance similarly, e.g. is the RRR = 2 for all metals, or only for pure metals, or is this true only for OFHC Cu under our particular set of conditions? The overall temperature variation of the Lorenz number for stainless steel is similar to that exhibited by L_c, although the values of the respective Lorenz numbers differ by a factor of 10. If L_c for stainless steel contacts resembled that of bulk stainless steel, then it could be argued that grain boundaries present in the steel are like pressed contacts, and that oxides in the grain boundaries are primarily responsible for the observed bulk thermal and electrical behavior. It is also of interest to see if there is a critical load at which the oxide layer is ruptured, allowing the underlying metal to extrude through the oxide and make metallic contact.

There are several improvements which could be made to the present experiment. Moving the knife-edge clamps closer together would reduce the bulk contribution to the measured resistance, permitting greater resolution at higher temperatures. This comes at the expense of greater

difficulty in assembling the contact sample to the mounting block.

The load application could be modified by running a strong wire from outside the cryostat to the contact in such a way, so that by hanging weights on the wire outside the cryostat, that tension in the wire applies the load to the contact. This would eliminate uncertainties with the Cu-Be spring constant, its Young's modulus variation with temperature and differential thermal contraction. Unfortunately, the amount of free space inside the cryostat is very small. At least three small radius right angle turns are probably necessary to run the wire to the cold tip of the cryostat. It would be difficult to achieve this without undue friction at the turns, neglecting of course, the need for a low friction, vacuum tight feedthrough.

The first improvement which should be made, is interfacing the experiment to a versatile and robust computer controlled data acquistion system. For T > 150K, the typical equilibration time is 40min, for one (1) data point. Computer controlled data acquisition would make this experiment a good deal less tedious.